Aerodynamic Performance of High Turning Airfoils and the Effect of Endwall Contouring on Turbine Performance

Santosh Abraham

Srinath V. Ekkad

Co-chair

Wing F. Ng

Co-chair

Rakesh K. Kapania

Mark R. Paul

Uri Vandsburger

Aerodynamic Performance of High Turning Airfoils and the Effect of Endwall Contouring on Turbine Performance

Santosh Abraham

ABSTRACT

Gas turbine companies are always focused on reducing capital costs and increasing overall efficiency. There are numerous advantages in reducing the number of airfoils per stage in the turbine section. While increased airfoil loading offers great advantages like low cost and weight, they also result in increased aerodynamic losses and associated issues. The strength of secondary flows is influenced by the upstream boundary layer thickness as well as the overall flow turning angle through the blade row. Secondary flows result in stagnation pressure loss which accounts for a considerable portion of the total stagnation pressure loss occurring in a turbine passage. A turbine designer strives to minimize these aerodynamic losses through design changes and geometrical effects. Performance of airfoils with varying loading levels and turning angles at transonic flow conditions are investigated in this study. The pressure difference between the pressure side and suction side of an airfoil gives an indication of the loading level of that airfoil. Secondary loss generation and the 3D flow near the endwalls of turbine blades are studied in detail. Detailed aerodynamic loss measurements, both in the pitchwise as well as spanwise directions, are conducted at 0.1 axial chord and 1.0 axial chord locations downstream of the trailing edge. Static pressure measurements on the airfoil surface and endwall pressure measurements were carried out in addition to

downstream loss measurements. The application of endwall contouring to reduce secondary losses is investigated to try and understand when contouring can be beneficial. A detailed study was conducted on the effectiveness of endwall contouring on two different blades with varying airfoil spacing. Heat transfer experiments on the endwall were also conducted to determine the effect of endwall contouring on surface heat transfer distributions. Heat transfer behavior has significant effect on the cooling flow needs and associated aerodynamic problems of coolant-mainstream mixing.

One of the primary objectives of this study is to provide data under transonic conditions that can be used to confirm/refine loss predictions for the effect of various Mach numbers and gas turning. The cascade exit Mach numbers were varied within a range from 0.6 to 1.1. A published experimental study on the effect of end wall contouring on such high turning blades at high exit Mach numbers is not available in open literature. Hence, the need to understand the parametric effects of endwall contouring on aerodynamic and heat transfer performance under these conditions.

ACKNOWLEDGEMENTS

I would like to express my sincere gratitude to my advisors, Dr. Srinath Ekkad and Dr. Wing Ng for their continuous guidance throughout the course of this project. The discussions, encouragement and critiques provided by them were of great essence to the progress of this work. My special thanks to them for their patience and faith in me and also for funding me. I am indebted to my colleague, Kapil Panchal who was instrumental in the CFD validation of the work presented in this dissertation. A special thanks to Anthony Malandra and Andrew Lohaus from Siemens Energy for their inputs and valued suggestions that led to the successful completion of this project.

I would like to thank my committee members Dr. Rakesh K. Kapania, Dr. Mark Paul and Dr. Uri Vandsburger for their valuable suggestions. I am also grateful to my colleagues, Song Xue, Colin Reagle, Michael Strover and everyone else in our research group who helped me make all those successful runs in the tunnel. Special thanks to the staff in the Mechanical Engineering machine shop, especially Bill Songer who was instrumental in the quick and high quality fabrication of the required hardware.

The task of writing this dissertation was made a lot easier, thanks to the efforts of my dear wife Tracy James. I would like to express my gratitude to her for putting up with me and managing to keep me sane over the past three years. Finally, I am forever indebted to my parents, P.K. Abraham and Sherly Abraham for their prayers and encouragement over all these years.

TABLE OF CONTENTS

LIST OF FIGURES

LIST OF TABLES

NOMENCLATURE

C_{ax} — Blade Axial Chord Length

M — Isentropic Mach Number $= \sqrt{\left[\left(\dfrac{p_{01}}{p_s}\right)^{\frac{\gamma-1}{\gamma}} - 1\right]\dfrac{2}{\gamma-1}}$

p_{01} — Inlet Total Pressure measured $0.45\ C_{ax}$ upstream of the cascade

p_{02} — Exit Total Pressure

p_{s2} — Exit Static Pressure

PS — Pressure Surface

SS — Suction Surface

h — Airfoil span

s — Pitch

x — Axial Coordinate

ω — Loss coefficient $= \dfrac{p_{01}-p_{02}}{p_{01}-p_{s2}}$

β_1 — Blade inlet metal angle

β_2 — Blade exit metal angle

Z — Zweifel coefficient $= 2\dfrac{s}{C_{ax}}\cos^2\beta_2(tan\beta_1 - tan\beta_2)$

h — Heat transfer coefficient

α — Thermal diffusivity

k — Thermal conductivity

T_m — Mainstream temperature

T_w — Wall temperature

T_i — Initial wall temperature

t — Time

1.0 INTRODUCTION

Gas turbines are widely used in land-based power plants and for aircraft propulsion. High efficiency levels have been achieved in the performance of gas turbine though years of research and development. However, there is room for more improvement and this requires a thorough understanding of the complex flow structures seen in turbines. Aerodynamic losses in turbines can be broadly broken down into profile losses, secondary losses and leakage losses. Viscous effects in airfoil boundary layers, shock waves seen near the trailing edge of the airfoil and trailing edge flow separation constitute the profile losses. Secondary flows are those generated when the wall boundary layer is turned through an angle by an adjacent curved surface (airfoil). Tip leakage losses are the losses arising due to the flow leakage over the tips of the rotor.

Highly loaded airfoils are advantageous as they result in lowering the cost due to a reduction in the number of airfoils required at each stage. However, increasing the loading could lead to an increase in secondary losses. The thickness of the upstream boundary layer as well as the airfoil turning angle influences the strength of the secondary flow observed near the endwalls. The secondary flow results into stagnation pressure loss which accounts for a considerable portion of the total stagnation pressure loss occurring in a turbine passage. Research on secondary flow has gained a lot of importance due to the effect it has on the turbine efficiency. However, majority of these studies have been conducted at subsonic flow conditions [[1][2][3]] and there is less information on the performance of blades at transonic flow conditions with high turning angles operating at varying incidences, as is investigated in this study. Prakash et al. [4] studied the effect that airfoil loading has on aerodynamic losses at subsonic conditions and found that as the loading level increases, higher suction side

1

separation occurs. Corriveau *et al.* [5] analyzed the performance of aft loaded and front loaded airfoils with moderate turning angles at transonic conditions and established that aft-loaded blades yielded considerably lower losses, but deteriorated at higher Mach numbers, while the front loaded airfoils showed poor performance. In a similar study at low speeds, Funazaki *et al.* [6] found that the front loaded airfoils in their design, exhibited better performance in terms of mid span losses. The works of Popovic *et al.* [7], and Zoric *et al.* [8], [9] revealed high profile loss for aft loaded airfoils and high secondary losses for front loaded airfoils. Benner *et al.* [10] conducted experiments at low speed on airfoils with differing leading edge geometries and concluded that the leading edge geometry has very little influence on the secondary flow. Low speed studies were conducted by MacIsaac *et al.* [11] to analyze effect of turbulent Reynolds stresses in secondary flows. Jouini *et al.* [12], [13] investigated the flow field for transonic linear turbine cascades at design and off-design conditions. Taremi *et al.* [14], [15] studied the variation of losses between low turning (90˚) and high turning (112˚) cascades.

Performance of five different airfoils at transonic flow conditions with high turning angles operating at varying incidences is investigated in this study. Loss systems provide predictions for pressure losses as the various geometric and aerodynamic parameters are varied. The objective of this study is to provide data at transonic conditions that can be used to confirm/refine loss predictions for the effect of various Mach numbers and gas turning. Notable recent efforts in computational fluid dynamics codes involve the work of Praisner and Clark [16], [17] and Menter *et al.* [18], [19]. Many researchers have previously used quasi-linear cascade design with divergent end walls, similar to the one used in the present study, in order to achieve loading distribution similar to that of a real engine. A similar quasi 2D cascade was used by Nagel *et al.* [20] with the same goal in mind. With present day stringent norms set by the government for clean and efficient engines and the ever-growing

competition in the market, gas turbine manufactures need to optimize every component of the engine. The need for low cost, compact and fuel efficient engines are apparent. Improvements can be made by designing blades such that minimum losses are generated while making sure that the loading on the blade is maximized in order to reduce the number of airfoils in each stage. The designer also needs to ensure that the turbine efficiency is maintained at off-design conditions.

End wall contouring has been widely studied during past two decades for secondary loss reduction in turbine passages. Secondary flows are created when a wall boundary layer is turned through an angle by an adjacent curved surface. Recent non-axisymmetric end wall contouring methods have shown more promise for loss reduction as compared to the axisymmetric end wall contouring methods used in initial studies. Onset of horseshoe vortex and development of secondary flow in turbine passages has been studied by many researchers. Controlling secondary flow within a turbine passage has been an area of active research for some time. During one of the earliest studies, Morris *et al*. [21] studied the effect of meridional endwall contouring and demonstrated a reduction in overall secondary loss by 25%. The non-axisymmetric end wall profile used in the study, however, did not show any promising results. The study was conducted at a very low Mach number and Reynolds number as compared to those encountered in modern HP turbines.

Kopper *et al*. [22] studied an axisymmetrically contoured vane passage at high exit Mach number of 0.85 and noted about 17% reduction in mass averaged total losses. The vane was a low turning angle (70˚) profile with a low aspect ratio of about 0.5. Mass contained in the secondary flow structures is a significant portion of the total mass flow in such cases. The secondary losses were over half of the total loss. The experiments conducted by Duden *et al*. [23] with a different type of meridional end wall profiling, for a highly loaded turbine cascade with about 100˚turning, however, did not show any significant overall reduction in

overall losses. Many other researchers tried such axisymmetric end wall contouring, especially during 1990s, but none of the studies showed significant and definite improvement for high exit Mach number blades.

Saha *et al*. [24] with non axisymmetric contours reported reduction in mass averaged total losses by about 3.2% through numerical computations at low Mach numbers. During the low Mach number experimental investigations for this blade profile, Gustafson *et al*. [25] reported 50% reduction in mass averaged pressure losses. Prainser *et al*. [26] from numerical computations showed 12% reduction in total row-loss for the optimized end wall. However, the experimental results showed 25% reduction for the same geometry. The exit Mach number for their cascade was about 0.1, a very low value.

Most of these studies were done at low exit Mach numbers and for moderate turning airfoils. The only study that was performed at very high Mach number was done on an axisymmetrically profiled end wall of a vane. There has been no published computational or experimental study done on a high turning transonic blade at a high exit Mach numbers.

For the studies where numerical computations were used, CFD results often under predicted the magnitude of loss as well as the change in loss as compared to the experimental results. Snedden *et al*. [27] applied Durham cascade (ref. [28], [29]) hub profile to the annular end wall of a 1½ stage rotating rig and observed about 0.4% improvement in rotor efficiency. However, the rotor exit relative velocities were very low in the range of about 50 m/s.

Taremi *et al*. [32] recently studied the effect of endwall contouring on a transonic linear cascade with airfoils that have a turning angle ~112°. The cascades included one with loading levels higher than the other. This study concluded that contouring reduced the secondary losses for the higher loaded cascade and loss level changes were negligible for the

lower loaded cascade. Panchal *et al*. [33] presented various methods of endwall contouring methods and suggested that endwall contouring needs to be studied on a case to case basis.

A study on the effect of end wall contouring on a high turning blade with high design exit Mach number is not available in open literature. Endwall heat transfer could also be reduced with the reduction of secondary flow strength with non-axisymmetric contouring. Lynch *et al*. [30] found that heat transfer levels were reduced by 20% in regions of high heat transfer with contoured endwall as compared to a planar endwall. This study was also conducted at low Mach numbers in a low speed cascade.

In the present study, the effect of endwall contouring on aerodynamic losses and endwall heat transfer will be studied in detail for two different contoured endwalls and compared with a baseline planar endwall. The two contoured endwall geometries studied includes one optimized to reduce endwall heat transfer and another optimized to reduce aerodynamic total losses. The effect of varying the spacing between blades is also seen with the added effects of endwall contouring.

The blade profile used for the study represents a high turning (~127˚), high exit Mach number (0.87) profile of the first stage of an HP turbine blade.

2.0 TEST FACILITY

A schematic of the transonic cascade wind tunnel at Virginia Tech is shown in Figure 1. The wind tunnel is a blow down facility capable of a twenty second run time. The air supply is pressurized by a four-stage Ingersoll-Rand compressor and stored in large outdoor tanks. The maximum tank pressure used for transonic tests is about 2068 kPa (300psig). A control valve is used to regulate the flow from the tanks to the test section. During a run, the upstream total pressure is held constant by varying the opening of a butterfly valve controlled by a computerized feedback circuit. There is additionally a safety valve upstream of the control valve to start and stop the tunnel. The airfoil isentropic exit Mach number is varied by changing the upstream total pressure.

The cascade test section, as shown in Figure 2, consists of 6 airfoils resulting in 5 passages, with a controlled bleed flow above the first airfoil. The airfoils are mounted on a rotatable window, which allows for changes in incidence angles as and when required. Airfoil 3 is considered as the center airfoil and is instrumented to measure the static pressure at midspan. Airfoil 2 is instrumented on the pressure side and Airfoil 4 is instrumented on the suction side, for midspan static pressure measurements to ensure flow periodicity in the two passages adjacent to the center airfoil. In order to ensure good flow periodicity it is essential that the stagnation streamlines for the outer airfoils of the cascade are identical. A headboard, positioned upstream of the cascade is instrumental in controlling the incoming flow by preventing an induced incidence angle effect on the leading edges of the airfoils. The headboard is used to create and control a flow bleed that prevents the flow from turning prior to reaching the leading edge of the airfoils. Good inlet flow conditions can be achieved by careful adjustment of the headboard angle which aids in maintaining uniform and periodic flow through each airfoil passage and ensuring that the flow angle gradient ahead of the

cascade is zero. A slot located 0.45 C_{ax} upstream of the cascade is used to measure the turbulence and velocity distribution at the inlet of the cascade. It is also used to measure inlet total pressure at midspan which is used as a reference total pressure for isentropic Mach number calculation. Tailboards are positioned at the top airfoil and bottom airfoil trailing edges to help guide the flow.
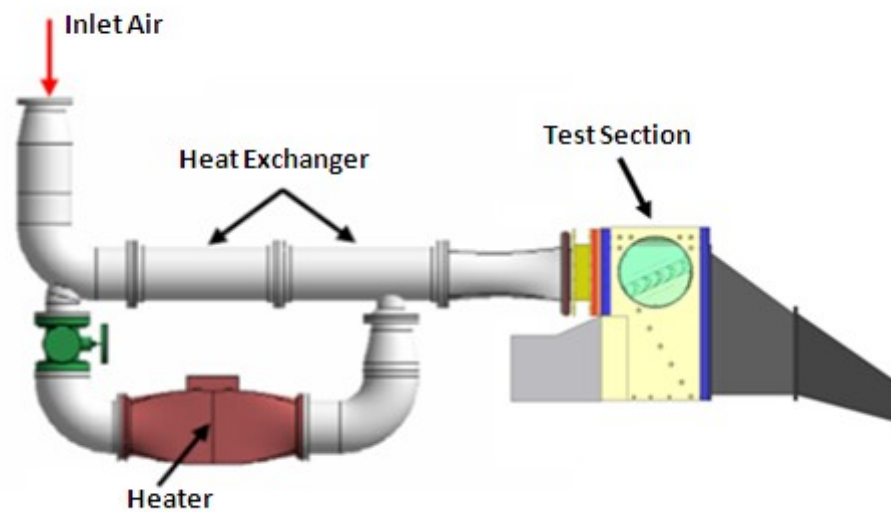
Figure 1: Virginia Tech transonic cascade wind tunnel
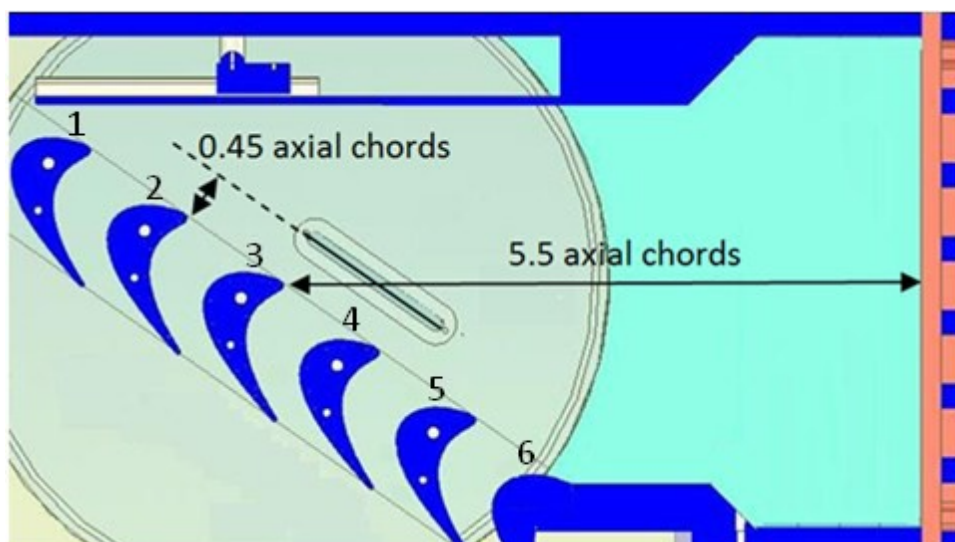
Figure 2: Test section

With an intention to obtain a ratio of inlet Mach number to exit Mach number that is representative to that encountered in a real engine and with the goal to simulate the airfoil and near end wall loading that is seen in an engine, the exit span is increased relative to the inlet span resulting in one end wall diverging from inlet to exit at a 13° angle, which simulates the required leading edge loading in a quasi 2-D cascade. The airfoil span increases by about 16% linearly in the axial direction, from inlet to exit of the cascade as shown in Figure 3.
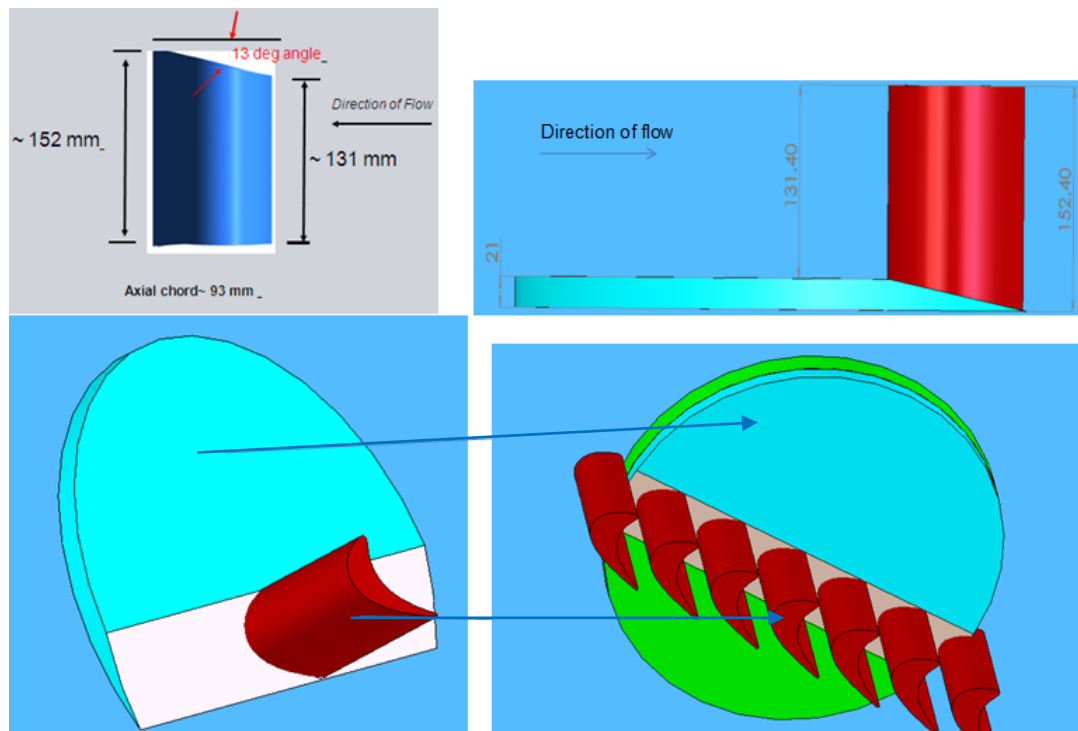
Figure 3: Change in inlet span relative to exit span

Instrumentation and data acquisition

Inlet Flow Measurements

A turbulence grid is placed 5.5 C_{ax} upstream of the cascade as shown in Figure 2 to obtain the desired level of turbulence. Aerodynamic measurements were made on a plane 0.45 C_{ax} upstream of the airfoil leading edge. The measurements covered one and a half airfoil pitches and extended from midspan to near the endwall. A pitot probe was used to

measure the inlet velocities at midspan and also to estimate the boundary layer thickness. Pitchwise traverse measurements were made to establish uniformity of incoming flow. A single line hot-wire probe was employed to measure the inlet free stream turbulence intensity based on isotropic turbulence assumption.

Static Pressure Measurements

The center airfoil and the two adjacent airfoils were instrumented with pressure taps placed at the midspan. In order to estimate the inlet and exit Mach numbers, static pressure taps were positioned on the end walls of the cascade on a plane 0.5 C_{ax} upstream of the airfoil leading edges and 0.5 C_{ax} downstream of the airfoil trailing edges.

Loss coefficient measurements

Performance of five airfoils at transonic flow conditions with high turning angles operating at varying incidences is investigated in this study. For the baseline case (airfoil A) the loss coefficient measurements were carried out at both 0.1 as well as 1.0 axial chord downstream from the blade trailing edge. A 5-hole probe was used to capture the velocity profiles in both the spanwise as well as in the pitchwise direction. The pitchwise line averaged loss coefficient was measured at midspan for Mach numbers varying from 0.6 to 1.1 and for incidence angles -10, 0 and +10. The spanwise area averaged loss coefficient was measured at different spanwise locations for the design exit Mach number and the design incidence angle. For the remaining 4 airfoils, a Kiel probe was used to measure all of the above mentioned quantities.

3.0 UNCERTAINTY ANALYSIS

The equation of loss coefficient is:

$$\omega = \frac{p_{t\_in} - p_{t\_ex}}{p_{t\_in} - p_{s\_ex}} \qquad [1]$$

Using Kline and McClintock's method

$$w_\omega = \left[\left(\frac{\partial \omega}{\partial p_{t\_in}} w_{pt\_in} \right)^2 + \left(\frac{\partial \omega}{\partial p_{t\_ex}} w_{pt\_ex} \right)^2 + \left(\frac{\partial \omega}{\partial p_{s\_ex}} w_{ps\_ex} \right)^2 \right]^{\frac{1}{2}}$$

Where w = uncertainty $\qquad [2]$

$$\frac{\partial \omega}{\partial p_{t\_in}} = \frac{1 - \omega}{(p_{t\_in} - p_{s\_ex})} \qquad [3]$$

$$\frac{\partial \omega}{\partial p_{t\_ex}} = -\frac{1}{(p_{t\_in} - p_{s\_ex})} \qquad [4]$$

$$\frac{\partial \omega}{\partial p_{s\_ex}} = \frac{\omega}{(p_{t\_in} - p_{s\_ex})} \qquad [5]$$

Hence, from [2-5]

$$w_\omega = \left[\left(\frac{1 - \omega}{(p_{t\_in} - p_{s\_ex})} w_{pt\_in} \right)^2 + \left(-\frac{1}{(p_{t\_in} - p_{s\_ex})} w_{pt\_ex} \right)^2 + \left(\frac{\omega}{(p_{t\_in} - p_{s\_ex})} w_{ps\_ex} \right)^2 \right]^{\frac{1}{2}}$$

$$\Rightarrow \frac{w_\omega}{\omega} = \frac{1}{(p_{t\_in} - p_{s\_ex})} \left[\left(\left(1 - \frac{1}{\omega} \right) w_{pt\_in} \right)^2 + \left(\frac{w_{ptex}}{\omega} \right)^2 + \left(w_{ps\_ex} \right)^2 \right]^{\frac{1}{2}} \qquad [6]$$

Also, the Mach number definition is based on p_{t_in} and p_{s_ex}. Therefore [6], after

substituting, $\frac{p_{t\_in}}{p_{s\_ex}} = \left(1 + \frac{\gamma - 1}{2} M_{iso}^2 \right)^{\frac{\gamma}{\gamma - 1}}$ becomes

$$\frac{w_\omega}{\omega} = \frac{1}{p_{s\_ex}\left[\left(1+\frac{\gamma-1}{2}M_{iso}^2\right)^{\frac{\gamma}{\gamma-1}}-1\right]}\left[\left(\left(1-\frac{1}{\omega}\right)w_{pt\_in}\right)^2 + \left(\frac{w_{ptex}}{\omega}\right)^2 + \left(w_{ps\_ex}\right)^2\right]^{\frac{1}{2}}$$ [7]

Hence, for a given Mach number and related p_{s_ex}, we can calculate uncertainty in experimental results for a given value of loss coefficient, if the uncertainties in individual variables are known. Let's look into it.

Uncertainty in p_{t_in}: All the pressure (p_{t_in}) is measured using 20 psi range 9816-2675 module. Instrument accuracy is 0.05% FS, which is $\pm 0.01\,psi$. Also, we use mean of the acquired data points along the run when inlet total pressure remains fairly constant. Hence, the unsteadiness resulted due to dispersion of inlet total pressure values around the mean is about $\pm 0.38\,psi$. Hence, the uncertainty in measurement of inlet total pressure is actually based on the confidence that the value of mean inlet total pressure will be within a given range when the experiments are repeated with identical. A quick look from two experimental runs with identical settings on two different days shows about 0.05 psi difference in value. Hence, the uncertainty can be given as,

$w_{pt\_in} = \pm 0.06\,psi$ (Instrument accuracy + uncertainty due to unsteadiness of total pressure)

[8]

 Uncertainty in p_{t_ex}: Here the instrument accuracy remains same. Now, even at 1 axial chord downstream, the flow is not completely mixed out and hence when we average the total pressure values along mid-span pitch, the variation will be more than that present in measurement of inlet total pressure due to additional variation of total pressure on account of presence of wake. Again, the uncertainty is based on the repeatability of the mean value of p_{t_ex}. A conservative value of ± 0.07 is estimated. Hence,

$w_{pt\_ex} = \pm 0.09\,psi$ [9]

Uncertainty in p_{s_ex}: p_{s_ex} is the wall static pressure measured 0.5 axial chord downstream. The values are generally below 2.5 psi and hence the instrument accuracy is 0.15 %FS, i.e. $\pm 0.03\ psi$. Also, the variation of static pressure is about $\pm 0.38\ psi$. Hence, similar to the previous cases

$$w_{ps\_ex} = \pm 0.10\ psi \tag{10}$$

Hence, uncertainty in all the variables is of same order, say w_{exp}, and hence, the equation [7] becomes,

$$\frac{w_\omega}{\omega} = \frac{W_{exp}}{p_{s\_ex}\left[\left(1+\frac{\gamma-1}{2}M_{iso}^2\right)^{\frac{\gamma}{\gamma-1}}-1\right]}\left[\left(1-\frac{1}{\omega}\right)^2 + \left(\frac{1}{\omega}\right)^2 + 1\right]^{\frac{1}{2}} \tag{11}$$

Now, for 55° and 45° inlet angle the loss coefficient range is about 0.08 to 0.12 and for 65° inlet angle it is about 0.20 to 0.22.

Now the components, $\left(1-\frac{1}{\omega}\right)^2, \left(\frac{1}{\omega}\right)^2, 1$ and $\left[\left(1-\frac{1}{\omega}\right)^2 + \left(\frac{1}{\omega}\right)^2 + 1\right]$ have been plotted against this loss coefficient range of 0.08 to 0.22 in Figure 4.

It can be observed that:

(1) Uncertainty in p_{s_ex} has insignificant contribution to total uncertainty

(2) Uncertainty in p_{t_ex} gives highest contribution to the final uncertainty value.

(3) Uncertainty due to p_{t_in} and that due to p_{t_ex} are comparable.

(4) High uncertainty at low loss coefficient values.

Hence, getting more accurate values of p_{t_ex} repeatedly is very important.
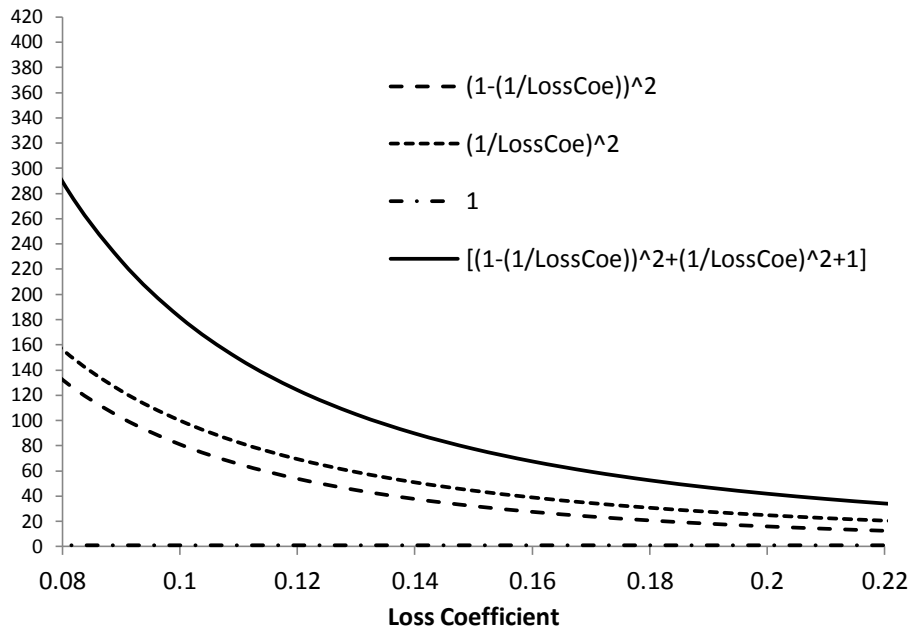
Figure 4: Contribution of Different Components

It was observed that the uncertainties do not change much for different values of p_{s_ex} and M_{iso}. Hence, variation in uncertainty (eqn. [11]) for different M_{iso} and related p_{s_ex} is plotted below.
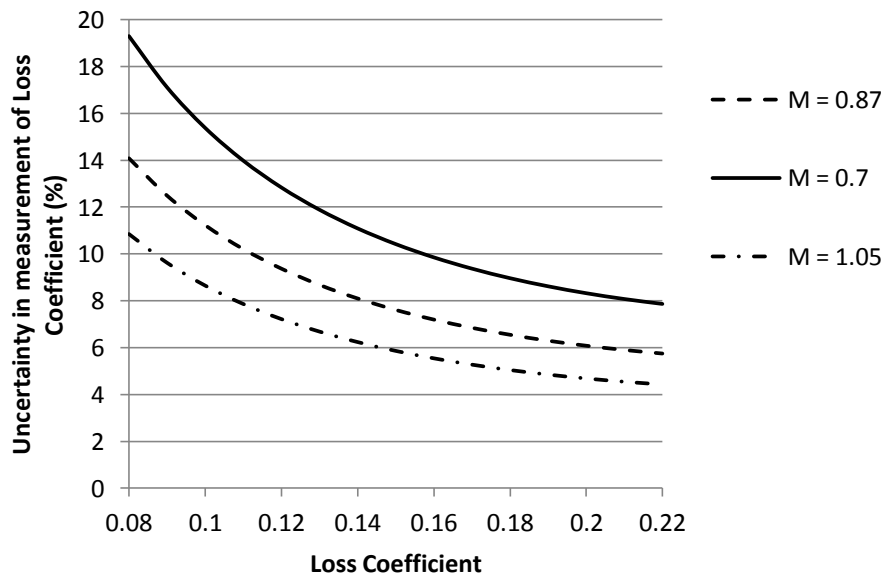
Figure 5: Variation in uncertainty with loss coefficient and Mach number

A value of $w_{exp} = \pm 0.07\, psi$ was taken for plotting the graphs in Figure 5. It can be observed that percentage uncertainty is inversely proportional to the loss coefficient value.

Finally a 20% uncertainty @ $\omega = 0.08$ means $\Delta\omega = \pm 0.016$ and 8% uncertainty @ $\omega = 0.22$ results in $\Delta\omega = \pm 0.0176$. And hence, the largest uncertainty in loss coefficient can be given as,

$$\omega_{actual} = \omega_{measured} \pm 0.0176 \qquad\qquad [12]$$

4.0 EFFECT OF INCIDENCE ANGLE ON AIRFOIL AERODYNAMIC PERFORMANCE

Motivation

This section presents detailed measurements of midspan total pressure losses, secondary flow field, static pressure measurements on an airfoil in a transonic turbine airfoil cascade. Numerous low-speed experimental studies have been carried out to investigate the performance of turbine cascades. Profile and secondary loss correlations have been developed and improved over the years to include the induced incidence and leading edge geometry and to reflect recent trends in turbine design. All of the above investigations have resulted in better understanding of flow field in turbine passages. However, there is still insufficient data on the performance of turbine blades with high turning angles operating at varying incidences angles at transonic Mach numbers. In the present study, measurements were made at +10, 0 and -10 degree incidence angles for a high turning turbine airfoil with 127˚ turning. The design inlet angle of the airfoil is 55˚. The exit Mach numbers were varied within a range from 0.6 to 1.1. Additionally, the exit span is increased relative to the inlet span resulting in one end wall diverging from inlet to exit at 13 degree angle. This was done in order to obtain a ratio of inlet Mach number to exit Mach number which is representative to that encountered in real engine and simulates the blade and near end wall loading that is seen in an engine.

Inlet Flow Measurements

Well-documented inlet boundary conditions are needed for CFD calculations. Aerodynamic inlet spanwise measurements on a plane 0.5 axial chord upstream of the blade

leading edge plane were measured. The primary measurement passage measured an isotropic turbulence intensity level of 8%. It is worth mentioning here that Gregory-Smith and Cleak [31] studied the influence of inlet turbulence intensity on secondary flows and concluded that it had very little influence on the flow field and loss behavior. The upstream flow uniformity was established with a maximum deviation of ±1% in normalized pressure.

Static Pressure Measurements

The surface isentropic Mach number was obtained from the ratio of the measured surface static pressure at midspan to the total pressure upstream of the cascade. The local Mach number distribution on the blade surface was measured for varying exit Mach numbers at 3 different incidence angles. Figure 6 shows the Mach number distribution on the blade surfaces at midspan for the center 3 blades at design conditions. The periodicity of flow through the passages was satisfactory and was established for all the cases that were studied.
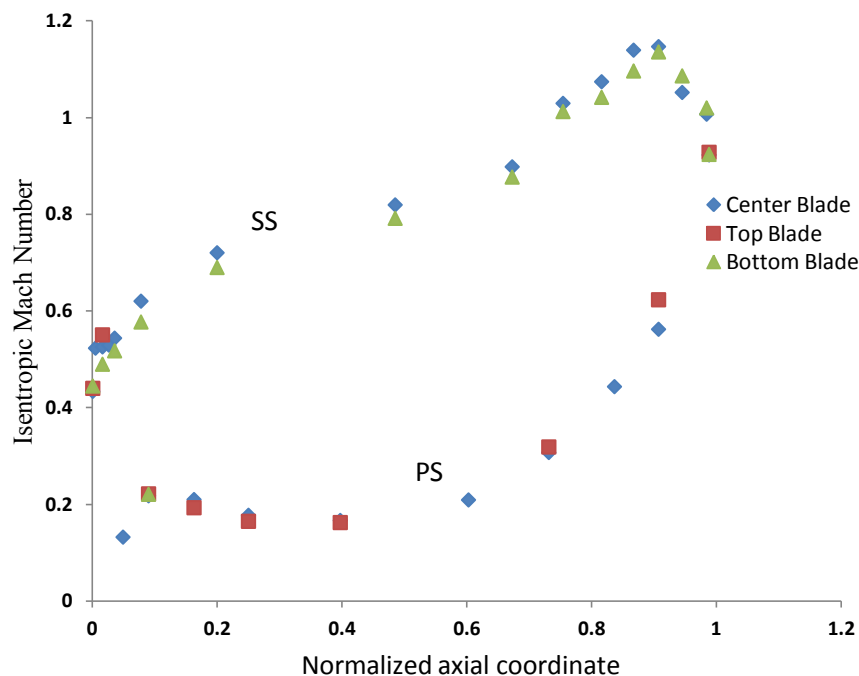
Figure 6: Flow Periodicity in the Cascade

Figure 7 shows the comparison of midspan blade loading between experimental values and CFD analysis results at 0 degree incidence and design Mach number. It can be seen that there is a very good agreement between experiments and CFD analysis. The CFD results presented in this section were provided by Siemens Energy.
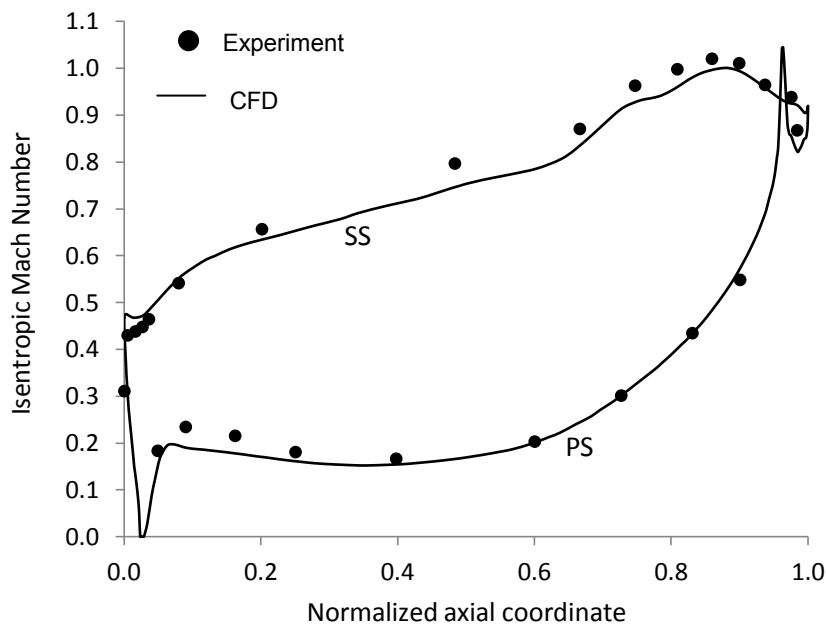
Figure 7: Midspan blade loading from CFD analysis and experiments at design condition

The effects of the exit Mach number on the surface Mach number distribution at the design incidence angle as well as the two off-design incidence angles are shown in Figure 8(a), (b) and (c). It is evident from the figure that the pressure side distribution does not vary significantly with the variation in exit Mach number. The pressure surface loading remains almost constant from about 75 percent of the axial chord up to the trailing edge. At higher exit Mach numbers, a normal shock impinges on the suction side and as the Mach number increases further, the shock becomes sharper and migrates more towards the trailing edge.
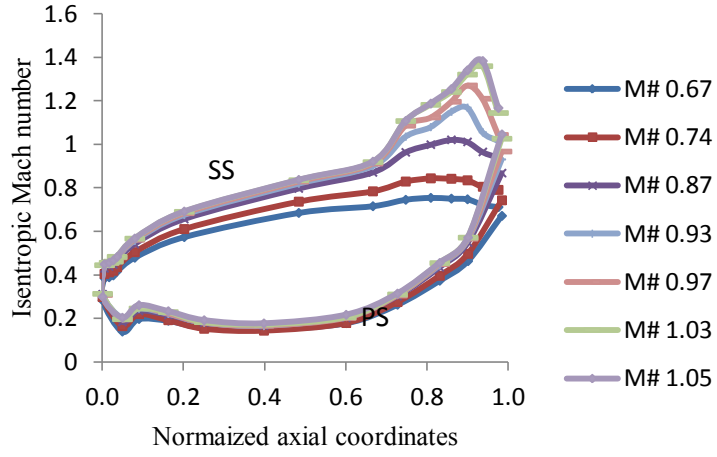
(a) Design incidence
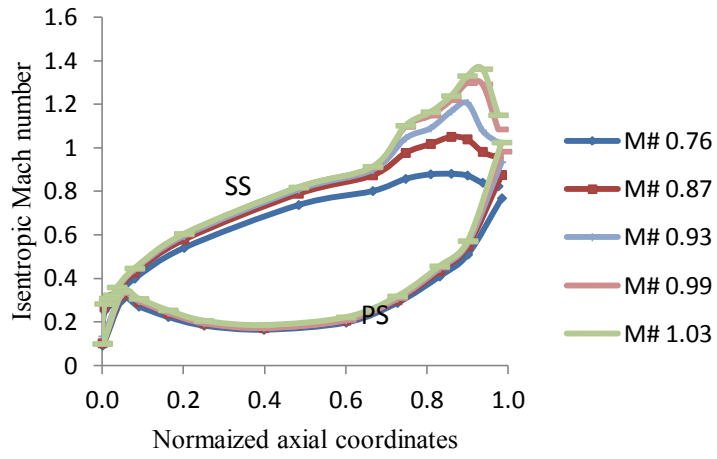
(b) -10.0 deg off-design incidence
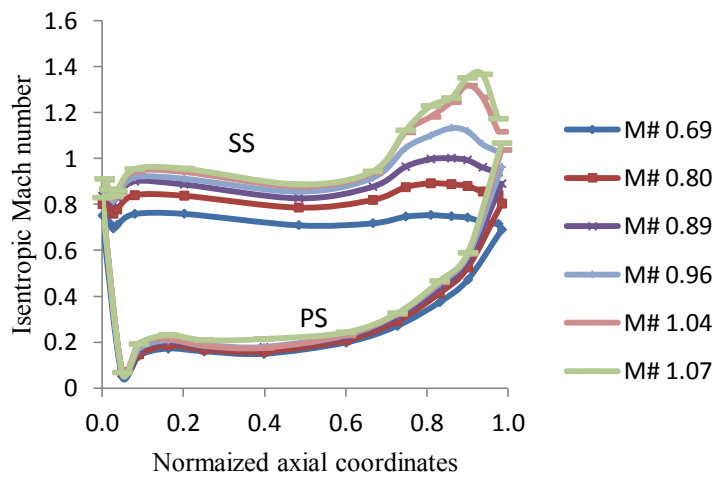
(c) +10.0 deg off-design incidence

Figure 8: Effect of Mach number on blade loading

The effect of varying incidence angle reveals large changes in the loading distribution in the vicinity of the leading edge. As the positive incidence increases a strong suction peak develops on the suction side near the leading edge (Figure 8(c)). The dip in Mach number distribution on the suction side for +10 degrees incidence angle case at 0.5 normalized axial coordinate is because of flow separation due to high turning of the airfoil. As the incidence angle reduces to -10 degrees the leading edge loading considerably decreases (Figure 8(b)).

Loss coefficient measurements:

Figure 9 shows a 2-D profile of the losses 0.1 axial chord downstream from the trailing edge of the cascade at the design exit Mach number and at the design incidence angle measured at various spanwise locations using a 5 hole probe. Regions of higher losses are clearly visible near the end walls and are a result of complex vortices arising due to the secondary flows. Pressure gradients in the passage caused by the boundary layer velocity distribution and flow stagnation on the blade result in the creation of secondary flows in the end wall region. These pressure variations force the flows toward the end wall and also lead to the development of two legs of the leading edge vortex. The turning angle of the flow between the airfoils results in the creation of a strong pressure gradient across the passage. This gradient influences the paths of the two legs of the horseshoe vortex and also the low velocity flow near the end wall. The pressure side leg of the horseshoe vortex which is forced to flow in a downward direction combines with the low velocity flow near the end wall and forms the passage vortex. The passage vortex drifts from the pressure side leading edge toward the suction side trailing edge of the adjacent airfoil. As this vortex approaches the suction side, it lifts off the end wall, adheres along the suction side and moves downstream in the passage. At the same time the suction side horseshoe vortex remains close to the end wall until it meets the passage vortex. It then wraps itself around the passage vortex instead of

adhering to the suction surface, lifts off the end wall and continues downstream along the suction side. As we go further downstream from the trailing edge plane, these vortices mix out.
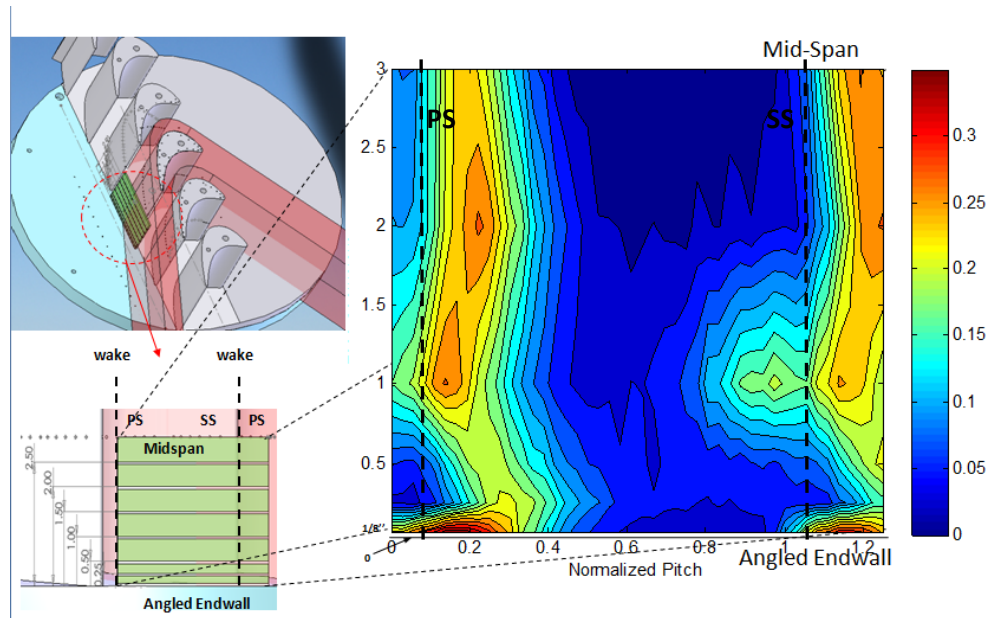
Figure 9: Loss coefficient at 0.1 axial chord downstream

The losses are also measured 1.0 axial chord downstream from the trailing edge of the cascade at different incidence angles and varying exit Mach numbers and are represented in Figure 10. For both the design incidence angle as well as the -10˚ off design incidence angle, at low exit Mach numbers the loss coefficients remain mostly unaltered. In other words, at lower subsonic exit Mach numbers, the losses are relatively the same. However for the +10 degree case, the flat behavior is not evident. The rise in losses as the exit Mach number decreases could be due to the increased loss production in the suction side boundary layer on the frontward part of the blade. This behavior at higher incidence angles was also observed by Jouini [12]. As the exit Mach number increases, the shocks become stronger and, as expected, the loss coefficient begins to rise for all incidence angles.

All the loss profiles were compared with corresponding results from CFD analysis, as shown in Figure 11 (a), (b) and (c) for 0 incidence angle, -10˚ incidence and +10˚ incidence respectively. A good match between CFD predictions and experimental loss measurements were observed. However, for the +10˚ case CFD under predicted the loss values as compared to the experimental values. This could be due to the presence of a large amount of separated flow on the suction side as seen from the loading distribution at high incidence angles, which may not be accurately captured. Sudden rise of total pressure loss at near sonic and supersonic isentropic Mach numbers as observed in experiments is also evident in CFD predictions. Even though the losses for -10 degree case are the least, the work output derived will also be least due to the reduced overall blade loading.
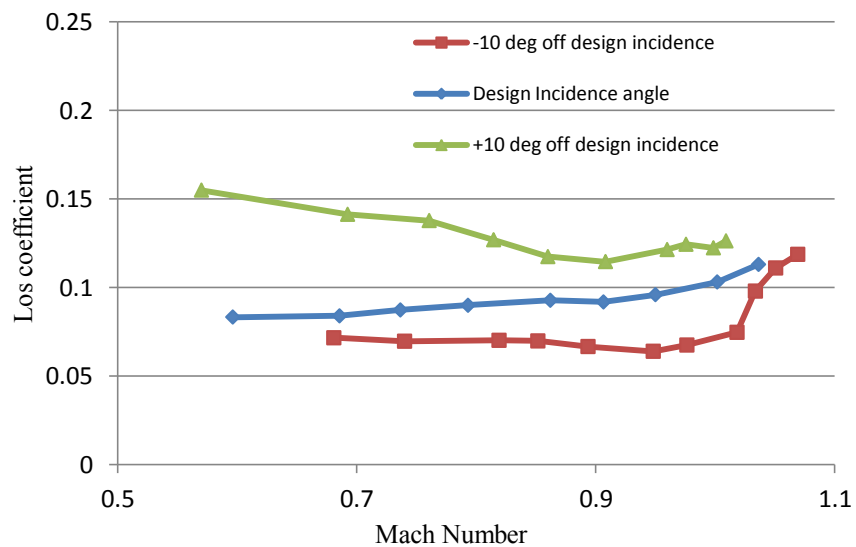
Figure 10: Midspan average loss coefficient at 1.0 axial chord
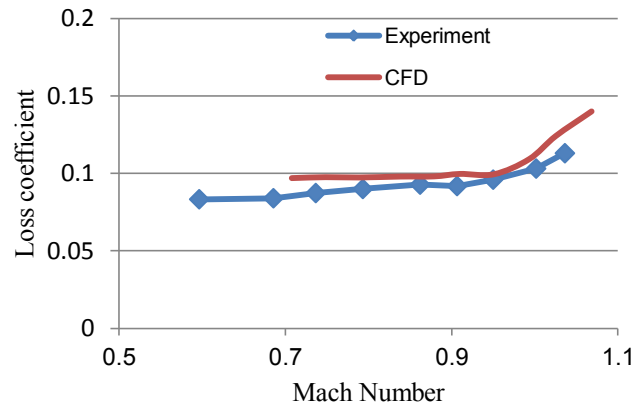
(a) Design incidence
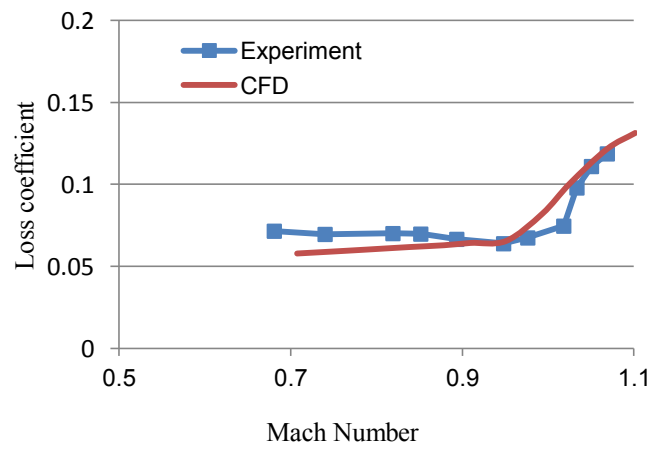
(b) -10 deg off design incidence
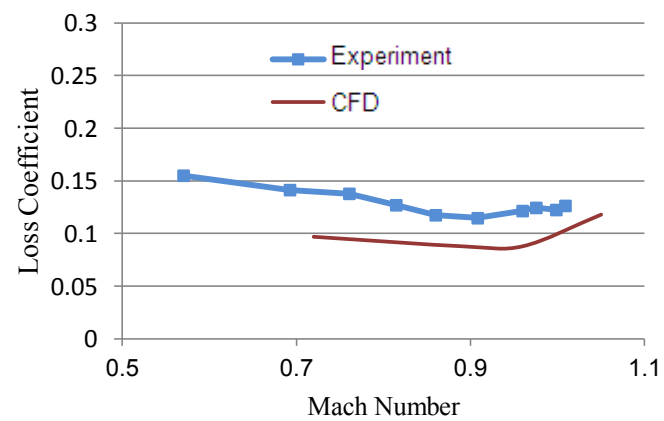
(c) +10 deg off design incidence

Figure 11: Loss coefficient measurements at 1.0 axial chord downstream

Conclusions

Experimental measurements and numerical predictions for a high turning, high loading turbine blade have been carried out at design and off design conditions in a linear transonic cascade wind tunnel.

The results show that at a given incidence angle, the effect of variation of exit Mach number is felt only toward the trailing edge region of blade and the loading at the leading edge remains almost same for different Mach numbers. However, at off-design incidence angles, the leading edge loading changes considerably reducing the overall loading in comparison to that obtained at design angle. The blade loading results from experiment and CFD analysis agree very well.

The loss coefficient contours 0.1 axial chord downstream of the cascade show presence of strong secondary vortices contributing to high total pressure loss. Experimental results show high lift-off of the vortex core.

The loss coefficient measurements 1.0 axial chord downstream of the cascade show minimum mixed-out midspan loss coefficient for -10 incidence angle case, where as that in the case of +10 degree incidence angle is the highest due to the presence of large amount of separated flow on the suction side. It was also observed that the losses rise sharply at near sonic and supersonic isentropic Mach numbers.

5.0 EFFECT OF AIRFOIL SHAPE ON AIRFOIL AERODYNAMIC PERFORMANCE

Motivation

It is advantageous to reduce the number of airfoils to the possible extent, since each individual airfoil adds to the overall weight and expense. With the added features such as special materials using expensive manufacturing processes, cooled airfoils with complex internal flow passages reduction of the number of airfoils is important. Performance of three airfoils at transonic flow conditions with high turning angles operating at varying incidences is investigated in this study. Loss systems provide predictions for pressure loss as the various geometric and aerodynamic parameters are varied. The objective of this study is to provide data at transonic conditions that can be used to confirm/refine loss predictions for the effect of various Mach numbers and gas turning. The three airfoils being studied (airfoils A, B and C) are designed for the same velocity triangles (inlet/exit gas angles and Mach number). Airfoil curvature and true chord are varied to change the variation in loading vs. chord. The goal is to see if a given type of loading distribution (more front loaded, more aft loaded, etc.) results in better performance (less pressure loss). Measurements are made at +10, 0 and -10 degree incidence angles for high turning turbine airfoils with ~127 degree turning. The cascade exit Mach numbers were varied within a range from 0.6 to 1.1.

Airfoil Geometries

While this section contains several discussions of airfoil flow physics and fluid mechanics, the main focus of this study was to analyze and compare the aerodynamic

performance of three turbine airfoil designs. Figure 12 shows the cross sectional geometries of the three airfoils being studied, oriented so that the axial chord is on the x-axis. All three airfoils are high turning transonic airfoils with identical flow angles and the same axial chord length as shown in Table 1. Therefore the Zweifel coefficient, given by equation 12 would be the same for all three airfoils.

$$Z = 2\frac{s}{C_{ax}}\cos^2\beta_2(tan\beta_1 - tan\beta_2) \hspace{2cm} [12]$$

The Zweifel coefficient, an aerodynamic loading index of cascade, provides a reliable and basic method for making an initial estimate of the minimum solidity and number of required airfoils. Investigations of the midspan surface loading profile, profile losses, spanwise losses and area averaged total losses were conducted to determine the performance characteristics for the airfoil designs.

The stagger angle and the unguided turning angle are detrimental parameters that affect the loading distribution. The stagger angle is the angle between the line joining the leading and trailing edge of the airfoil to the engine axial direction. The unguided turning angle is the amount of turning that the fluid undergoes over the rear section of the airfoil extending from the airfoil throat to the trailing edge. It can be seen from Table 1 that the unguided turning angle for blade B is the highest and that for blade C is the lowest while the stagger angle for all three airfoils are almost the same.
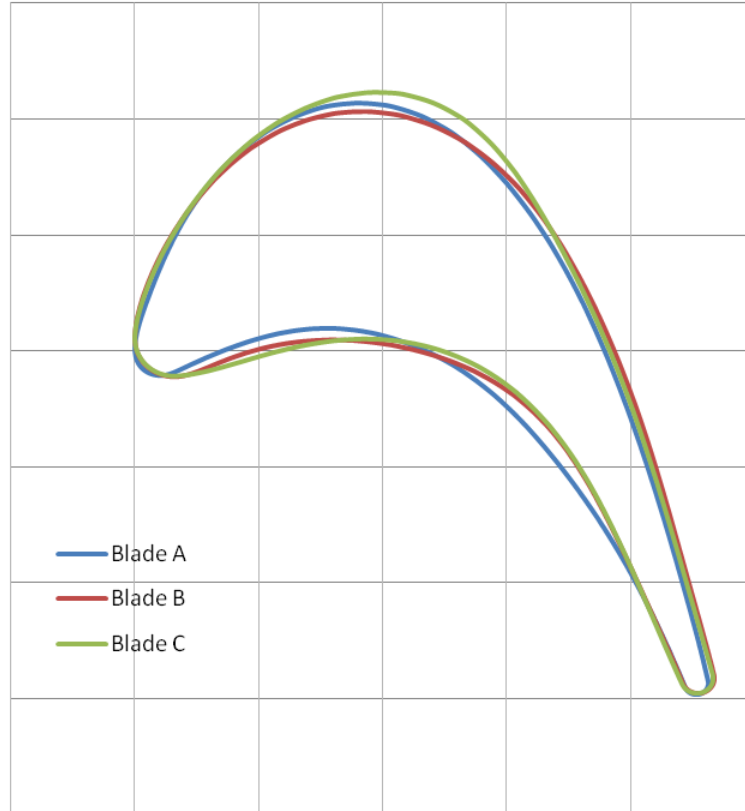
Figure 12: Cross sectional geometries of the three airfoils

Cascade Parameters	Airfoil A	Airfoil B	Airfoil C
Axial chord length	93mm	93mm	93mm
Blade span(trailing edge)	152mm	152mm	152mm
Blade pitch	91mm	91mm	91mm
Inlet metal angle β_1	55°	55°	55°
Exit metal angle β_2	-72°	-73°	-71°
Stagger angle	32.27	32.14	33.21
Unguided turning angle	15.7	19.65	9.7

Table 1: Design parameters for Airfoils A, B and C

Static Pressure Measurements

The periodicity of flow through the passages was satisfactory and was established for all the cases that were studied using midspan pressure taps on the center airfoil and its adjacent airfoils. The local Mach number distribution on the three airfoil surfaces were measured for varying exit Mach numbers at 3 different incidence angles.

Figure 13 shows the loading on the airfoils at design conditions. The loading on the suction side is relatively higher around midchord for airfoil A, than for airfoils B and C due to axial redistribution of loading. The suction surface loading differences were by design from changes in airfoil shape and curvature. It is apparent that airfoil B is highly aft loaded. The unguided turning flow for airfoil B is the highest. Compared to airfoil A, airfoil B reveals a considerable amount of aft diffusion which will result in higher profile losses downstream. The profile losses resulting from different airfoil loadings are studied in detail in further sections.

Figure 14, Figure 15 and Figure 16 shows the effect of Mach number variation on the airfoil loading for the three airfoils at design incidence angle as well as for the two off-design incidence angles. As the positive incidence increases to + 10 degrees a strong suction peak develops on the suction side near the leading edge and as the incidence angle reduces to -10 degrees the leading edge loading considerably decreases. In other words, the loading on the three airfoils change from aft loading for the -10 degree incidence angle cases, to front loading for the +10 degree incidence angle cases. For all cases there is no significant change on the pressure side loading, up to near trailing edge, with varying exit Mach numbers. For all higher exit Mach number cases (> 0.9) the loading on the suction side remains relatively the same, from leading edge to 0.7 normalized axial coordinate as the exit Mach number increases. This can be attributed to the choking of the flow in the blade passage. For the +10

degree incidence angle cases for all three airfoils, a mild deceleration is noticeable on the suction surface from the leading edge to mid-chord. As a result the suction side boundary layer will tend to be thicker for these cases as compared to the other two cases, which will result in higher losses for these cases.
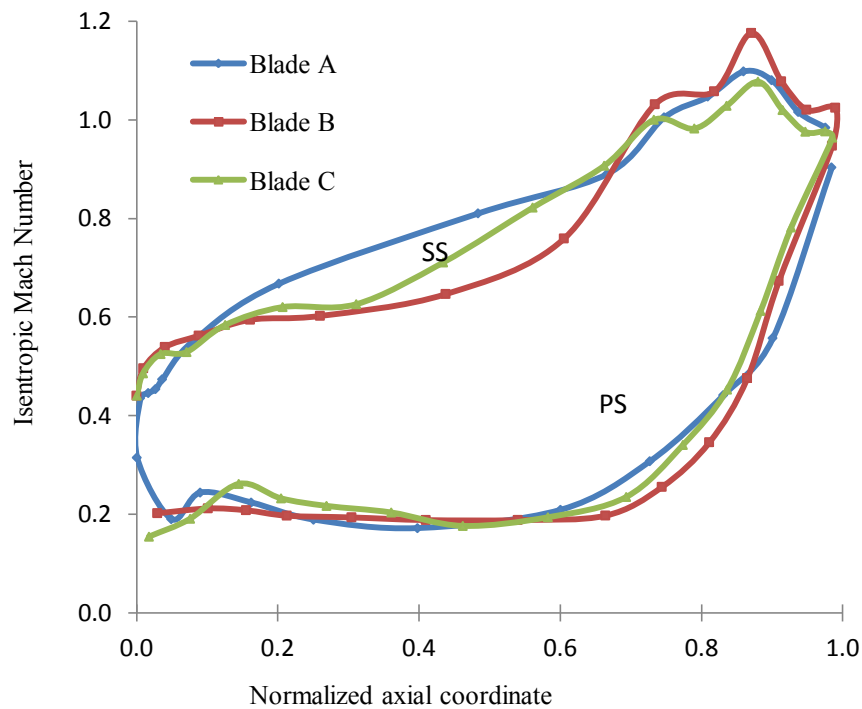
Figure 13: Loading distribution on the three airfoils at design condition

At higher exit Mach numbers a normal shock impinges on the suction side and as the Mach number increases further, the shock becomes sharper and migrates more towards the trailing edge for all cases tested. Note that while all airfoils experience the shock at higher Mach numbers, the magnitude of the resulting pressure gradient (velocity drop) as a function of the exit Mach number and the rate at which the shock appears and grows vary between the three airfoil designs. The shocks are less prominent on airfoil A which would result in the other airfoils showing higher losses due to the shock effect.
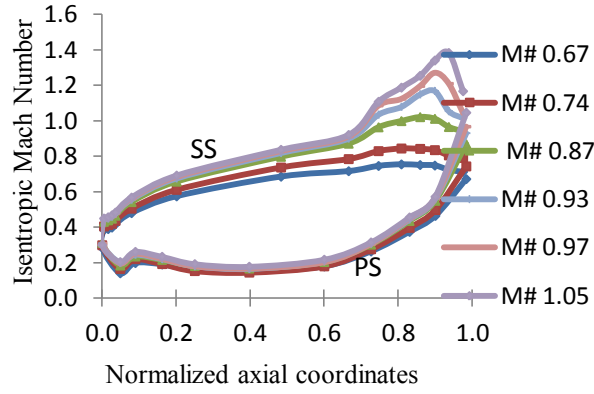
(a) Design incidence
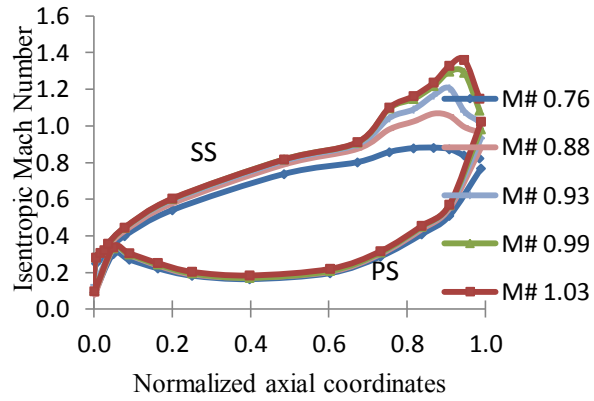
(b) -10 deg off design incidence
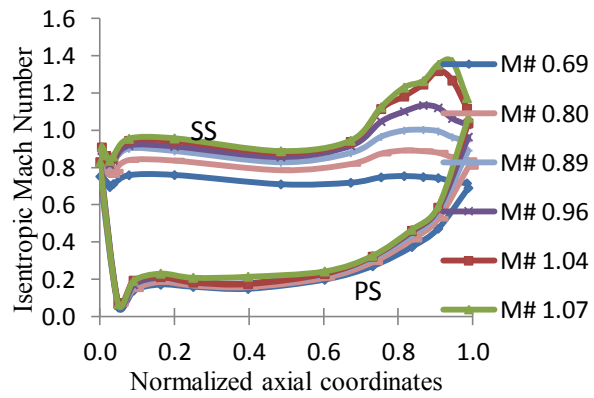
(c) +10 deg off design incidence

Figure 14: Effects of Mach number on airfoil loading for blade A
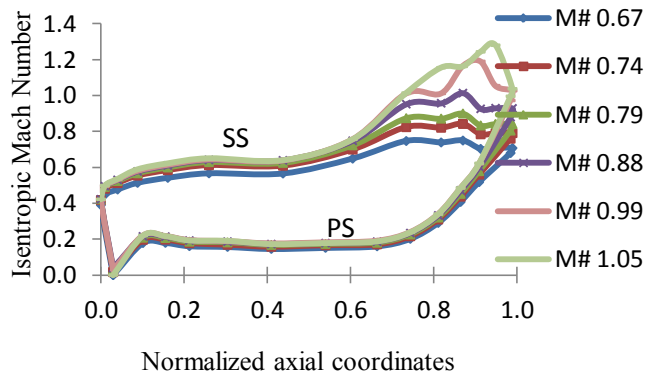
(a) Design incidence
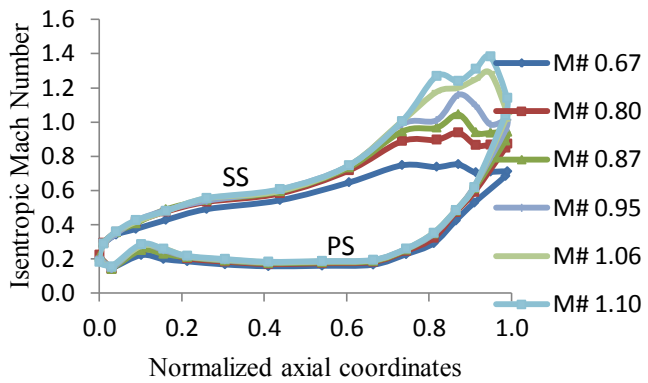
(b) -10 deg off design incidence
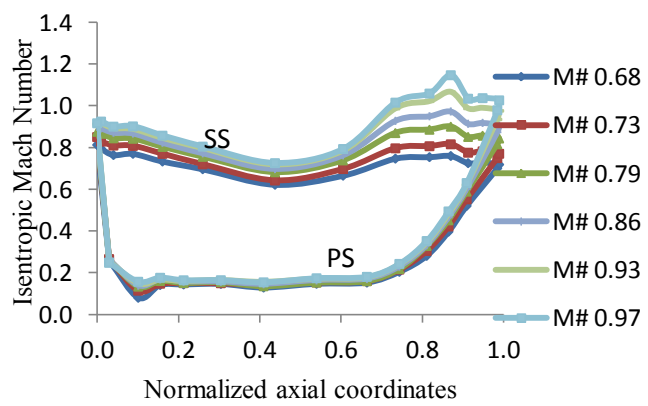
(c) +10 deg off design incidence

Figure 15: Effects of Mach number on airfoil loading for blade B
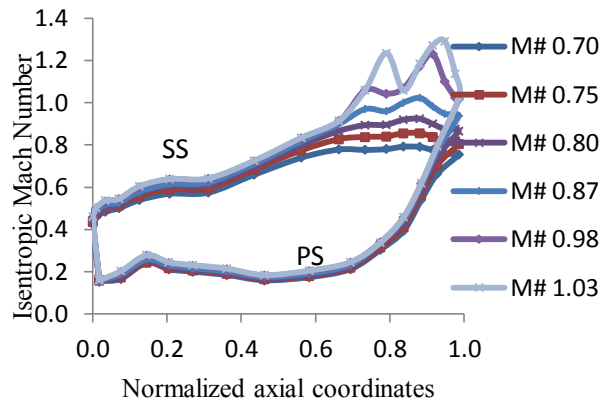
(a) Design incidence
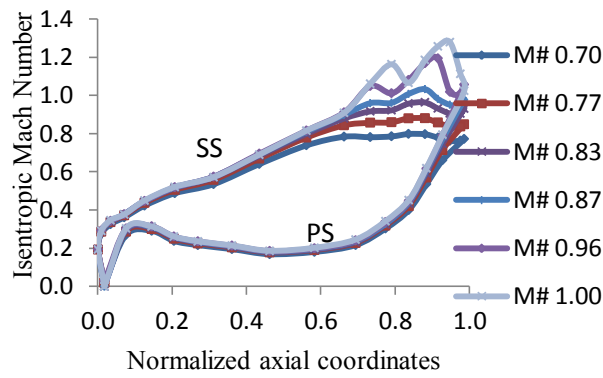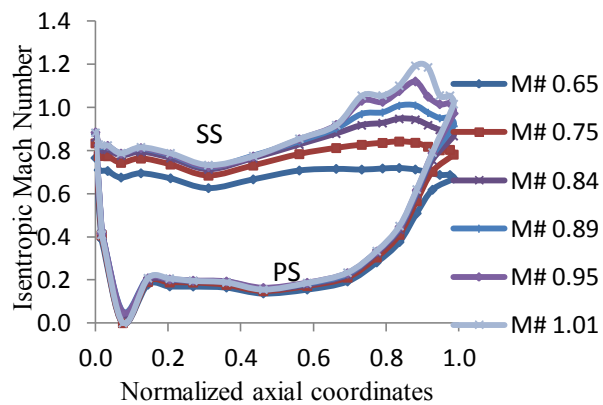
(b) -10 deg off design

(c) +10 deg off design incidence

Figure 16: Effects of Mach number on airfoil loading for blade C
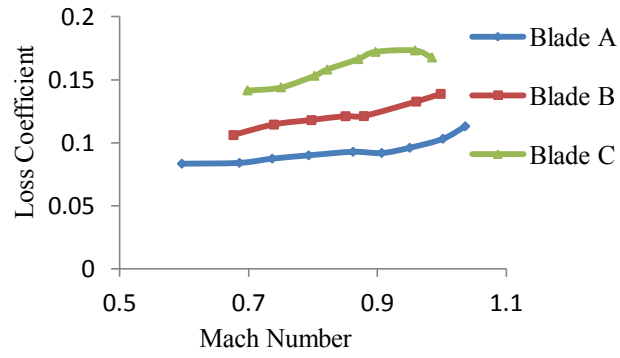
(a) Design incidence
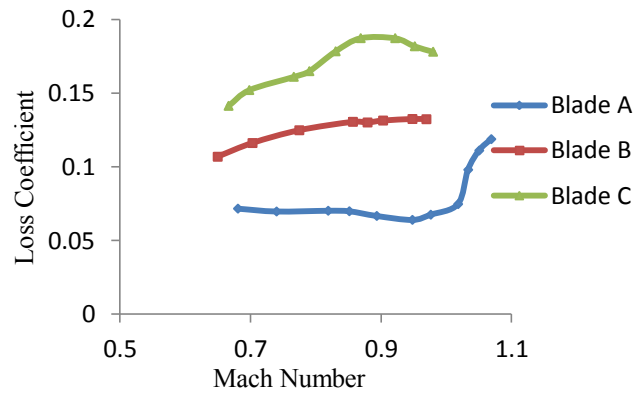
(b) -10 deg off design incidence
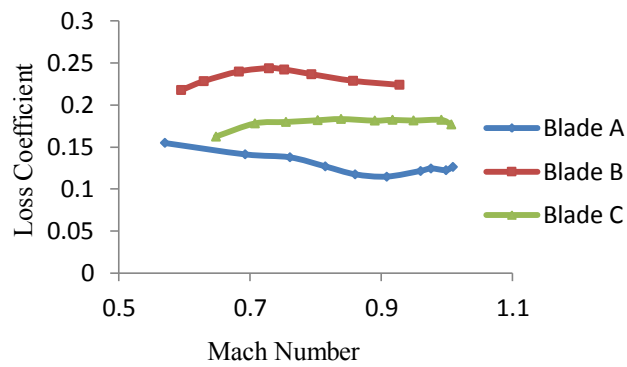
(c) +10 deg off design incidence

Figure 17: Loss coefficient measurements at 1.0 axial chord downstream

Loss coefficient measurements 1.0 axial chord downstream:

Profile Losses:

Profile losses are associated with boundary layer growth over the blade profile and include separation loss under adverse conditions of extreme turning angles or high inlet Mach numbers. The pitchwise line averaged loss coefficients are measured 1.0 axial chord downstream from the trailing edge of the cascade using a traversing Kiel probe at midspan at the different incidence angles and varying exit Mach numbers and are represented in Figure 17. From the analysis of the airfoil loading we concluded that airfoil B showed a significant amount of aft diffusion as compared to airfoil A, which therefore results in higher profile losses for airfoil B. The term aft diffusion refers to the static pressure rise or the drop in Mach number from the peak location to the trailing edge on the suction side. When the aft diffusion becomes excessive, flow separation on the suction surface occurs, which results in high losses. Aft diffusion decreases as the loading moves forward, as in the case of Blade A. Airfoil C is also more aft loaded than airfoil A. Another factor that ensures lower losses for airfoil A is the fact that the oblique shocks originating at the trailing edge of the adjacent airfoil and impinging on the rear of the suction surface on airfoil A at higher Mach numbers are considerably less than those on the other two airfoils. This will favorably affect the losses for airfoil A. For the design incidence angle cases as well as for the -10 degree incidence angle cases, airfoil C sees the strongest shock and corresponding drop in Mach number. This in turn increases the direct total pressure losses through the shock wave. The aft diffusion for these two incidence angle cases seems to be more prominent for airfoil C which also directly influences the total pressure downstream of the cascade. These factors make the losses for airfoil C more prominent at zero incidence and negative incidence angles. For the +10 degree cases, the losses are higher than the other two incidence angle cases for all three airfoils. The rise in losses is due to the increased loss production in the suction side boundary layer on the

frontward part of the airfoil as can be seen from the loading. Also airfoil B sees a considerable amount of flow deceleration on the frontward suction side for the +10° incidence angle case, which leads to larger suction side boundary layer, which in turn increases losses. This explains higher losses for airfoil B than the other two airfoils at higher incidence angles.

Secondary Losses:

Secondary losses arise from secondary flows which are always present when a wall boundary layer is turned through an angle by an adjacent curved surface. Profile losses are the losses measure at midspan, where we assume that the secondary flow does not play a major role in loss generation. So the losses obtained at other span locations, away from midspan, after subtracting the profile losses, would be the secondary losses. Figure 18 shows the pitchwise line averaged losses measured at various spanwise locations measured 1.0 axial chord downstream from the trailing edge of the cascade at the design exit Mach number and design incidence angle, measured at various spanwise locations using a traversing Kiel probe. The suction side horseshoe vortex meets the passage vortex and then wraps itself around the passage vortex instead of adhering to the suction surface, lifts off the end wall and continues downstream along the suction side. This vortex is identified in Figure 18 by a region of high losses as compared to midspan losses. This region varies for the three airfoils from a normalized span around 0.70 to 0.85 in the experimental results. Airfoil A shows comparatively lower losses along the entire span. The losses due to secondary flows appear closer to the endwall for airfoil C as compared to the other airfoils. The overall area averaged losses obtained from experiments by taking the average of the pitchwise and spanwise losses at design condition are plotted in Figure 19. Airfoil A shows the lowest overall loss, which is

consistent with all of the previous analysis, while airfoils B and C exhibit higher (by almost 29%) and similar overall loss levels.
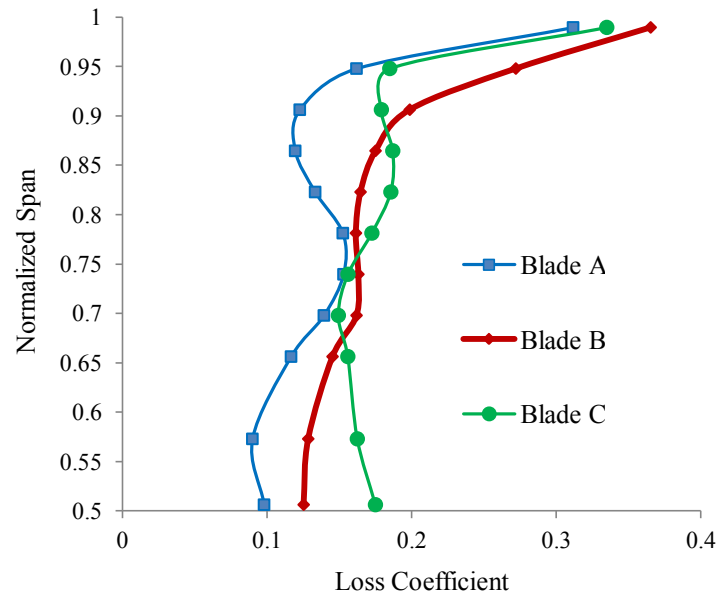
Figure 18: Spanwise Loss Variation at design condition
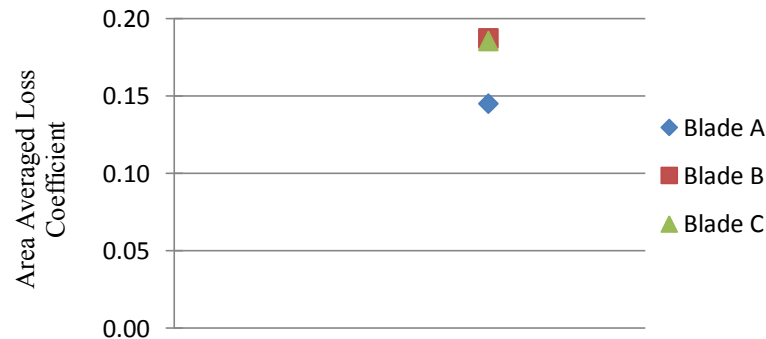
Figure 19: Area averaged losses at design condition

Conclusions

One of the goals of this study is to use the data to confirm/refine loss predictions for the effect of various Mach numbers and gas turning. Loss systems provide predictions for pressure loss as the various geometric and aerodynamic parameters are varied. Airfoils are then designed to produce the target velocity triangles. In this study experimental

measurements and numerical predictions for a high turning, high loading turbine airfoil have been carried out at design and off design conditions in a linear transonic cascade wind tunnel.

The effect of variation of exit Mach number on airfoil loading is felt mainly toward the trailing edge region of airfoil and the loading at leading edge remains almost same for different Mach numbers.

By studying the airfoil loading at different conditions and the corresponding loss levels, we can conclude that the losses are prominently governed by three physical phenomena:

- Deceleration of flow on the suction side of the airfoil plays a major role in higher loss production.
- With higher aft diffusion, flow separation on the rear part of the suction surface of the airfoil occurs, which leads to higher losses.
- Shocks originating from the trailing edge of the adjacent airfoil and impinging on the rear of the airfoil suction surface affect losses adversely.

6.0 EFFECT OF AIRFOIL TURNING ANGLE ON AIRFOIL AERODYNAMIC PERFORMANCE

Motivation

Performance of three airfoils with varying turning angles, operating at transonic flow conditions is investigated in this study. Airfoil curvature and true chord are varied to change the variation in loading vs. chord. Airfoils A, D and E are designed to different velocity triangles. Velocity triangle requirements (inlet/exit Mach number and gas angles) come from 1D and 2D models that include calibrated loss systems. These models are used to estimate the basic turbine flow path geometry (diameter, axial chord, number of stages, stage work splits/reactions, etc.) that will most efficiently produce the required turbine work for the specified boundary conditions (inlet total pressure, temperature and flow, exit pressure). Loss systems provide predictions for pressure loss as the various geometric and aerodynamic parameters are varied. Airfoils are then designed to produce the target velocity triangles. One of the goals of this test is to use the data to confirm/refine loss predictions for the effect of various Mach numbers and gas turning. The cascade exit Mach numbers were varied within a range from 0.6 to 1.1.

Airfoil Geometries

Figure 20 shows the cross sectional geometries of the three airfoils being studied, oriented so that the axial chord is on the x-axis. All three airfoils are high turning transonic airfoils with varying flow angles and the same axial chord length as shown in Table 2. Therefore the Zweifel coefficient would be different for all three airfoils. Investigations of the midspan surface loading profile, profile losses, spanwise losses and area averaged total losses

were conducted to determine the performance characteristics for the airfoil designs. The inlet angle for airfoil A is 9˚ more than that for airfoil D and 8˚ less than that for airfoil E with all blades having almost the same exit angles. Therefore airfoil E has the highest turning angle (138˚) and airfoil D has the lowest (120˚). The stagger angle and the unguided turning angle are detrimental parameters that affect the loading distribution. It can be seen from Table 2 that the unguided turning angle for blade D is the highest which will result in it showing high aft diffusion due to high flow separation on the suction side close to the trailing edge.
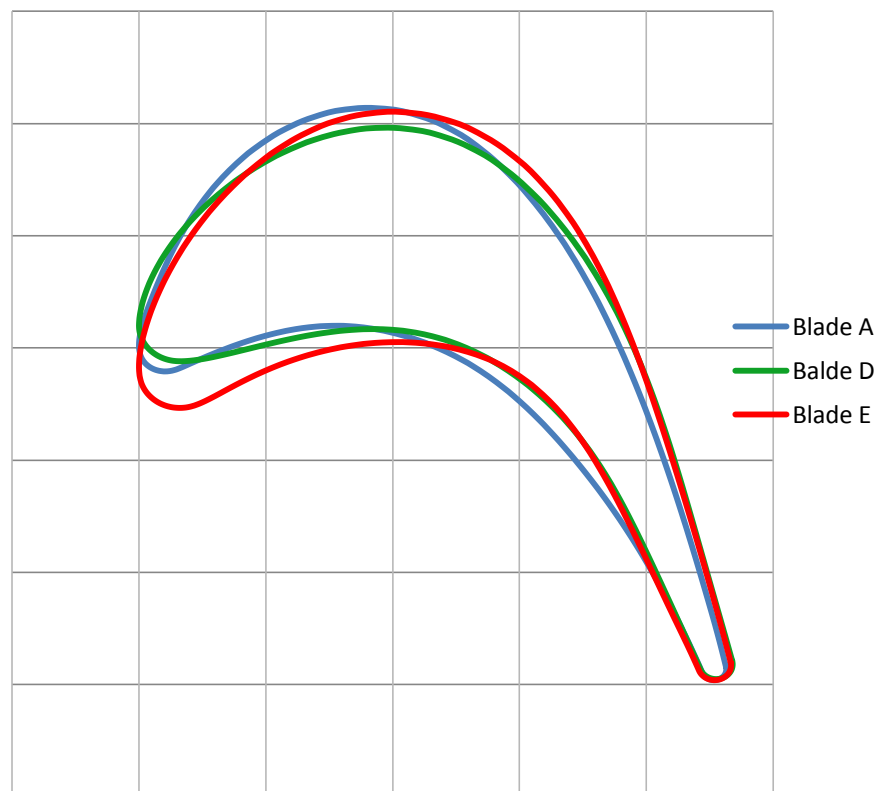
Figure 20: Cross sectional geometries of the three airfoils

Cascade Parameters	Airfoil A	Airfoil D	Airfoil E
Axial chord length	93mm	93mm	93mm
Blade span(trailing edge)	152mm	152mm	152mm
Blade pitch	91mm	91mm	91mm
Inlet metal angle β_1	55°	46°	63°
Exit metal angle β_2	72°	-74°	-75°
Stagger angle	32.27	32.96	29.12
Unguided turning angle	15.7	19.14	15.48

Table 2: Design parameters for Airfoils A, D and E

Static pressure measurements

The periodicity of flow through the passages was satisfactory and was established for all the cases that were studied using midspan pressure taps on the center airfoil and its adjacent airfoils. The local Mach number distribution on the three airfoil surfaces were measured for varying exit Mach numbers at the design incidence angle.

Figure 21 shows the loading on the airfoils at design conditions. Since airfoil D has a smaller inlet angle it is comparatively lightly loaded in the frontward part of the airfoil. It is highly aft loaded and a large amount of aft diffusion is evident, which adversely affects losses. The high aft diffusion is due to the high unguided turning angle on airfoil D. Airfoil E is more front loaded that the other two airfoils. Deceleration of flow is observed on the suction surface from normalized axial chord 0.2 to 0.5. This represents flow separation due to

high turning of the airfoil which leads to a thicker boundary layer on the suction surface and increased profile losses.

The effect of Mach number variation on the airfoil loading for the three airfoils at design incidence is shown in Figure 22. No significant change is observed on the pressure side loading, up to near trailing edge, with varying exit Mach numbers. For all higher exit Mach number cases (> 0.9) the loading on the suction side remains relatively the same from leading edge to 0.7 normalized axial coordinate as the exit Mach number increases. This can be attributed to the choking of the flow in the blade passage. At higher exit Mach numbers a normal shock impinges on the suction side near the trailing edge. This is similar to the analysis from the previous section.
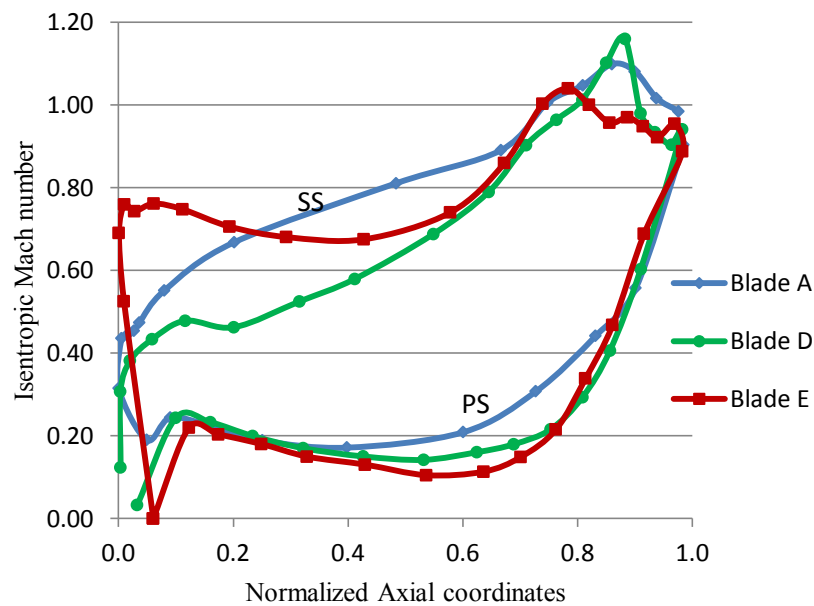
Figure 21: Loading distribution on the three airfoils
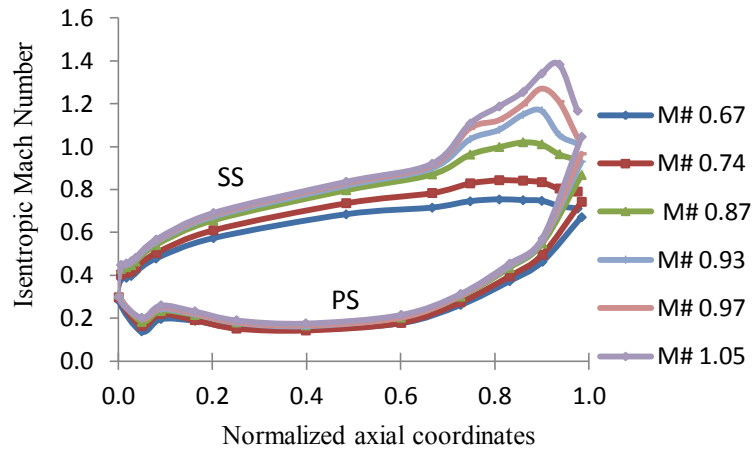
(a) Airfoil A
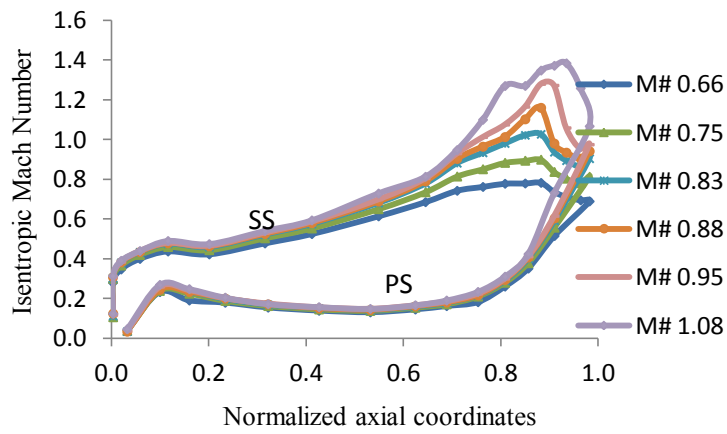
(b) Airfoil D
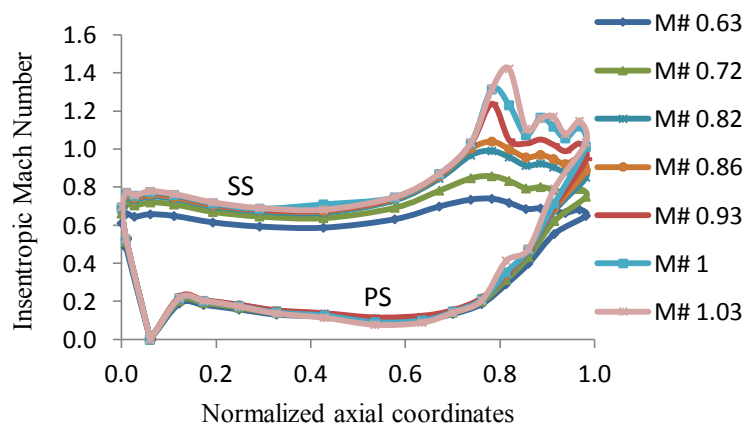
(c) Airfoil E

Figure 22: Effects of Mach number on airfoil loading at design incidence

Loss coefficient measurements 1.0 axial chord downstream:

Profile Losses:

Mid-span pitchwise line average loss is considered as profile loss. Profile losses are associated with boundary layer growth over the blade profile and include separation loss under adverse conditions of extreme turning. The pitchwise line averaged loss coefficients are measured 1.0 axial chord downstream from the trailing edge of the cascade using a traversing Kiel probe at midspan at the different incidence angles and varying exit Mach numbers and are represented in Figure 23. From the analysis of the airfoil loading we concluded that airfoil D showed a significant amount of aft diffusion as compared to the other two airfoils, which therefore results in higher profile losses for airfoil D. When the aft diffusion becomes excessive, flow separation on the suction surface occurs, which results in high losses. At lower Mach numbers the amount of aft diffusion for airfoil D reduces (Figure 22) and this in turn reduces the amount of losses generated as can be seen in Figure 23. Aft diffusion decreases as the loading moves forward, as in the case of the other two airfoils. Airfoil E is more front loaded than the other two airfoils. Deceleration of flow is observed on the suction surface from normalized axial chord 0.2 to 0.5. This represents flow separation due to high turning of the airfoil which leads to a thicker boundary layer on the suction surface and increased profile losses. These factors make the losses for airfoil D and E more prominent than for airfoil A.
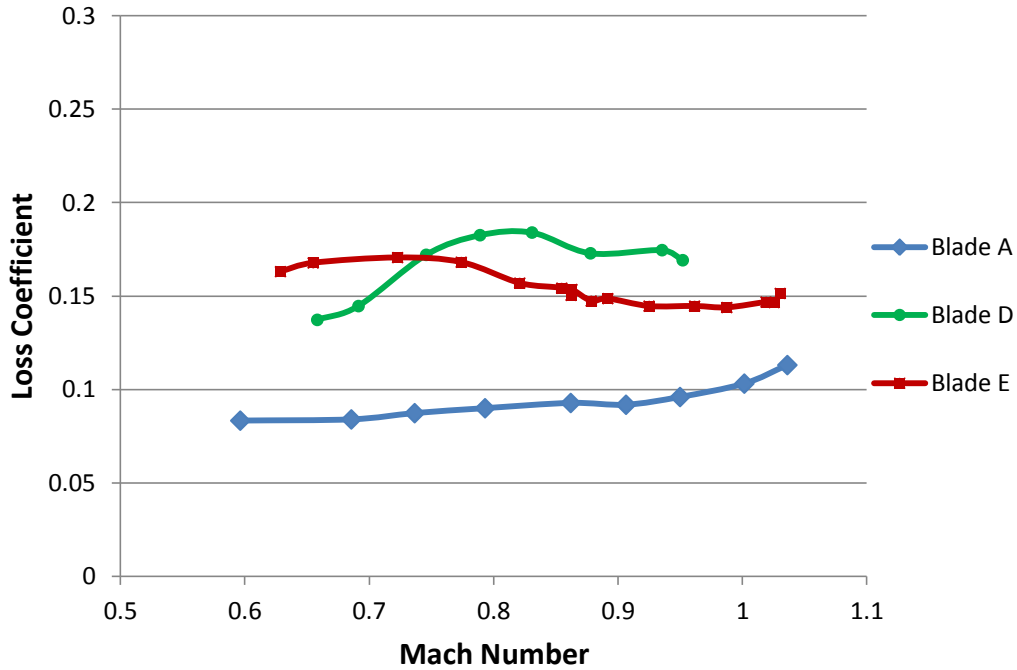
Figure 23: Loss coefficient measurements at 1.0 Cax downstream at design incidence

Secondary Losses:

The mechanism of secondary flow generation has been discussed in detail in the previous section. Figure 24 shows the pitchwise line averaged losses measured at various spanwise locations measured 1.0 axial chord downstream from the trailing edge of the cascade at the design exit Mach number and design incidence angle, measured at various spanwise locations using a traversing Kiel probe.

Although the profile losses for airfoils D and E are relatively of the same level, it can be seen from Figure 24 that the secondary losses are much higher for airfoil E. Secondary losses are usually higher when there is a large incidence angle. Secondary losses arise from secondary flows which are always present when a wall boundary layer is turned through an angle by an adjacent curved surface. Since the turning angle is highest for airfoil E, it is not surprising that it sees the highest secondary losses as compared to the other two airfoils.

The overall area averaged losses obtained from experiments by taking the average of the pitchwise and spanwise losses at design condition are plotted in Figure 25. Airfoil A shows the lowest overall losses, which is consistent with all of the previous analysis. Even though the secondary losses for airfoil D are relatively low, the overall area averaged loss for airfoil D (Figure 25) is still higher than that for airfoil A because it has high profile losses. Airfoil E with high secondary losses as well as high profile losses shows the highest overall area averaged loss at design conditions.
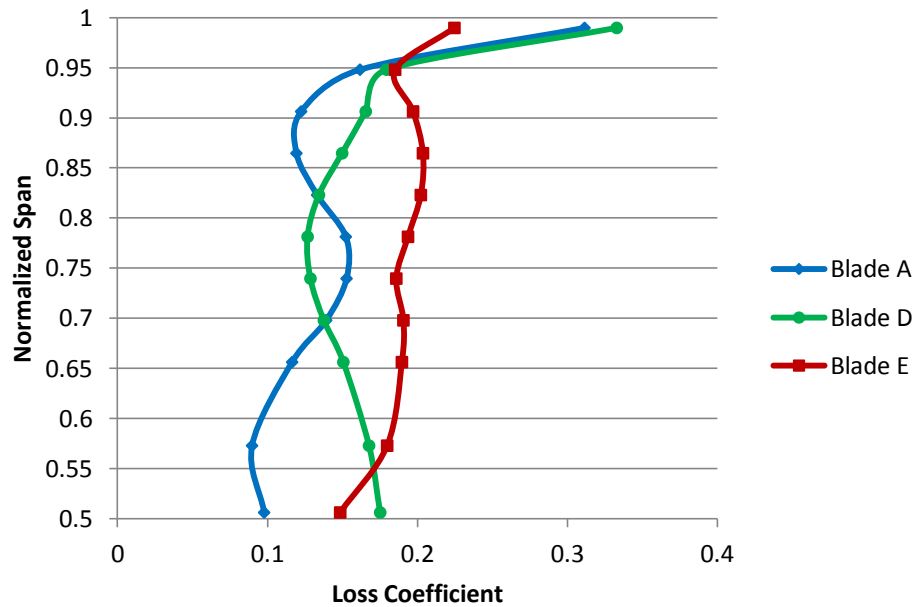
Figure 24: Spanwise Loss Variation at design condition
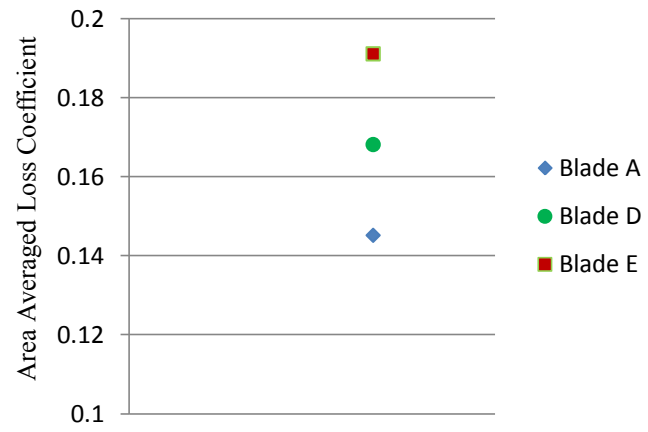
Figure 25: Area averaged losses at design condition

7.0 EFFECT OF ENDWALL CONTOURING ON TURBINE PERFORMANCE

Motivation

Endwall contouring has been widely studied during the past two decades for secondary loss reduction in turbine passages. Onset of horseshoe vortex and development of secondary flow in turbine passages has been studied by many researchers. Most of these studies were done at low exit Mach numbers and for moderate turning airfoils. There has been no published experimental study done on a high turning transonic blade at high exit Mach numbers. Endwall heat transfer could also be reduced by endwall contouring, with the reduction of the secondary flow strength.

The effect of endwall contouring on aerodynamic losses and endwall heat transfer will be studied in detail for a contoured endwall and compared with a baseline planar endwall. This study experimentally investigates the effect of end wall contouring on a transonic blade passage. The airfoil with the best performance with respect to total pressure losses evaluated from our studies from the previous sections was selected for this purpose (Airfoil A). This airfoil profile represents a high turning (~127˚), high exit Mach number (0.87) profile of the first stage of an HP turbine blade. A contoured endwall geometry which was optimized to reduce endwall heat transfer is studied here. Both aerodynamic as well as heat transfer performances of this contoured endwall are analyzed in detail.

Contoured endwall with the objective of improved heat transfer characteristics

The contoured endwall that was designed with the objective of enhanced heat transfer characteristics was studied in detail. The goal is to reduce heat transfer from the hot gas to the endwall. The contoured geometry shows similar trend for peak and trough locations to that found in literature. The end wall contouring was restricted up to the axial trailing edge. Five rapid prototype models using ABS material was manufactured with the contoured endwall being part of the airfoil, as shown in Figure 26. The airfoils are mounted on a rotatable window. The rest of the setup is similar to the baseline case which has been discussed previously.

5 passages with contoured endwall
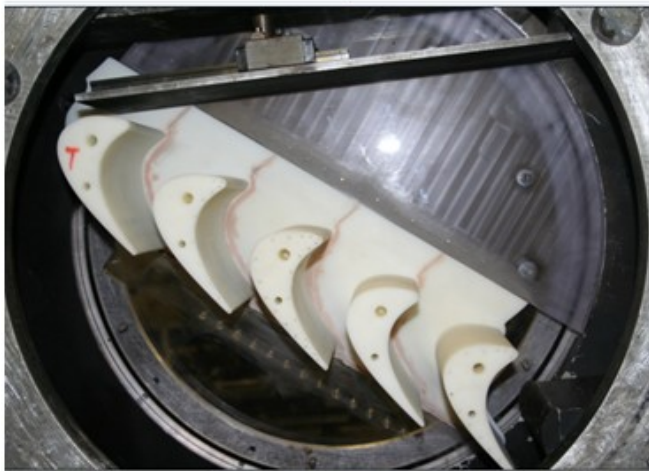
Rapid prototype model of airfoil A
with contoured endwall

Figure 26: Contoured endwall setup

Endwall contour geometry:
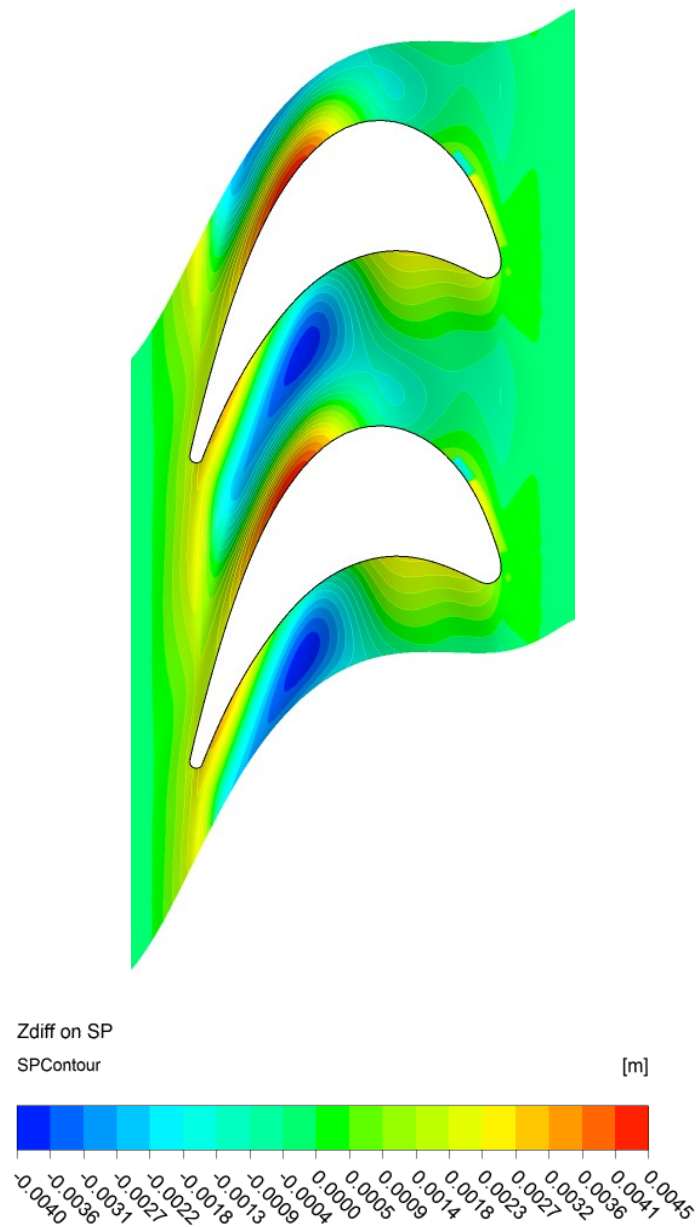
Figure 27: Endwall contour geometry

Figure 27 represents the endwall contour that was optimized to reduced heat transfer from the hot gas to the endwall. The contoured endwall design has a trough region which begins from the pressure side, around mid chord region and extends through the middle of the passage. A peak region is observed near the suction side as the trough region ends. The objective of these contours is to change the pressure gradient across the passage in an attempt

to alter the path of the unfavorable cross passage pitchwise movement of the passage vortex and cause it to move in a more favorable streamwise direction.

Loss coefficient:

The losses measured at midspan are considered to be the profile losses, where we assume that the secondary flow does not play a major role in loss generation. So the losses obtained at other span locations, away from midspan, are the sum of profile and secondary losses.

Figure 28 shows the pitchwise line averaged total losses measured 0.1 axial chord downstream from the trailing edge of the cascade at the design exit Mach number and design incidence angle, measured at various spanwise locations using a traversing 5 hole probe for the baseline and contoured endwall designs. Figure 29 represents the 2D loss contour for the same condition mentioned above. High loss regions are observed near the endwalls and the wake of the trailing edge of the airfoils. Secondary flows are generated near the endwall region because of the boundary layer velocity distribution near the endwall and also due to the flow stagnation at the leading edge of the airfoil. When the low velocity, near-endwall flow encounters the airfoil leading edge, it rolls up into two legs of the horseshoe vortex at a point called the saddle point. The leg that moves to the pressure side of the airfoil sees the large pressure gradient existing in the passage and moves across the passage in an unfavorable pitchwise direction and meets the suction side leg of the horseshoe vortex. The vortex then lifts off from the endwall and begins moving up (spanwise) near the suction side surface, as it continues downstream. This vortex is identified in Figure 28 by a region of high losses as compared to midspan losses at a normalized span around 0.85.

The objective of endwall contouring is to reduce the strength of the passage vortex and redirect it. The contours try to make the passage vortex move in a streamwise direction,

thereby reducing its strong pitchwise component. Delaying the pitchwise progression of the passage vortex will also delay the meeting of the passage vortex and the suction side horseshoe vortex. This will make the lift off occur further downstream, thereby delaying the spanwise movement of the vortex. As we go further downstream from the trailing edge plane, these vortices mix out. 1.0 axial chord downstream of the trailing edge this vortex has lifted further away from the endwall and can be seen in Figure 30 at a normalized span around 0.75. From the two 2D contours of loss coefficient plotted at 0.1 C_{ax} downstream and 1.0 C_{ax} downstream (Figure 31), it is evident that the flow has mixed out considerably at the location further downstream of the trailing edge.

Not much difference in total losses is seen between the baseline planar endwall and contoured endwall designs. From Figure 29, the strength of the passage vortex, around 1 inch from the endwall, as well as the losses close to the endwall, has reduced slightly for the contoured endwall case. However as we go further away from the endwall there is a small increase in the losses. This could be due to increased blockage in the passage due to the geometry of the contoured endwall. The contoured endwall is not successful in its objective of altering the pressure gradient across the passage. This could be because the contouring is not aggressive enough. The heights of the peaks and troughs cannot be large, because the slopes of the contours would be too steep. To resolve this problem, in the next phase of this project, the spacing between the airfoils is increased. This enables the contour design to be more aggressive in terms of peak and trough heights, due to the added area in the passage. This makes the contour slopes more gradual and smooth in its transition from peak to trough regions. In later chapters we see that endwall contouring is successful in its objective of altering the path of the passage vortex when the spacing between the airfoils is increased.
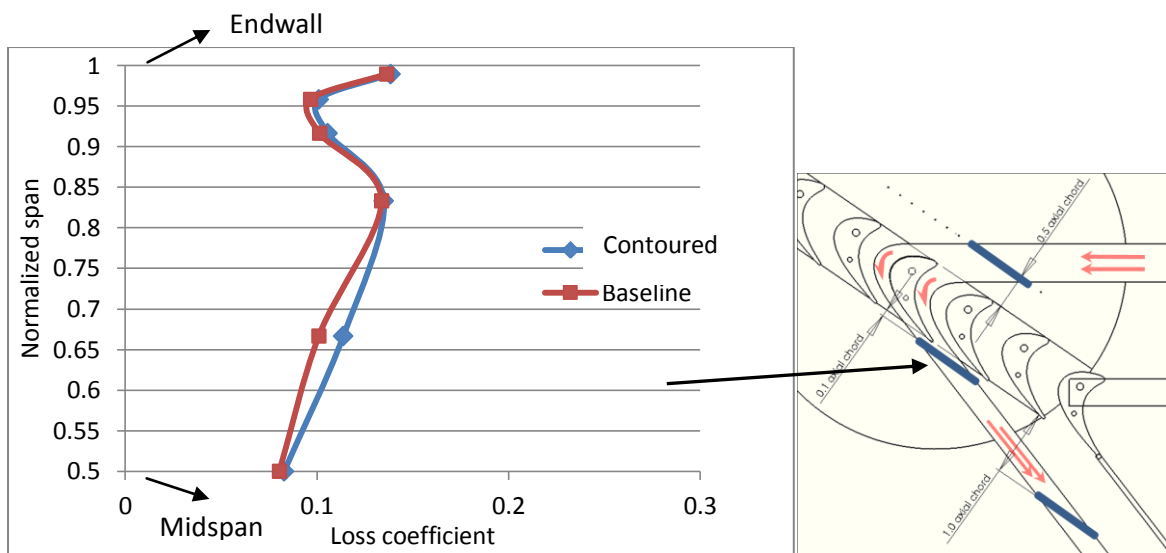
Figure 28: Spanwise Loss Variation at 0.1 C$_{ax}$
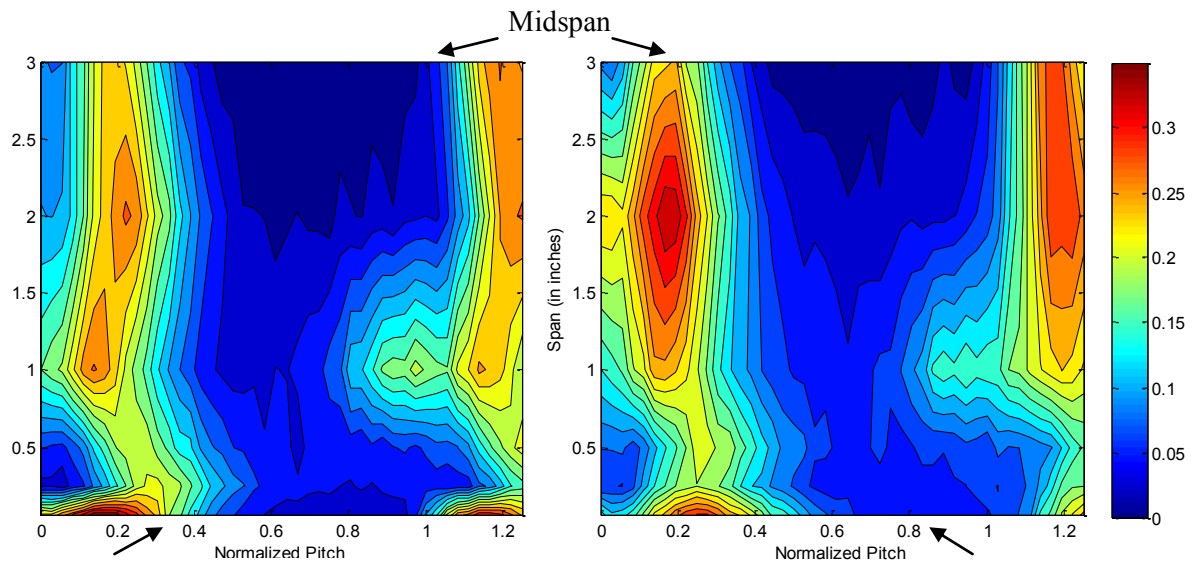
Figure 29: 2D loss contour of baseline vs. HT contoured endwall at 0.1 C$_{ax}$
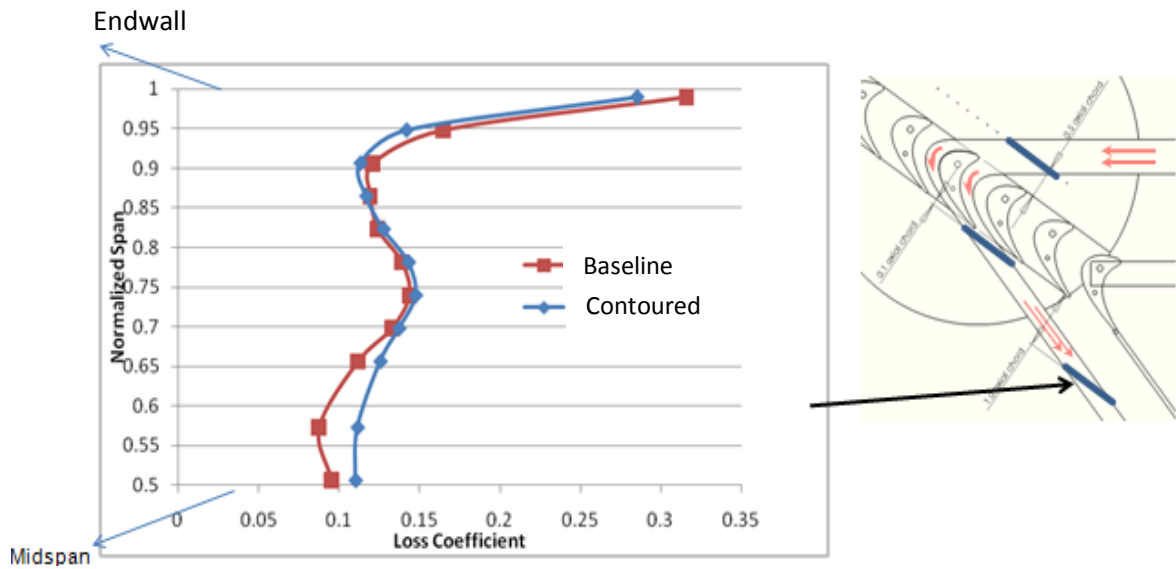
Figure 30: Spanwise Loss Variation at 1.0 Cax
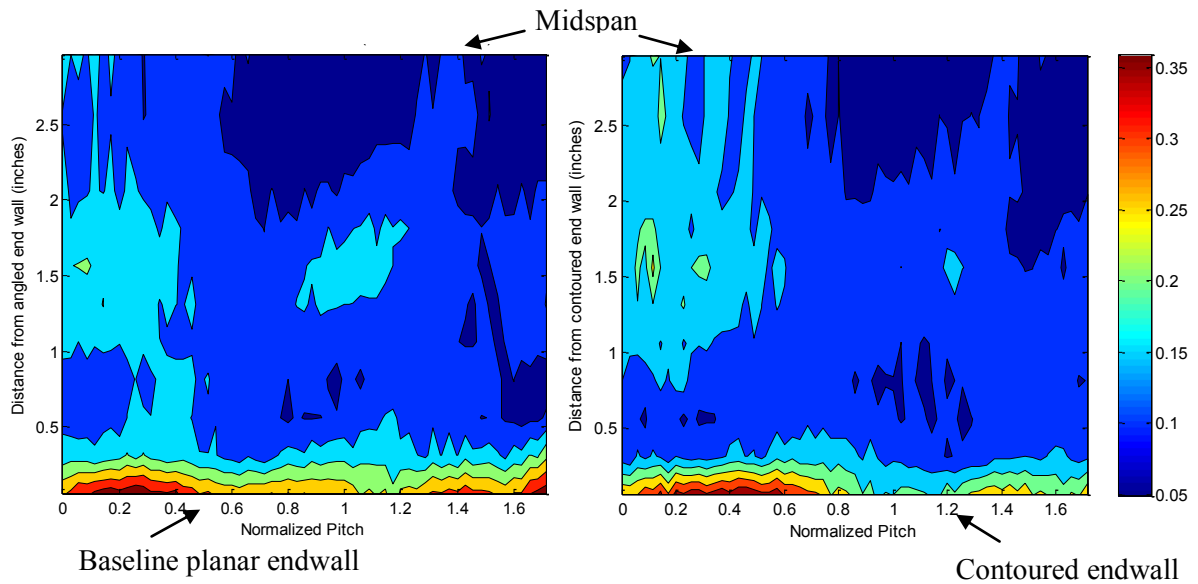
Figure 31: 2D loss contour of baseline vs. HT contoured endwall at 1.0 C_{ax}

52

Endwall heat transfer study:

The effect of endwall contouring on heat transfer characteristics is studied in this section. One of the objectives of endwall contouring is to reduce the heat transfer from the hot gas to the endwall. Figure 1 shows the heater and the heat exchanger section in the Virginia Tech transonic cascade. A butterfly valve just upstream of the test section is closed, thereby creating a closed loop in the heater section. The heater and a fan are turned on and the passive heat exchanger that consists of a mesh of copper wires is heated. When the upstream temperature is 200°F (93°C), the butterfly valve is opened and the valve to the heater section is closed and the tunnel is started. The heated air passes through the turbulence grids and into the test section. An IR camera is positioned to capture the temperature on the endwall through a special IR transparent window made of Zinc Selenide as shown in Figure 32.
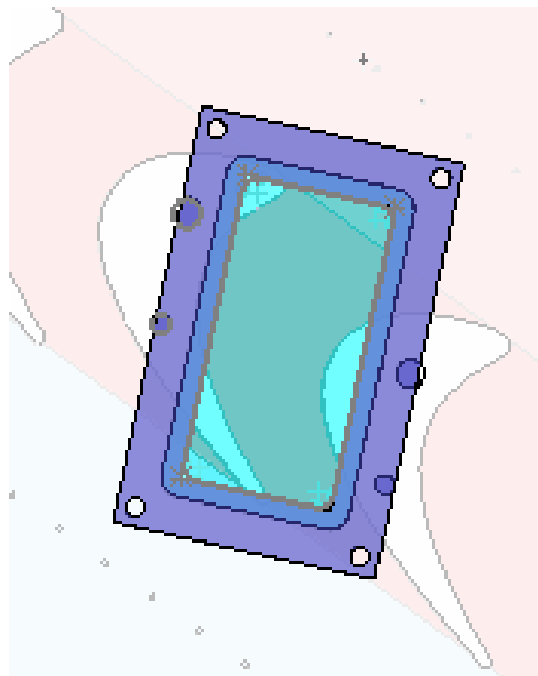
Figure 32: IR window showing the endwall view seen by the IR camera

To increase the IR transmissivity, an anti reflective coating was added onto the Zinc Selenide window. The entire test section was painted black, in order to reduce reflected radiation and increase the endwall emissivity. Surface thermocouples were positioned in situ for IR camera calibration purposes.

Heat transfer data reduction:
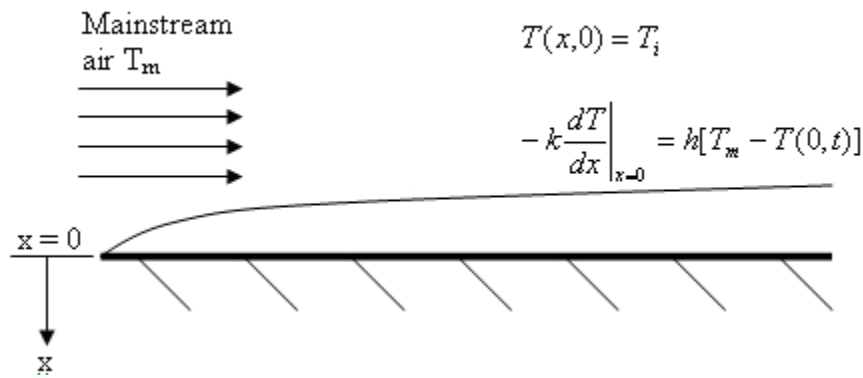
Figure 33: Heat transfer at the endwall

The endwall is initially at a uniform temperature T_i at time $t = 0$.

At time $t > 0$, hot stream of air at temperature T_m is sent into the test section.

Balancing the thermal energy on the endwall surface and applying the convective boundary condition we get.

$$\frac{\partial^2 T}{\partial^2 x} = \frac{1}{\propto}\frac{\partial T}{\partial t} \qquad [13]$$

$$T = T_i \text{ at t=0} \qquad [14]$$

$$-k\frac{\partial T}{\partial x} = h(T_w - T_m) \text{ at } x = 0 \text{ and } t \geq 0 \qquad [15]$$

$$T = T_i \text{ at } x = \infty \text{ and } t \geq 0 \qquad [16]$$

Where,

T_w = Endwall surface temperature

T_m = Mainstream air temperature

T_i = Initial surface temperature of the endwall

$\propto$ = Thermal diffusivity

k = Thermal conductivity

t = time for which data is reduced

h = heat transfer coefficient

On solving the above equation, we get the transient response of the endwall surface due to convective heat load applied by the hot mainstream air.

$$\frac{T_w - T_i}{T_m - T_i} = 1 - exp\left(\frac{h^2 \propto t}{k^2}\right) erfc\left(\frac{h\sqrt{(\propto t)}}{k}\right)$$
[17]

For the above solution to be valid, the endwall is assumed to be semi infinitely thick. Therefore the thermal pulse generated at one boundary of the endwall ($x = 0$) does not reach the other end. The thermal diffusivity of the material governs how fast the thermal pulse travels within the body. The depth to which the pulse travels is given by:

$$Penetration\ depth\ =\ \sqrt{(\propto t)}$$
[18]

The endwall is made of ABS(Acrylonitrile butadiene styrene), which has a very low value of thermal diffusivity and only the first 5 seconds of data are used to calculate the value of h. The penetration depth is about 0.5 mm, which is much smaller than the thickness of the endwall and therefore the semi-infinite assumption is valid.

The only unknown value in equation 17 is h. T_w and T_m are captured at each time interval (t) by the IR camera and a thermocouple respectively. T_i is the first image captured on the endwall by the IR camera at time $t = 0$. Figure 34 shows the temperature variance of the endwall when the tunnel runs. The images are captured by the IR camera at a rate of 10 images per second and the data is reduced between $t = 0 \ secs \ and \ t = 5 \ secs$.
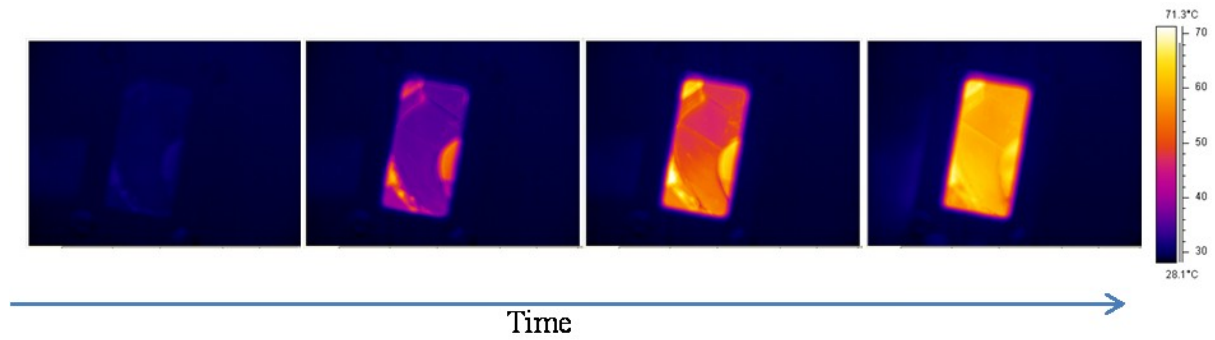
Figure 34: Raw IR images during run time

Heat transfer results:

The heat transfer experiments were conducted at the design Mach number (0.87) and design incidence angle (55°) for the cascade with the baseline endwall and the cascade with contoured endwall. The heat transfer coefficient was calculated and the results are shown in Figure 35. Slight reduction in the heat transfer coefficient values were seen in the middle of the passage, but high heat transfer regions are observed as the flow reaches the pressure side aft region nearing the trailing edge. Negligible change was observed when the overall area averaged heat transfer coefficients were compared between the two cases. This goes hand in hand with the analysis from the aerodynamic testing of this contoured endwall. The key point is that the contours are not successful in significantly altering the cross passage flow of the passage vortex.
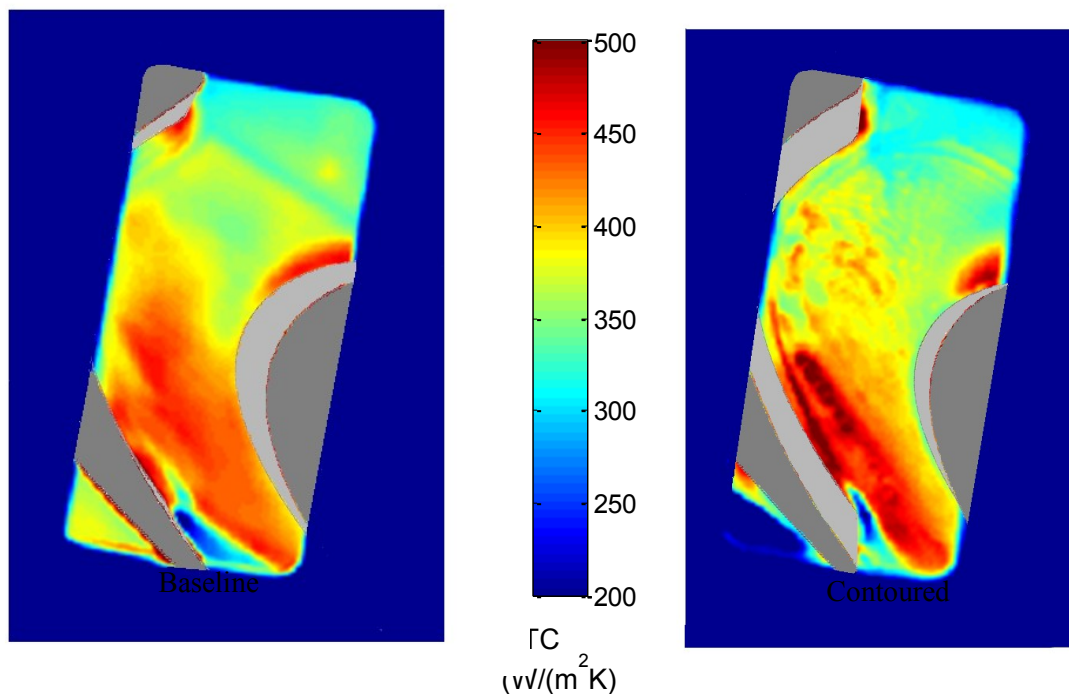
Figure 35: Heat transfer comparison between baseline and contoured endwall

However, in the next phase of the project, where the spacing between the airfoils is increased, we see that endwall contouring is indeed successful in changing the flow path of the secondary vortices.

Conclusions:

Similar to the conclusion derived from the aerodynamic study on the effect of endwall contouring, no benefits were observed in the heat transfer study as well. This is not surprising, since both the aerodynamic as well as heat transfer characteristics are closely associated with each other. Reduction in aerodynamic losses is achieved by reducing the strength of the passage vortex and redirecting it in a more streamwise direction. Heat transfer coefficient on the endwall is reduced by reducing the pitchwise direction of the passage vortex. Since the contouring in this study did not succeed in significantly altering the passage vortex flow path, no improvement was observed in both the heat transfer as well as aerodynamic studies. The objective in both the cases is to reduce the cross passage pitchwise flow of the passage vortex. From both the aerodynamic and heat transfer study of endwall contouring, negligible change in secondary flow characteristics were observed.

The contribution of the secondary losses in this cascade is small as compared to the profile losses. If the spacing between the two airfoils were increased, there would be more area in the passage for the contouring to have a bigger impact in altering the passage vortex. Also, the airfoil would be more loaded, thereby increasing the difference between the pressure side and suction side pressure distribution on the airfoil. This will create a larger cross passage pressure gradient, leading to stronger secondary flow generation and larger contribution of secondary losses to the total pressure losses. Another advantage of increasing the area of the passage, obtained by increasing the spacing, is that the contours can be more aggressively designed without creating steep gradients in the trough and peak regions.

To further investigate the influence of endwall contouring in alerting secondary flow patterns, a study on a cascade with increased spacing between the airfoils was undertaken and is discussed in the subsequent chapters.

8.0 STUDY OF AERODYNAMIC LOSSES ON CASCADE WITH INCREASED AIRFOIL SPACING

Motivation

Detailed experimental results of the midspan total pressure losses, secondary flow field, and static pressure measurements on two linear, high-turning turbine cascades at transonic conditions are studied. The airfoils in the two cascades being studied are identical and their aerodynamic loading levels are varied by increasing the pitch of one cascade by 25% with respect to the other. The turbine cascades are referred to as B1-SP (pitch = 91 mm) and B1-IP (pitch = 113 mm). Cascade B1-IP, with its increased pitch, has a Zweifel coefficient increased by 25%. The airfoils have a turning angle of ~127°. Measurements are made at design and off-design conditions, at exit Mach numbers ranging from 0.71 to 0.95. The exit span of the airfoils are increased relative to the inlet span with the intention of obtaining a ratio of inlet Mach number to exit Mach number that is representative to that encountered in a real engine. This results in one end wall diverging from inlet to exit at a 13 degree angle, which simulates the required leading edge loading as seen in an engine. The objective of this study is to investigate the variation in airfoil loading distribution, on changing the pitch, and the effect it has on aerodynamic performance in terms of pressure losses. Detailed loss measurements, both in the pitchwise as well as spanwise directions are conducted at 0.1 Cax and 1.0 Cax locations downstream of the trailing edge.

Over the years, profile and secondary loss correlations have been developed and improved and they reflect recent trends in turbine design. Research on secondary flow has been prominent due to the effect it has on the turbine efficiency. Almost a third of the total

losses in turbines are due to end wall losses. The advantages of highly loaded airfoils are manifold. They result in a reduction in the number of airfoils required per stage. While increased loading offers advantages like low cost and weight, they also result in increased losses. The strength of the secondary flow is influenced by the upstream boundary layer thickness as well as the overall flow turning angle. The secondary flow results in stagnation pressure loss which accounts for a considerable portion of the total stagnation pressure loss occurring in a turbine passage.

Results and Discussions

Static Pressure Measurements

Airfoil static pressure at midspan for the center airfoil in the cascades was used to calculate the surface isentropic Mach number. The experimental uncertainty was established at ±0.1%. The periodicity of flow through the passages was satisfactory and was established for all the cases that were studied using midspan pressure taps on the center airfoil and its adjacent airfoils. The local Mach number distribution on the airfoil surfaces were measured for exit Mach numbers varying from 0.70 to 0.95. Figure 36 shows the comparison of midspan airfoil loading between experimental values and CFD analysis results at design Mach number for the airfoils. It can be seen that there is a reasonably good agreement between experiments and CFD analysis. The CFD results shown were provided by Siemens Energy.
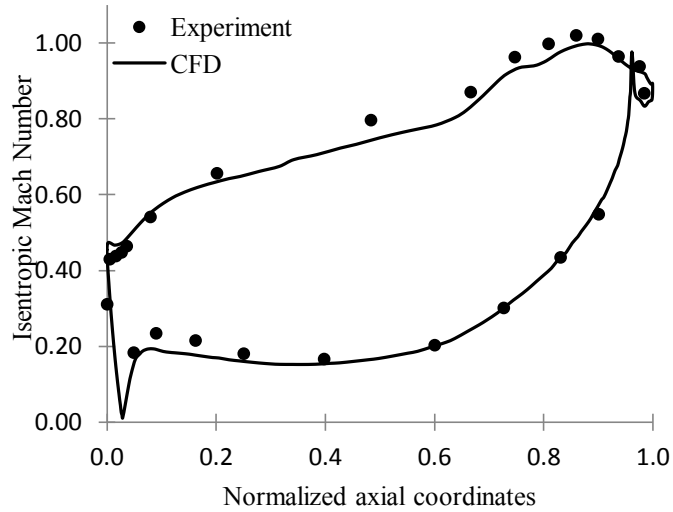
(a) Airfoil B1-SP at design incidence angle
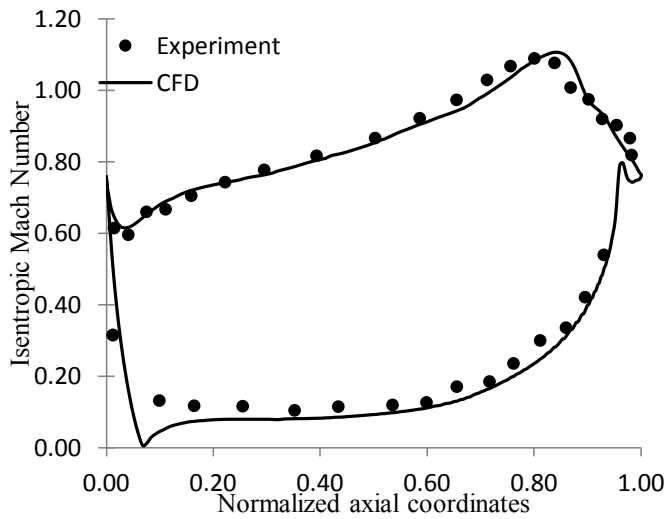
(b) Airfoil B1-IP at design incidence angle

Figure 36: Midspan airfoil loading from CFD analysis and experiments at design

Mach number

Figure 37 compares the loading on the airfoils at design conditions. As expected, B1-IP with the increased pitch, and therefore the increased Zweifel coefficient, is more loaded as compared to B1-SP. Both the airfoils exhibit mid to aft-loading characteristics. The highly loaded B1-IP airfoil is expected to produce higher losses. Increased loading essentially means

higher local velocities on the suction side surface, and higher static pressure on the pressure side surface for airfoil B1-IP. The larger local velocity on the suction side surface for airfoil B1-IP creates a region of local supersonic flow on the aft portion, making it prone to be adversely affected by shock waves. The loading on B1-IP also exhibits a higher level of aft diffusion or flow separation near the suction side trailing edge which will result in additional profile losses downstream. Since the difference in static pressure on the suction side relative to the pressure side is larger for B1-IP, the strength of the passage vortex will be higher. This will, in turn, result in higher secondary losses as well. Detailed analysis of this phenomenon is discussed in the next section.
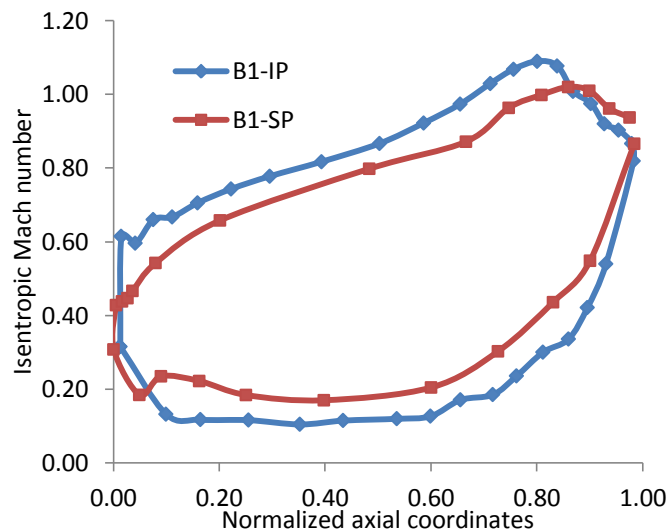
Figure 37: Loading distribution on the airfoils in the two cascades

The effect of Mach number variation on the airfoil loading for the two cascades is shown in Figure 38. For all cases there is no significant change on the pressure side loading, up to near trailing edge, with varying exit Mach numbers. For the two higher Mach number cases, in both the cascades, the loading on the suction side remains relatively the same from the leading edge to ~0.7 normalized axial coordinate. This can be attributed to the choking of the flow in the blade passage. As the exit Mach number increases, the level of aft diffusion

63

also increases for both the cascades. This will result in a thick or separated boundary layer near the suction side trailing edge which will contribute to the profile losses at higher Mach numbers.
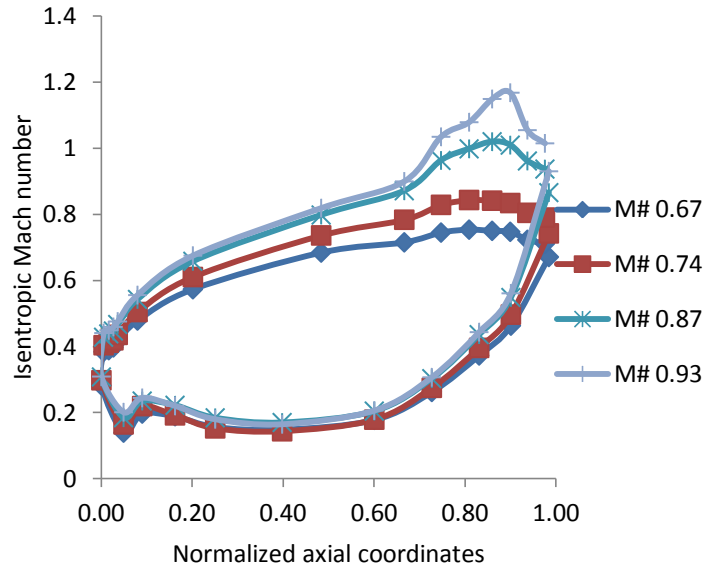
(a) B1-SP
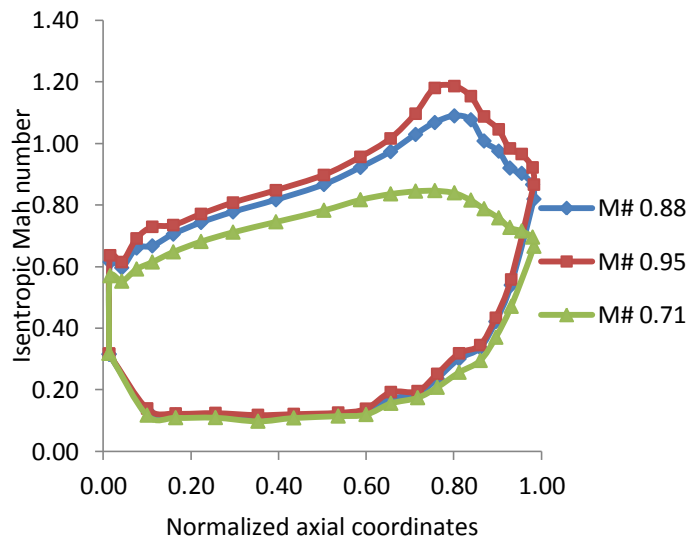
(b) B1-IP

Figure 38: Effects of Mach number on airfoil loading

Loss coefficient measurements:

Pitchwise as well as spanwise measurements were made to obtain a complete loss profile at 0.1 Cax as well as 1.0 Cax downstream from the trailing edge for the two cascades. Therefore a combination of profile losses as well as secondary losses is measured. Measurements are made at a total of 60 points during each run, across a distance of over one pitch length. Profile losses are associated with boundary layer growth over the blade profile and include separation loss under adverse conditions of extreme turning angles or high inlet Mach numbers. Shocks/boundary layer interactions also contribute to profile losses. Secondary losses arise from secondary flows which are always present when a wall boundary layer is turned through an angle by an adjacent curved surface.

Figure 39 shows a 2-D profile of the losses for the two cascades, 0.1 axial chord downstream from the trailing edge of the cascade at the design exit Mach at various spanwise locations. The spanwise measurements were taken during multiple runs with a traversing 5 hole probe, from midspan to inclined endwall. Regions of higher losses are clearly visible near the end walls and are a result of complex vortices arising due to the secondary flows. Pressure gradients in the passage caused by the boundary layer velocity distribution and flow stagnation on the blade result in the creation of secondary flows in the end wall region. These pressure variations force the flows toward the end wall and also lead to the development of two legs of the leading edge vortex. The turning angle of the flow between the airfoils results in the creation of a strong pressure gradient across the passage. This gradient influences the paths of the two legs of the horseshoe vortex and also the low velocity flow near the end wall. The pressure side leg of the horseshoe vortex which is forced to flow in a downward direction combines with the low velocity flow near the end wall and forms the passage vortex. The passage vortex drifts from the pressure side leading edge toward the suction side trailing edge

of the adjacent airfoil. As this vortex approaches the suction side, it lifts off the end wall, adheres along the suction side and moves downstream in the passage. At the same time the suction side horseshoe vortex remains close to the end wall until it meets the passage vortex. It then wraps itself around the passage vortex instead of adhering to the suction surface, lifts off the end wall and continues downstream along the suction side.

In the previous section, where we studied the airfoil loading, we observed that the highly loaded B1-IP airfoil exhibits a larger difference in airfoil static pressure between the suction side surface and the pressure side surface. This creates a larger pressure gradient across the passage for B1-IP cascade as compared to the B1-SP cascade. Due to this, the pressure side leg of the horseshoe vortex, in the B1-IP case, is forced to move sharply across the passage, to the suction side surface of the adjacent airfoil. This strong vortex meets the suction side leg of the horseshoe vortex and then lifts off the endwall earlier than in the case of B1-SP cascade where the pressure gradient is relatively less. This vortex is identified in Figure 39 and Figure 40 by a region of high losses at a normalized span of around 0.15 to 0.25 for the B1-SP cascade, while it is higher (normalized span ~ 0.25 to 0.50) and stronger for the B1-IP case. The line averaged losses in the pitchwise direction at each span location is calculated and plotted in Figure 40. An increase in the overall area averaged loss coefficient of ~35% is observed for the B1-IP cascade.

Figure 39: 2D profile of losses measured experimentally at 0.1 Cax downstream
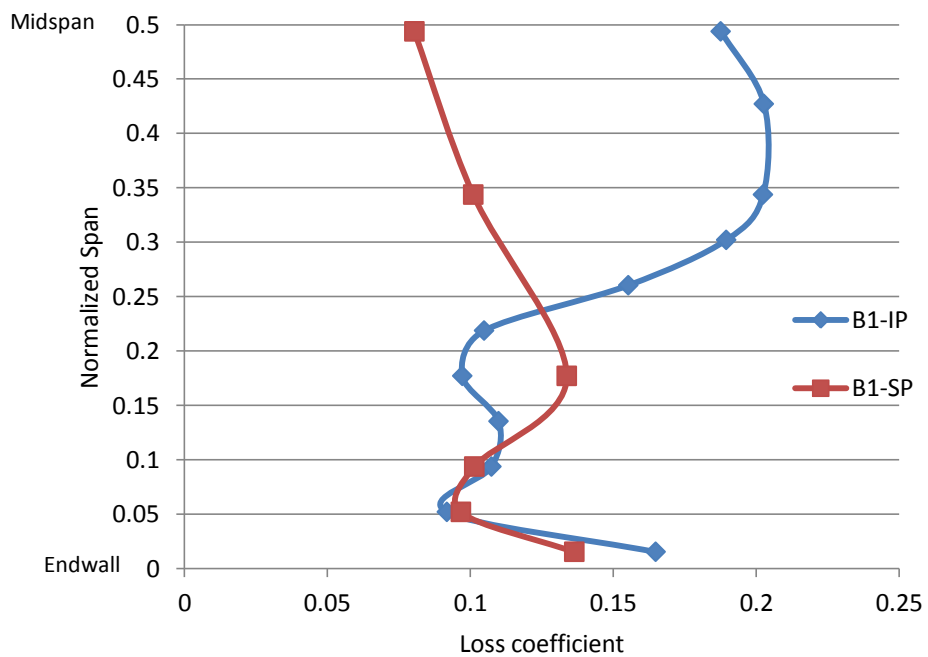
Figure 40: Spanwise variation of losses: 0.1 Cax downstream

As we go further downstream from the trailing edge plane, the vortices mix out and at 1.0 axial chord downstream, the losses are almost completely mixed out. With the objective of studying these mixed out losses, measurements are made at $1.0\ C_{ax}$ downstream from the trailing edge of the cascade at varying exit Mach numbers. For both the cascades, there is a

rise in losses observed as the exit Mach number increases, as can be seen in Figure 41. Both the airfoils exhibit an increase in the level of aft diffusion at higher exit Mach numbers. The term aft diffusion refers to the static pressure rise or the drop in Mach number from the peak location to the trailing edge. When the aft diffusion becomes excessive, flow separation on the suction surface occurs, which results in high losses. Increase in losses is seen at higher Mach numbers also due to the fact that the local velocities on the suction side, at higher Mach numbers, create a local supersonic flow, thus making it prone to shock waves.
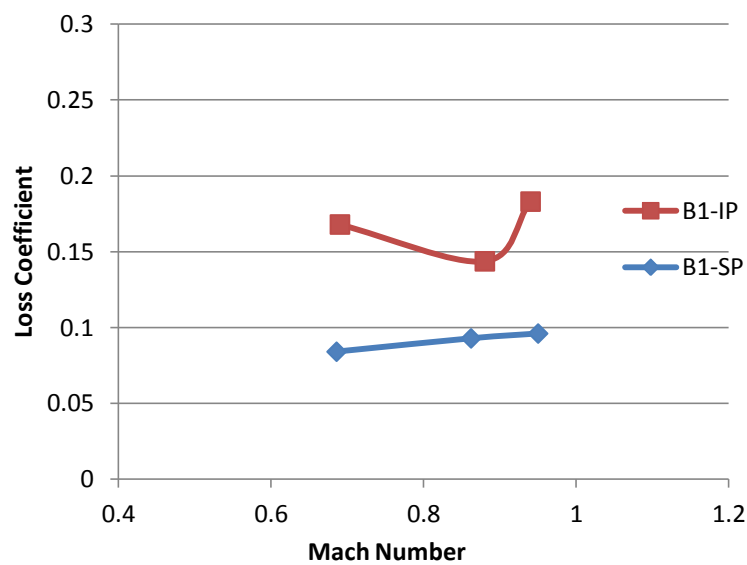
Figure 41: Loss vs. M#: 1.0 Cax downstream

The spanwise variation of losses was measured at 1.0 C_{ax} downstream for both the cascades at the design condition. Figure 42 shows a 2-D profile of the losses for the two cascades, at the design exit Mach at various spanwise locations, measured using a Kiel probe. Figure 43 represents the line averaged losses in the pitchwise direction, at each span location.

From the plots below, it is evident that the losses are more mixed out as compared to the losses measured at the $0.1C_{ax}$ location. The strength of the passage vortex, for both the cascades, has reduced due to mixing at the $1.0C_{ax}$ location. It is still higher and stronger for

the B1-IP case, consistent to what was observed at the $0.1 C_{ax}$ location. The mixed out losses are higher across the entire span for the B1-IP cascade and an increase in the overall area averaged losses of ~ 27% was seen.
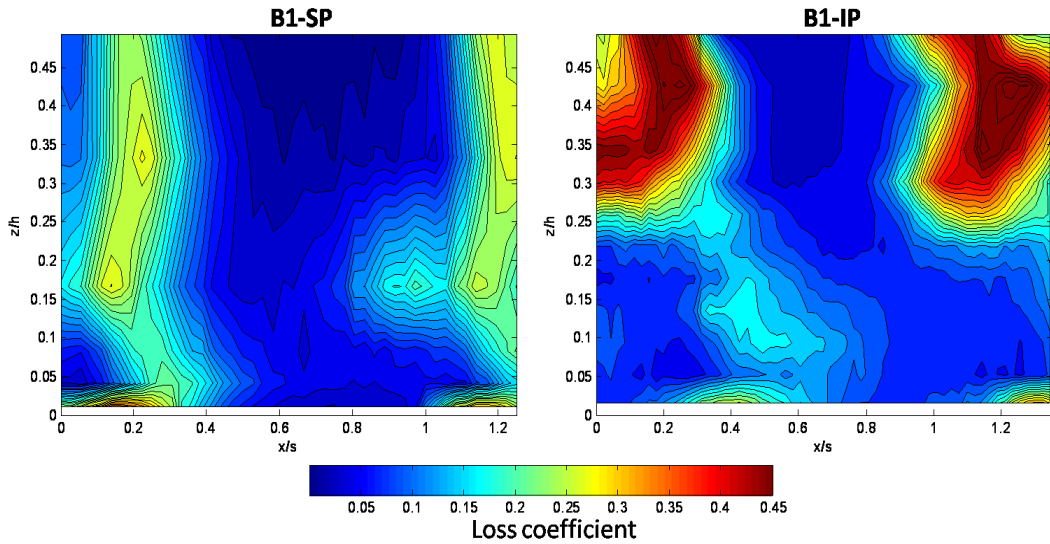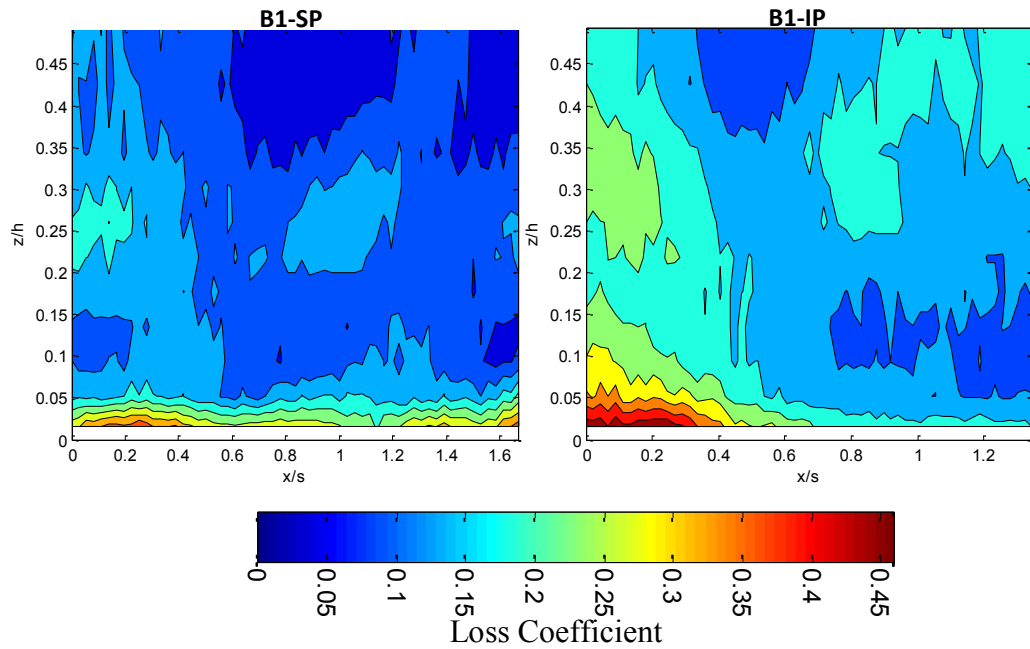

Figure 42: 2D profile of losses measured experimentally at 1.0 Cax downstream
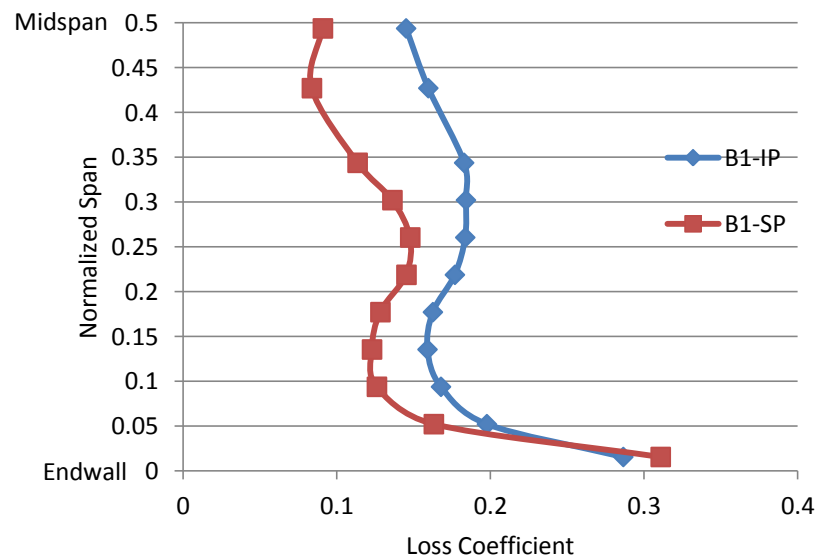
Figure 43: Spanwise variation of losses: 1.0 Cax downstream

Conclusions

In this study experimental measurements and numerical predictions for two high turning, high loading turbine airfoil cascades have been carried out at design and off design conditions in a quasi linear transonic cascade wind tunnel. The variation of airfoil loading and change in loss generation for the two cascades was studied in detail.

The increased loading on the cascade with the higher pitch, resulted in an increased pressure gradient across the passage, which caused stronger secondary vortices that contribute to high total pressure loss. The adverse pressure gradient across the passage, made the location where the passage vortex meets the suction surface shift closer towards the leading edge region. Higher lift-off of the vortex core was also seen in the case of the increased pitch cascade. The cascade with the increased pitch saw an increase in overall area averaged losses of 35% at 0.1 Cax downstream from the trailing edge of the cascade and 27% increase in mixed out losses measured at the 1.0 Cax downstream location. The variation of losses at midspan with Mach number was also studied. Flow separation on the suction side near the trailing edge and shocks originating from the trailing edge of the adjacent airfoil and impinging on the rear of the airfoil suction surface affect profile losses adversely.

Loss systems provide predictions for pressure loss as the various geometric and aerodynamic parameters are varied. The results from this study are used to provide data at transonic conditions that can be used to confirm/refine loss predictions for the effect of various Mach numbers and airfoil loading. The work presented up till here is part of a comprehensive study on loss generation by high turning turbine airfoils and leads up to a study on the effect of endwall contouring on secondary losses.

9.0 EFFECT OF ENDWALL CONTOURING ON AIRFOIL AERODYNAMIC PERFORMANCE (CASCADE WITH INCREASED PITCH)

Motivation

This section presents a detailed experimental and numerical study on the effect of endwall contouring in a quasi 2D cascade, operating at transonic conditions. Aerodynamic performance of two contoured endwalls are studied and compared with a baseline (planar) endwall. The first contoured endwall was generated with the goal of reducing secondary losses (Aero-optimized contoured endwall) and the second endwall was generated with the objective of reduced heat transfer from the hot gas to the endwall (HT-optimized contoured endwall). Midspan total pressure loss, secondary flow field, airfoil and endwall static pressure measurements were measured. The cascade exit Mach numbers range from 0.71 to 0.95 and the turning angle of the airfoil is ~ 127°. The inlet span of the airfoils was reduced with respect to the outlet span with the intention of obtaining a realistic inlet/exit Mach number that is observed in a real engine. The results reveal that the Aero-Optimized contoured endwall provides a significant reduction in overall total pressure losses. An experimental study on the effect of end wall contouring on such a high turning blade at high exit Mach numbers is not available in open literature.

Instrumentation and Data Acquisition

Inlet Flow Measurements

Aerodynamic measurements were made on a plane $0.45C_{ax}$ upstream of the airfoil leading edge. Pitchwise traverse measurements were carried out using a pitot probe to ensure

uniformity of incoming flow and inlet velocity profiles. Pitchwise traverse measurements were made at different span locations in multiple runs to estimate the boundary layer thickness. A turbulence grid is placed $5.5C_{ax}$ upstream of the cascade as shown in Figure 2 to obtain the desired level of turbulence. A single wire hot-wire probe was employed to measure the inlet free stream turbulence intensity based on an isotropic turbulence assumption.

Static Pressure Measurements

Static pressure taps are positioned on the cascade endwalls on a plane $0.5C_{ax}$ upstream of the cascade that serves to confirm the incoming flow periodicity. They are also positioned $0.5C_{ax}$ downstream of the cascade to estimate the exit Mach numbers. Midspan loading of the center airfoil was measured by instrumenting the center airfoil with pressure taps. The adjacent airfoils were also instrumented to verify flow periodicity between the passages. Endwall static pressure measurements were measured by positioning 16 pressure taps, equally spaced in the pitchwise and spanwise direction on the endwall, with the objective of capturing the endwall pressure gradient variation across the passage with and without endwall contouring.

Loss coefficient measurements

Pitchwise traverse measurements were made at different spanwise locations at $0.1\ C_{ax}$ and $1.0\ C_{ax}$ downstream of the cascade trailing edge. The spanwise area averaged loss coefficient was measured at 11 different spanwise locations during multiple runs, from midspan to the inclined endwall for the design exit Mach number for both the cascades.

Midspan loss measurements were made at off design Mach numbers as well. A 5 hole probe was used to make measurements at the $0.1C_{ax}$ location. Mixed out losses were measured at $1.0C_{ax}$ location using a Kiel probe.

Endwall Contour Geometries

Aero-optimized contoured endwall

HT-optimized contoured endwall
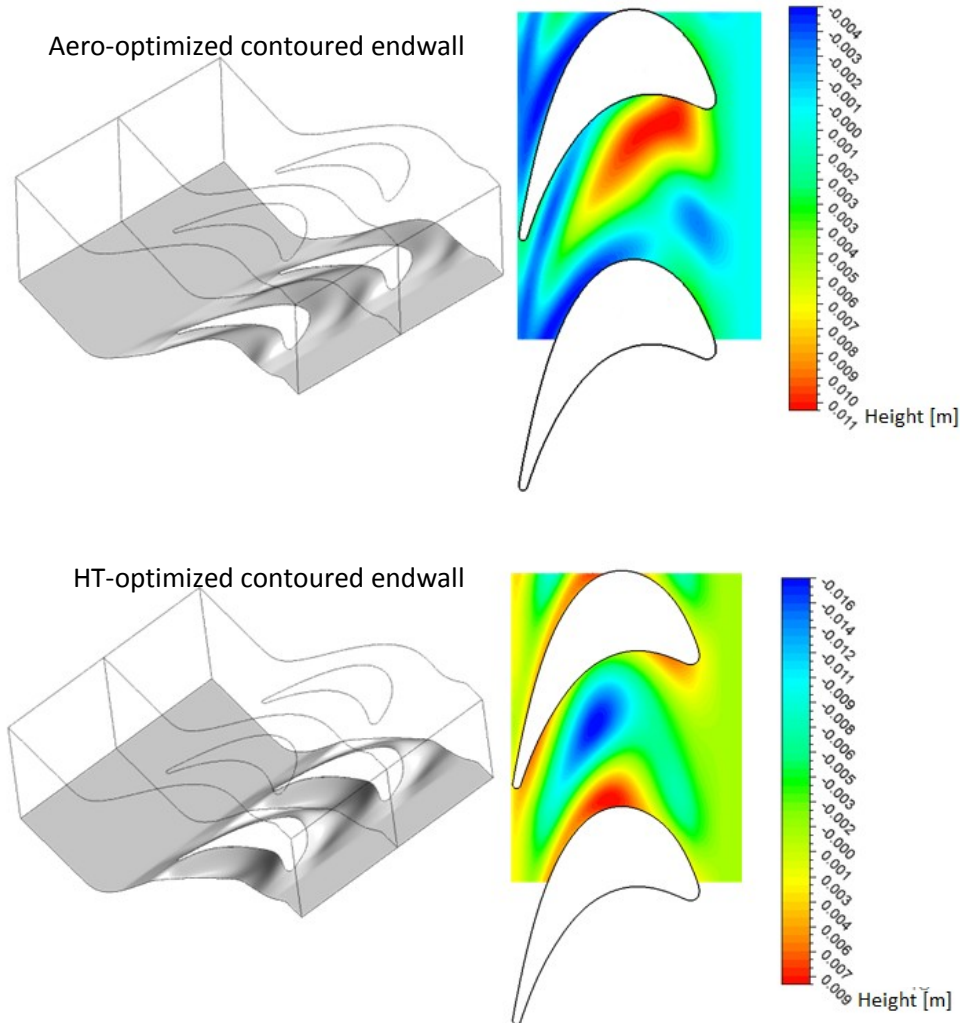
Figure 44: Endwall contour geometries

Figure 44 represents the two endwall contours being studied. The Aero-optimized contoured (AO-C) endwall has a peak region starting near the leading edge pressure side that extends towards mid passage and a trough region along the suction side of the airfoil from ~0.2 normalized axial chord up to near the trailing edge. In later sections, we can see that this

peak region succeeds in delaying the progression of the passage vortex from the pressure side to the suction side. The heat transfer optimized contoured (HTO-C) endwall has a strong trough region near the middle of the passage and a peak region near the airfoil suction side. This causes the passage vortex to slightly diffuse across the passage before reaching the suction side surface. Detailed discussions on the variation of flow along the contoured endwalls are carried out in the later sections.

Results and Discussions

Inlet Flow Measurements

The velocity profile of the incoming flow was measured on a plane $0.45C_{ax}$ upstream of the airfoil leading edge and was used as the incoming flow profile in the CFD calculations. The primary measurement passage isotropic turbulence intensity level as measured by a single wire hot-wire probe was 8%. The upstream flow uniformity was established with a maximum deviation of $\pm 1\%$ in normalized pressure.

Static Pressure Measurements

Airfoil static pressure at midspan for the center airfoil in the cascades was used to calculate the surface isentropic Mach number. The experimental uncertainty was established at $\pm 0.1\%$. The periodicity of flow through the passages was satisfactory and was established for all the cases that were studied using midspan pressure taps on the center airfoil and its adjacent airfoils. The local Mach number distribution on the airfoil surfaces were measured for exit Mach numbers varying from 0.70 to 0.95. Figure 45 shows the comparison of midspan airfoil loading between experimental values and CFD analysis results at design

Mach number (baseline endwall) for the airfoils. It can be seen that there is a reasonably good agreement between experiments and CFD analysis.

In order to ensure that contouring of the endwall does not affect the midspan loading, experimental measurements were conducted to obtain the loading of AO-C airfoil at midspan. Figure 46 reveals that the change of loading due to endwall contouring at airfoil midspan is insignificant. This confirms that the mainstream flow path near midspan remains unaltered with endwall contouring and that the airfoil loading is not largely compromised. It can be concluded that the profile losses are mostly unaffected by endwall contouring.
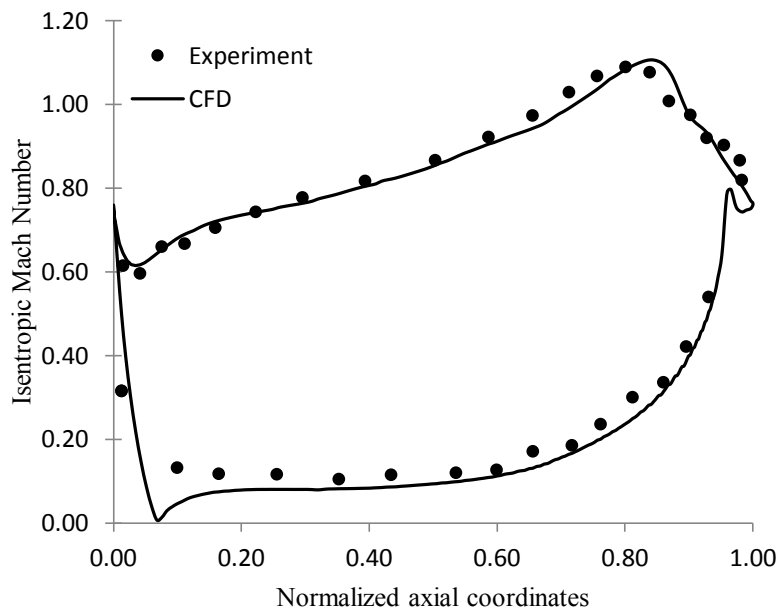
Figure 45: Midspan baseline airfoil loading from CFD and experiments (design Mach #)
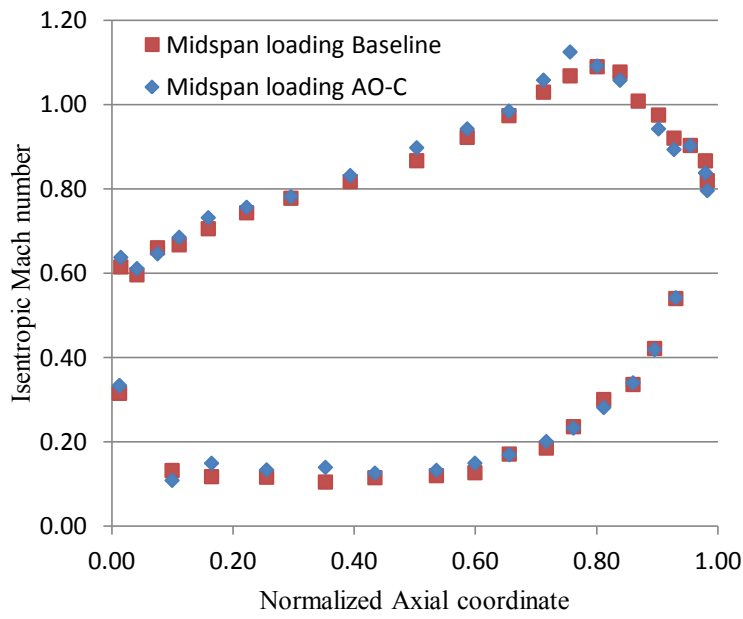
Figure 46: Midspan airfoil loading for the baseline case and AO-C case (design Mach #)
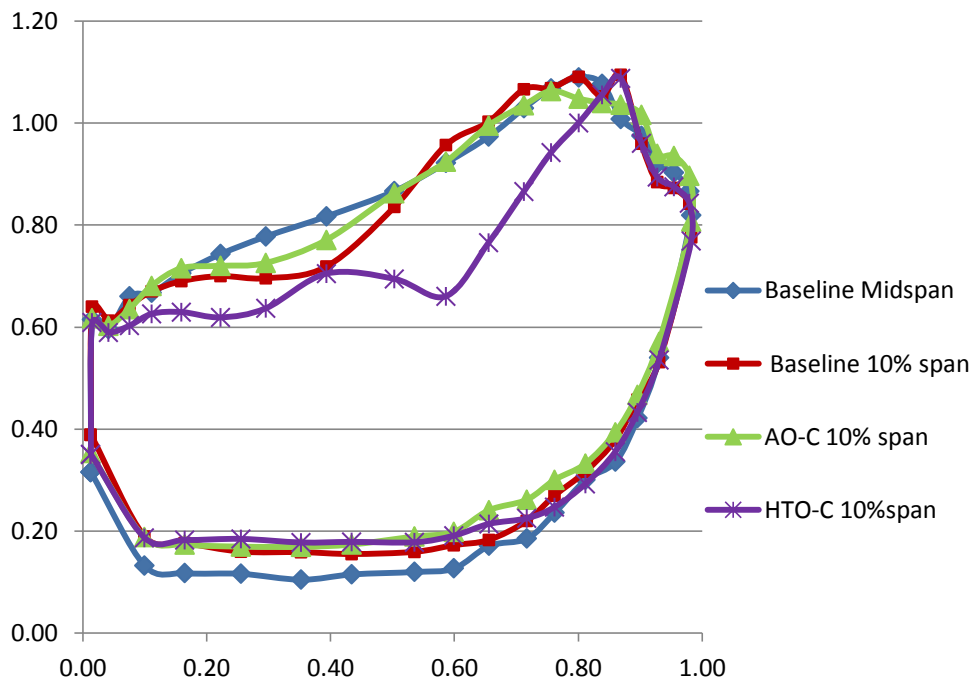
Figure 47: Variation of airfoil loading

The airfoil loading near the contoured endwall for the three cases is shown in Figure 47. All three cases show that the airfoils are relatively less loaded near the endwall as

compared to the midspan loading. Contouring of the endwall, changes the pressure distribution on the blade near the endwalls. The difference in pressure between the pressure side and the suction side, especially in the frontward part of the airfoil, directs the progression of the passage vortex. The strength and direction of the passage vortex is governed by the pressure gradient across the passage. The contoured endwalls alter this pressure gradient, thereby redirecting the endwall flow.
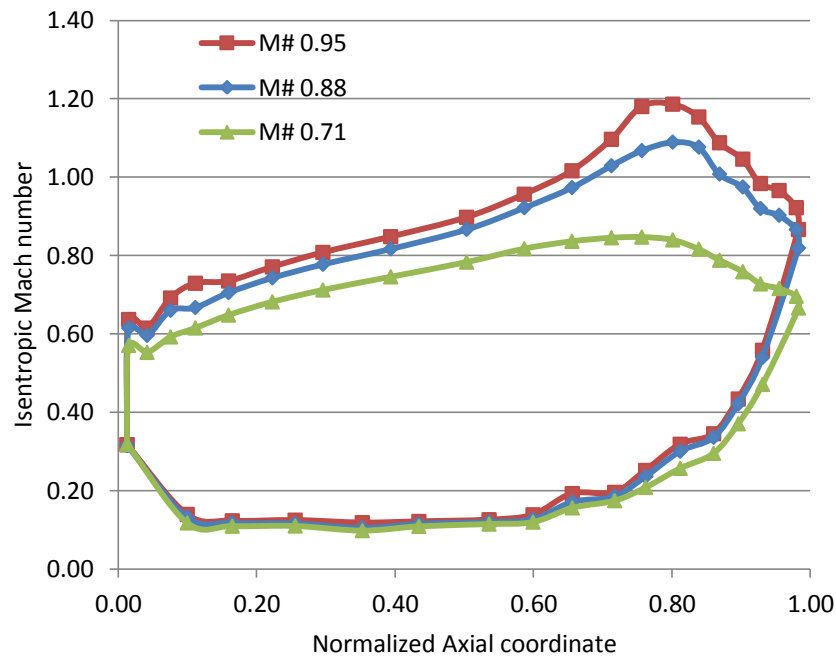
Figure 48: Variation of loading of with Mach number (Baseline midspan)

The effect of Mach number variation on the airfoil loading is shown in Figure 48. For all the cases, there is no significant change on the pressure side loading, up to near trailing edge, with varying exit Mach numbers. For the two higher Mach number cases, the loading on the suction side remain relatively the same from the leading edge to ~0.7 normalized axial coordinate. This can be attributed to the choking of the flow in the blade passage. Since the airfoils are more highly loaded as the Mach number increases, the pressure gradient across the passage will also be higher and therefore the strength of the passage vortex will be more.

The stronger the secondary flow structure, the larger will be the impact that endwall contouring has on secondary loss reduction. In other words, since the contribution of the secondary flow is larger in the case of the higher Mach number, the effect of endwall contouring may be more beneficial in loss reduction in this case.

Loss Measurements:

To capture the complete trend of the loss behavior, measurements were made across the pitch and span of the airfoils, at 0.1 Cax as well as 1.0 Cax downstream of the trailing edge of the cascades. Measurements are made at a total of 60 points during each run at each span location, across a distance of over one pitch length. Figure 49 represents a 2-D profile of the losses for the three cases, measured 0.1 Cax downstream of the trailing edge at the design exit Mach number. A 5 hole probe was traversed in the pitchwise direction at one spanwise location during each run. This was repeated at 11 different spanwise locations, from midspan to contoured endwall (flat endwall for the baseline case) to generate a 2D profile.

Regions of higher losses are clearly visible near the end walls and are a result of complex vortices arising due to the secondary flows. Pressure gradients in the passage caused by the boundary layer velocity distribution and flow stagnation on the blade, result in the creation of secondary flows in the end wall region. These pressure variations force the flows toward the end wall and also lead to the development of two legs of the leading edge vortex. The turning angle of the flow between the airfoils results in the creation of a strong pressure gradient across the passage. This gradient influences the paths of the two legs of the horseshoe vortex and also the low velocity flow near the end wall. The pressure side leg of the horseshoe vortex which is forced to flow in a downward direction combines with the low velocity flow near the end wall and forms the passage vortex. The passage vortex drifts from

the pressure side leading edge toward the suction side trailing edge of the adjacent airfoil. As this vortex approaches the suction side, it lifts off the end wall, adheres along the suction side and moves downstream in the passage. At the same time the suction side horseshoe vortex remains close to the end wall until it meets the passage vortex. It then wraps itself around the passage vortex instead of adhering to the suction surface, lifts off the end wall and continues downstream along the suction side.

The aero-optimized contoured (AO-C) endwall (Figure 44) has a protruded region which starts near the true leading edge of the airfoil and proceeds towards the suction side of the adjacent airfoil. This protrusion prevents the passage vortex or the pressure side leg of the horseshoe vortex from cutting sharply across the passage, from leading edge pressure side to suction side. The passage vortex tends to move across the passage due to the existing large pressure gradient. But the peaks on the contoured endwall try to guide this passage vortex along the pressure side of the airfoil, thereby delaying the progression of the passage vortex in the cross passage (pitchwise) direction. The passage vortex is guided along the favorable streamwise direction by the contours. The contours succeed in making the passage vortex meet the suction side leg of the horseshoe vortex further downstream, than in the baseline case. As the cross flow direction of the passage vortex, compared to the streamwise mainstream flow, is less intense in the aero-optimized contoured endwall case, the secondary losses generated will be lower. From Figure 49 and Figure 50, it is evident that the strength of the passage vortex is relatively less in the case of the aero-optimized endwall. This vortex is identified in the figures at a normalized span of 0.30 to 0.50 for the baseline case and 0.25 to 0.40 for the AO-C case. The contours have succeeded in restricting the amount of lift-off of the passage vortex. This is also due to the fact that the passage vortex was delayed in meeting the suction side leg of the horseshoe vortex, which is where the lift off originates. Reduction of losses can also be observed near the endwall because of the reduced cross flow.

Static pressure measurements were carried out on the endwalls to study the variation of endwall static pressure across the passage at all Mach numbers. As mentioned previously, the pressure variation across the passage is the dominant factor that determines both strength and direction of the passage vortex and thereby the secondary loss generation. A grid comprising of 16 static pressure taps were spaced equally across the pitch and chord of the passage as shown in Figure 51. The results indicate that the contours in the AO-C cascade manage to smoothen the pressure variations from the pressure side of the airfoil to the suction side of the adjacent airfoil. This alters the passage vortex path favorably by reducing the adverse pressure gradient, which is otherwise seen in the baseline case.

The line averaged losses in the pitchwise direction at each span location is calculated and plotted in Figure 50. A 3% reduction in overall area averaged loss coefficient is observed for the AO-C cascade. Further reduction in losses is seen as we go further downstream, where the complex secondary flows interact with each other.

The heat transfer optimized contoured (HTO-C) endwall has a peak region along most of the suction side surface of the airfoil with a deep trough near the middle of the passage. The peak region originates near the region where the passage vortex meets the suction side leg of the horseshoe vortex. The peak along this region pushes the passage vortex further downstream along the streamwise direction. Figure 49 and Figure 50 reveal that the passage vortex is less spread out as compared to the other two cases and is concentrated around normalized span ~ 0.4. There is no change in the overall area averaged losses for this case, as compared to the baseline case, although the trend of the secondary flows has been altered. From Figure 51, it is evident that the pressure variation along the passage has changed compared to the baseline case. However, the variation is not as smooth as in the AO-C case and the progression of the passage vortex across the passage is still quite strong. The objective of this contoured endwall is overall area averaged heat transfer reduction at the

endwall. At this point, it is worth mentioning that significant reduction in area averaged heat transfer was achieved for both the contoured endwalls studied, with small regions of increased hot spots.
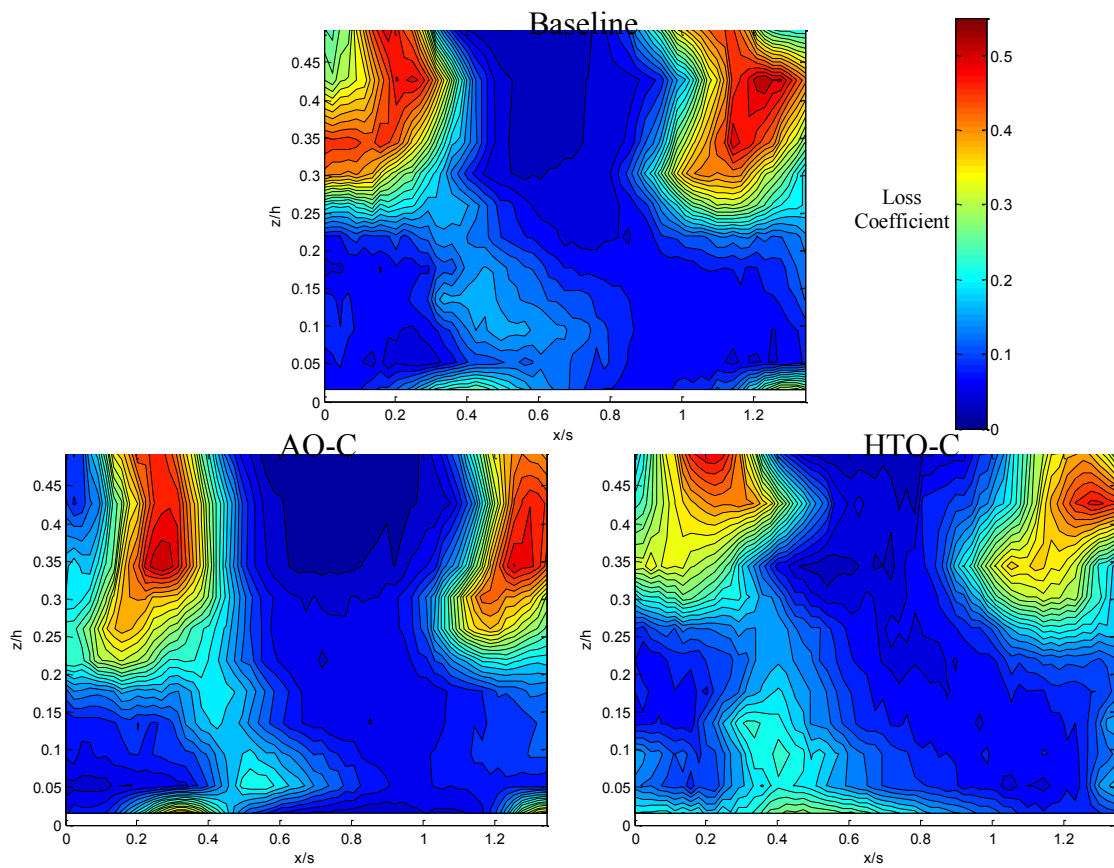

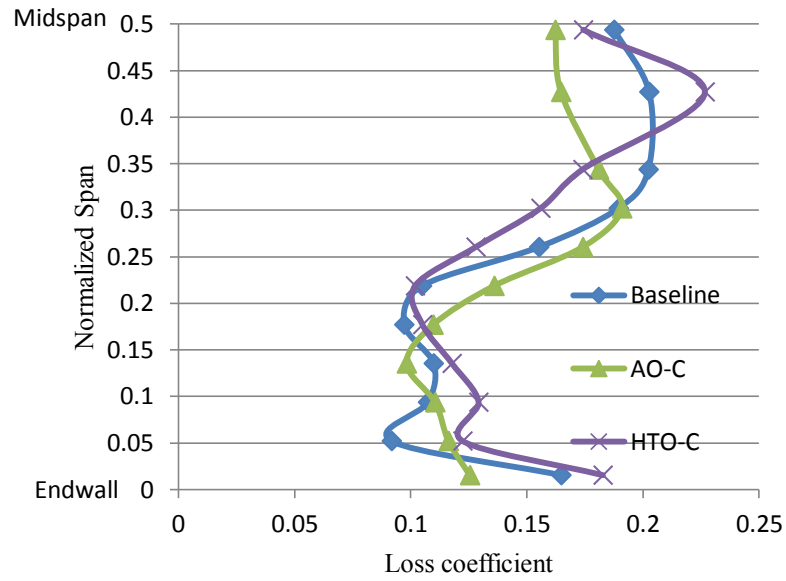Figure 49: 2D profile of losses measured experimentally at 0.1 Cax downstream
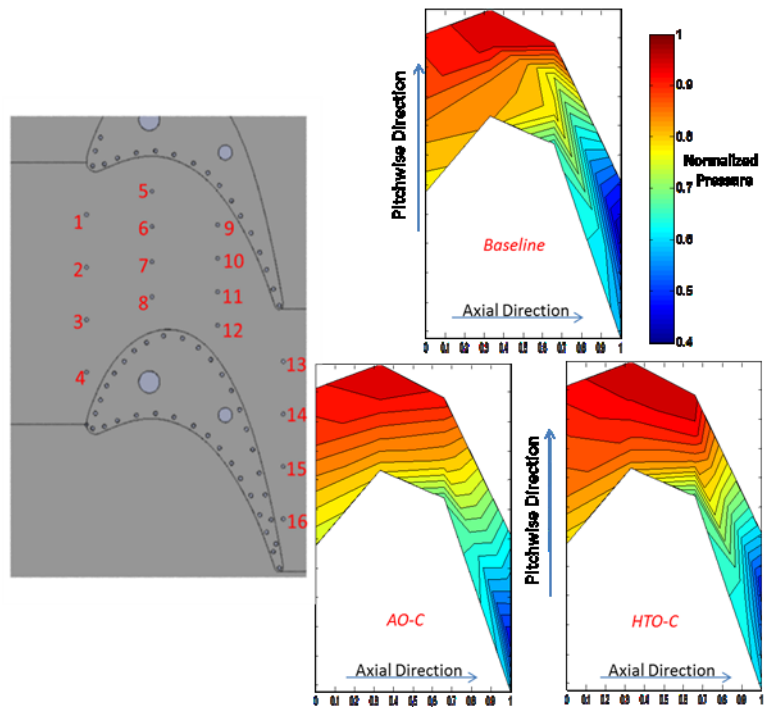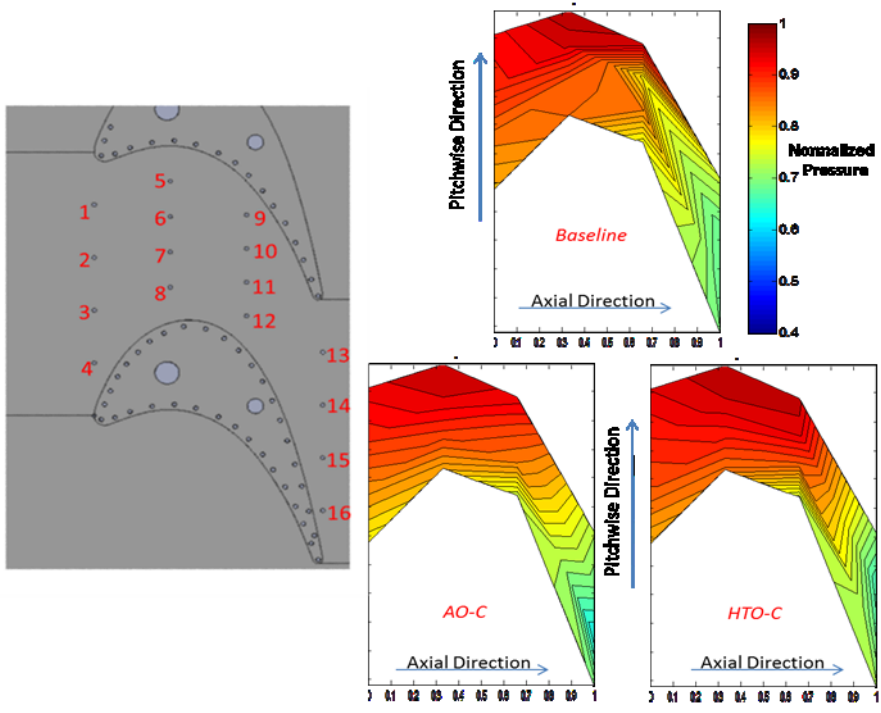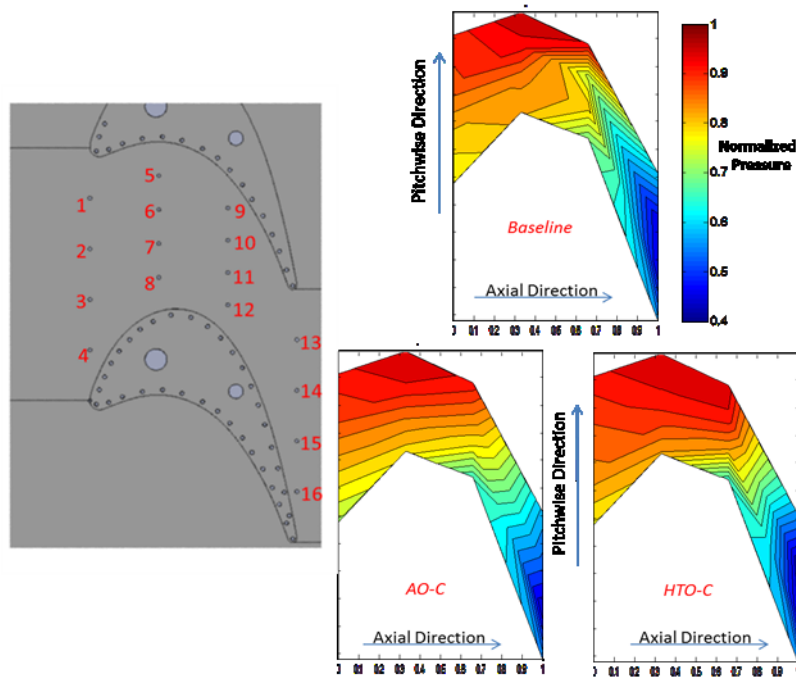
(design Mach #)

Figure 50: Spanwise variation of losses: 0.1 Cax downstream

(Experimental data at design Mach number)

(a) M# 0.87

(b) M# 0.71

(c) M# 0.95

Figure 51: Static pressure variation across the passage

As we go further downstream from the trailing edge plane, the vortices mix out and at 1.0 axial chord downstream, the losses are almost completely mixed out. With the objective of studying these mixed out losses, measurements are made at $1.0\ C_{ax}$ downstream from the trailing edge of the cascade at varying exit Mach numbers. A rise in losses is observed as the exit Mach number increases in the baseline case, as can be seen in Figure 52. The airfoils exhibit an increase in the level of aft diffusion at higher exit Mach numbers (Figure 48). The term aft diffusion refers to the static pressure rise or the drop in Mach number from the peak location to the trailing edge. When the aft diffusion becomes excessive, flow separation on the suction surface occurs, which results in high losses. Also, increase in losses is seen at higher Mach numbers due to the fact that the local velocities on the suction side, at higher Mach numbers, create a local supersonic flow, thus making it prone to shock waves.

As the Mach number increases, the difference in static pressure from the pressure side to the suction side of the airfoil increases, especially on the frontward portion of the airfoil. This pressure gradient plays a pivotal role in governing the strength and direction of the passage vortex. Therefore the secondary losses generated will be higher as the Mach number increases. The contours were generated to reduce losses at design Mach number. At the lower Mach number case the mixed out losses at midspan are almost equal for all three cases. The flow path of the passage vortex in the pitchwise direction will not be as steep as it is in the case of the higher Mach numbers. Therefore the contours may not play as major a role in favorably altering the passage vortex structures at the low Mach number case as it does at the higher Mach number cases. However, complete spanwise measurements need to be obtained to make a comprehensive conclusion on the benefits of endwall contouring at the off-design Mach numbers.
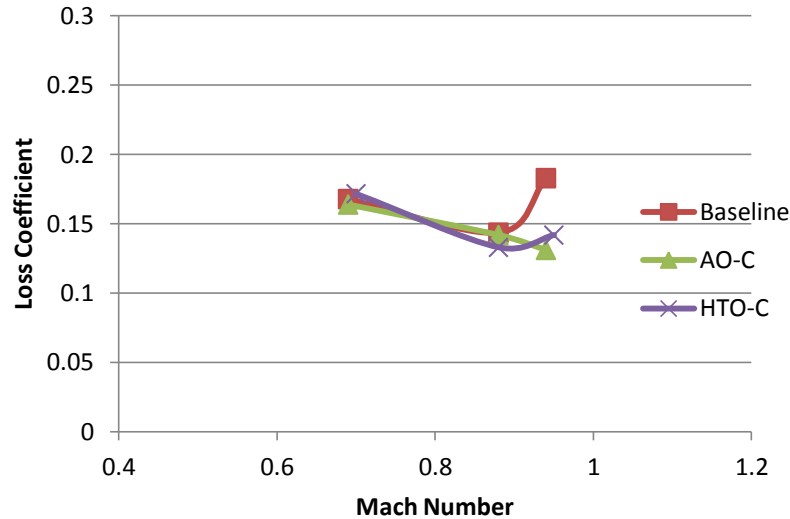
Figure 52: Loss vs. M#: 1.0 Cax downstream

The spanwise measurements made 1.0 C_{ax} downstream of the trailing edge are represented in Figure 53. It is evident that the losses are more mixed out as compared to the losses measured at the 0.1 C_{ax} location. The core region of the passage vortex, for all the cascades, has reduced due to mixing of the flow at the $1.0C_{ax}$ location.The line averaged losses in the pitchwise direction at each span location reveals that the losses in the case of AO-C are lower than the baseline case almost across the entire span. On calculating the overall area averaged loss coefficient (averaged across the entire span and pitch) a 17% reduction is achieved for the AO-C cascade. The endwall contours, in this case, have succeed in reducing the strength of the non-streamwise components of the velocity vector, which reduced the amount of mixed out losses as the flow goes further downstream. As observed at the 0.1 Cax location, the HTO-C cascade reveals no change in the value of the overall area averaged loss coefficient at the 1.0 Cax location as well, although variation of trend in the flow is visible.
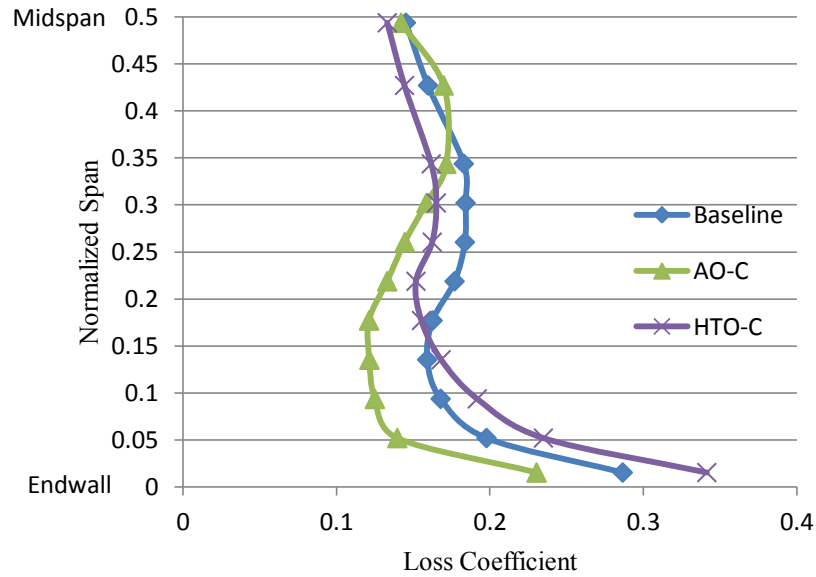
Figure 53: Spanwise variation of losses: 1.0 Cax downstream

(Design Mach number)

Conclusions

Experimental measurements were presented on the effect of endwall contouring on high turning, high loading turbine airfoil cascades in a quasi 2D transonic cascade wind tunnel. Two contoured endwalls, one with the objective of total pressure loss reduction and the other with the objective of reduced heat transfer from the hot gas to the endwall were tested. Traverse measurements and passage pressure measurements were carried out to study the interaction between the endwall secondary flow and the contoured endwalls.

The aero-optimized contoured (AO-C) endwall reduced the strength of the passage vortex that moves cross passage in the pitchwise direction. The contouring succeeds in delaying the meeting of the passage vortex and the suction side leg of the horseshoe vortex and thereby pulling down the vortex in the spanwise direction. A 3% reduction in area averaged losses was achieved at 0.1 Cax downstream of the trailing edge and a 17% reduction in mixed out losses was achieved at 1.0 Cax downstream location. The heat transfer

optimized contoured (HTO-C) endwall effected an altered pressure gradient across the endwall passage, which helps in moving the passage vortex in the stream wise direction. The heat transfer optimized case was not as effective in reducing the total pressure loss as the aero-optimized case. The overall area averaged loss coefficient, in this case, was comparable to the baseline case.

10.0 EFFECT OF AIRFOIL SPACING ON ENDWALL CONTOURING PERFORMANCE IN A TRANSONIC TURBINE BLADE PASSAGE

Motivation

Numerous studies on the effectiveness of endwall contouring in reducing secondary losses have been conducted. Most of these studies have shown promising results. However, the amount of improvement achieved varies considerably from study to study. Reduction in losses due to endwall contouring is highly dependent on blade loading, requiring case by case endwall contour studies. Designs with low aspect ratios, increased airfoil loading and more front loaded airfoils generally have secondary losses that are a significant portion of total losses. Endwall contouring can be more effective in such cases. To try and understand when contouring can be helpful and when it is futile, a study of endwall contouring on two cascades with varying loading levels is carried out. The loading levels of the two airfoils are varied by increasing the pitch of one cascade by 25% with respect to the other. Cascade IP, with its increased pitch, has a Zweifel coefficient increased by 25% compared to cascade SP. The airfoils have a turning angle of ~127°. Detailed loss measurements, both in the pitchwise as well as spanwise directions, are conducted at 0.1 Cax and 1.0 Cax locations downstream of the trailing edge. The results reveal that endwall contouring reduced the overall total pressure losses of the IP case considerably, while it was insignificant and caused very little change in secondary flow patterns for the SP case.

Static Pressure Measurements

Static pressure taps positioned 0.5 Cax upstream and 0.5 Cax downstream of the cascade are used to estimate the inlet and exit Mach numbers. Airfoil midspan loading was measured on the center airfoil at the design exit Mach numbers of 0.87. The adjacent airfoils were also instrumented in order to ensure flow periodicity between the passages of interest. The periodicity of flow through the passages was satisfactory and was established for all the cases. The comparison between the loading levels between the two airfoils as shown in Figure 54 shows that IP airfoil with its increased pitch is consistently loaded higher than the SP case. The IP airfoil has larger local velocities on the suction side and larger surface static pressure on the suction side surface. The larger pressure variation on airfoil IP causes a strong pressure gradient in the passage that causes the pressure side leg of the horseshoe vortex to migrate sharply across the passage (pitchwise direction) leading to higher losses. Further discussion of this phenomenon will follow in the next section.
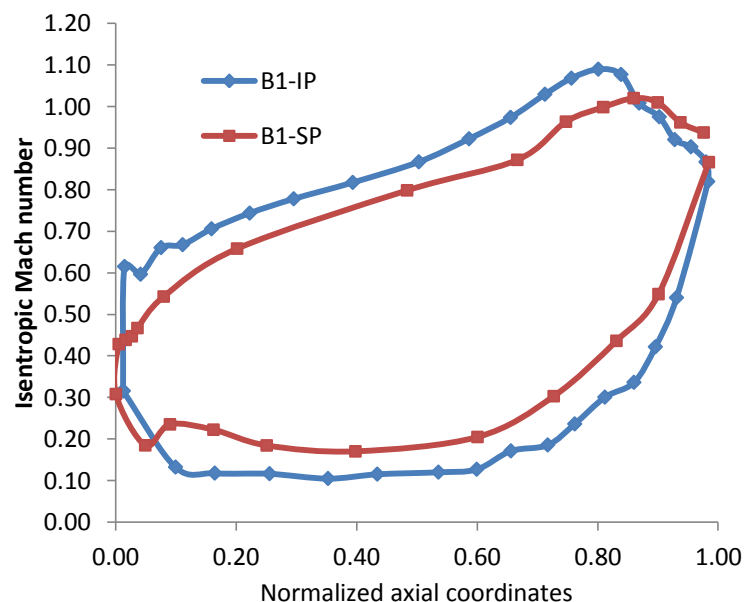

Figure 54: Loading distribution on the airfoils in the two cascades

Loss Measurements

Traverse measurements were made at 0.1 Cax as well as 1.0 Cax downstream from the trailing edge for the two cascades. Both pitchwise as well as spanwise measurements were made to obtain a complete 2D loss profile. Measurements are made at a total of 60 points during each run, across a distance of over one pitch length. Figure 56 shows a 2-D profile of the losses for the two cascades, 0.1 axial chord downstream from the trailing edge of the cascade at the design exit Mach at various spanwise locations. A 5 hole probe was traversed in the pitchwise direction at various span locations, from midspan to flat/contoured endwall. The contour geometries for the SP cascade and the IP cascade (Aero-optimized geometry) were presented previously in Figure 27 and Figure 44 respectively.

Both the cascades show high loss regions near the endwalls. The difference in airfoil static pressure distribution between the suction side and pressure side, results in a strong pressure gradient in the passage. This along with the low velocity endwall flow and the flow stagnation near the airfoil leading edge gives rise to the horseshoe vortex. The vortex splits at the leading edge into two legs and progresses down either side of the leading edge of the airfoil. The pressure side leg of the horseshoe vortex migrates across the passage due to the strong pressure gradient mentioned before. The pressure side leg of the horseshoe vortex which is forced to flow in a downward pitchwise direction combines with the low velocity flow near the end wall and forms the passage vortex. Since the pressure gradient is larger in the IP case, the passage vortex is stronger and also migrates more sharply than in the SP case. The cross passage flow of the passage vortex results in large total pressure losses. The passage vortex goes on to meet the suction side leg of the horseshoe vortex near the suction side surface, lifts off the end wall, adheres along the suction side and moves downstream in the passage. At the same time the suction side horseshoe vortex remains close to the end wall

until it meets the passage vortex. It then wraps itself around the passage vortex instead of adhering to the suction surface, lifts off the end wall and continues downstream along the suction side.

From Figure 55 and Figure 56, it is evident that the strength of these vortices is much larger in the IP baseline case compared to the SP baseline case. Since the pressure gradient across the passage is larger in the IP baseline case, the passage vortex meets the suction side leg of the horseshoe vortex much earlier than in the SP baseline case. This makes the lift-off occur earlier in the passage, and by the time the flow exits the trailing edge region of the airfoil, the vortex has climbed up the span and is almost at midspan. This is identified in the plots from a region of normalized span ~ 0.25 to 0.50. Comparatively the vortex in the SP case is much lower (normalized span ~ 0.15 to 0.30) and the vortex core region is also smaller. The overall increase in area averaged loss coefficient is 35% more in the IP baseline case.

The important observation in the figure is that the contribution of the secondary losses to the total pressure loss in the SP baseline case is much smaller than in the IP baseline case. Since the lift-off is low and does not reach near midspan, we can assume that the profile losses for the SP case are the losses that are measured at midspan. For the IP case, however this assumption cannot be made since the secondary vortex core has reached the midspan region. The effect of the secondary flow is seen across the entire span of the IP airfoil passage. Since the contribution of the secondary losses in the SP case is significantly lower, benefits of endwall contouring are also limited. Profile losses are the major contributors in this case and endwall contouring cannot reduce those losses. However, in the IP case, as the secondary losses contribute heavily to the total pressure losses, the effect of endwall contouring is very beneficial. This is evident from the figures below, wherein reduction in the

strength of the passage vortex is clearly visible for the IP case. The endwall contouring also manages to bring down the vortex core in the spanwise region. This is achieved by delaying the meeting of the passage vortex and suction side leg of the horseshoe vortex, which is where the lift-off of the vortex occurs. The SP cascade shows very little variance of secondary flow structures with the inclusion of endwall contouring. The losses in the SP cascade are dominated by the profile losses. As the secondary losses are low in this case, there is not much room for improvement of secondary flow characteristics. Since the lift-off is comparatively lower than in the IP case, the flow of the passage vortex in the pitch wise direction is not as steep as in the IP case. In other words, the streamwise component (favorable) of the velocity vector is stronger in the SP case as compared to the IP case, which has a strong pitchwise component (unfavorable). Therefore endwall contouring does not make a big difference in changing secondary flow characteristics in the SP case. It is instrumental in altering the near-endwall passage flow in the IP case and the contours succeeds in directing the flow into a more streamwise direction thereby reducing the losses.

Figure 55: Spanwise variation of losses: 0.1 Cax downstream

(a) SP Cascade

(b) IP Cascade

Figure 56: 2D plot of losses with and without endwall contouring at 0.1 Cax location

Larger reduction of losses will be seen further downstream where these complex secondary flows mix with each other. In order to estimate these losses, measurements were made at 1.0 Cax downstream location. By the time the flow reaches this location, the vortices mix out and therefore the losses are almost completely mixed out. With the objective of

studying these mixed out losses, measurements are made at $1.0\,C_{ax}$ downstream from the trailing edge of the cascade. Similar to the procedure followed at 0.1 Cax location, spanwise variation of losses was measured at 1.0 Cax location using a traversing Kiel probe at the design Mach number of 0.87 and the results are plotted in Figure 57 and Figure 58.

As seen from the 01. Cax location, there is no significant effect of endwall contouring on the SP case. The secondary flow path was not altered and therefore the loss profile remains mostly unchanged. However, the reduction in losses for the IP case is rather significant. The contours altered the secondary flow path, making them move more in a streamwise direction than in the baseline case. Since the pitchwise and spanwise components of the flow were higher in the IP baseline case as compared to the contoured case, higher losses are seen due to unfavorable mixing as the flow moves downstream. With contouring, these pitchwise and spanwise components have been reduced and therefore mixing losses are more limited than in the baseline case. Contouring of the endwall resulted in a 3% reduction in area averaged losses at 0.1 Cax downstream of the trailing edge and a 17% reduction in mixed out losses at 1.0 Cax downstream location for the IP case.
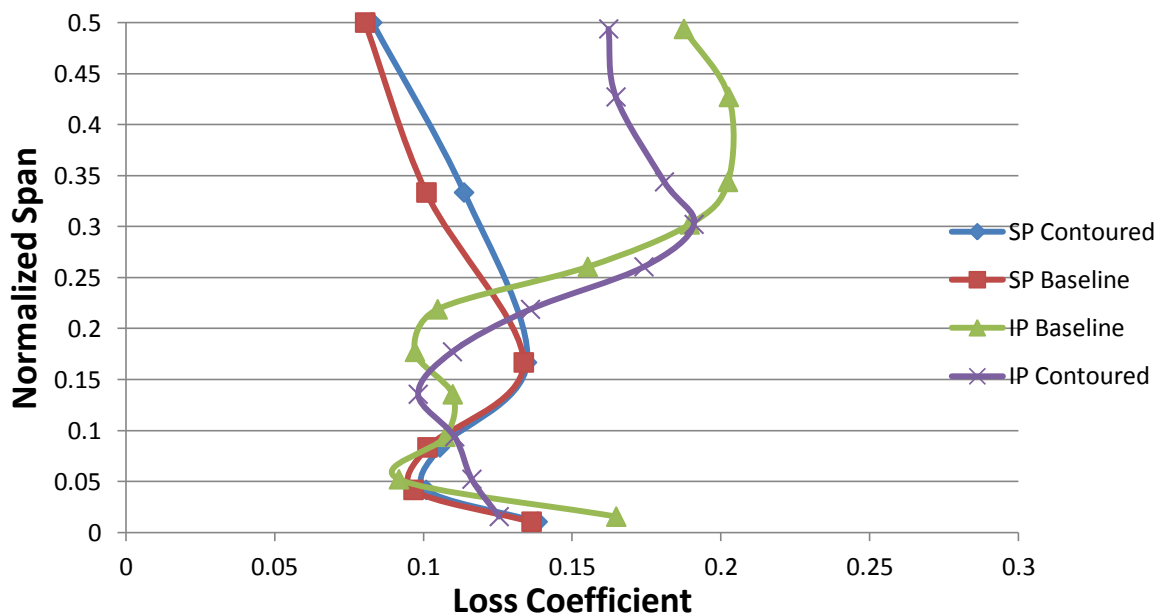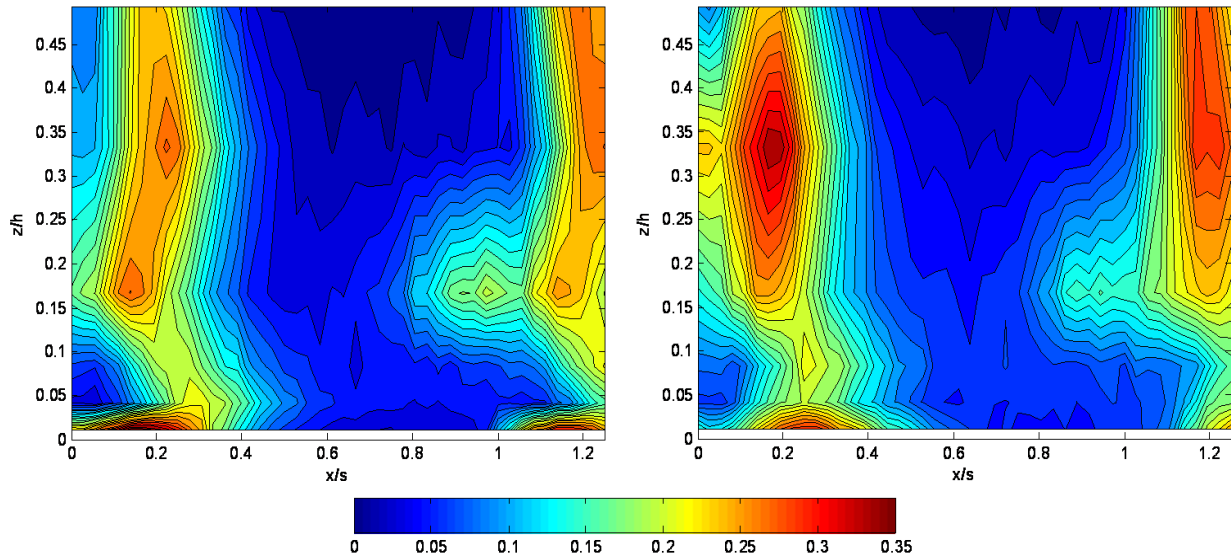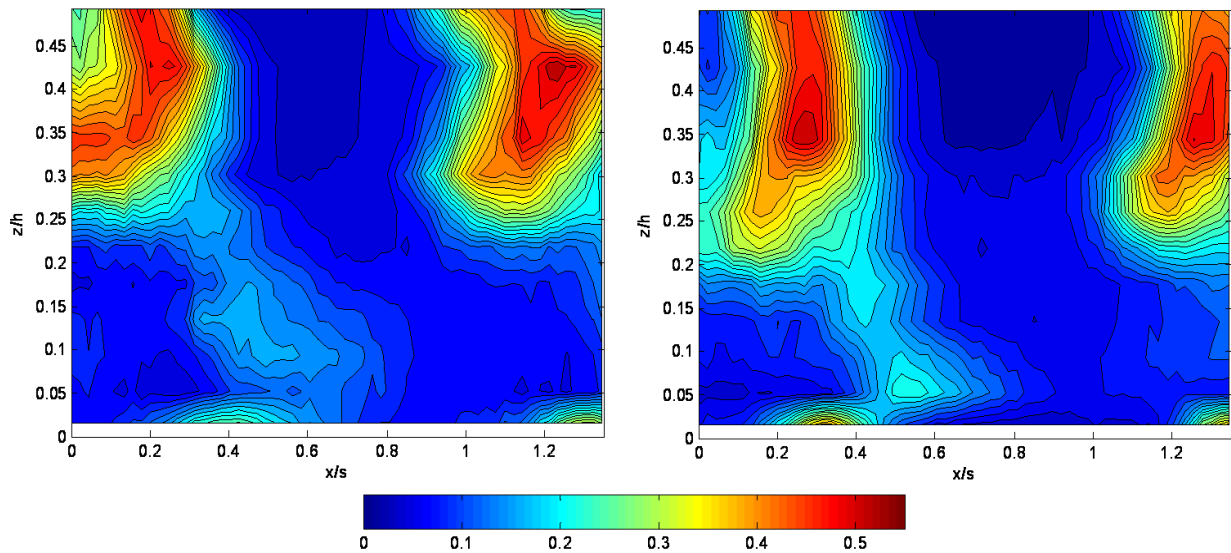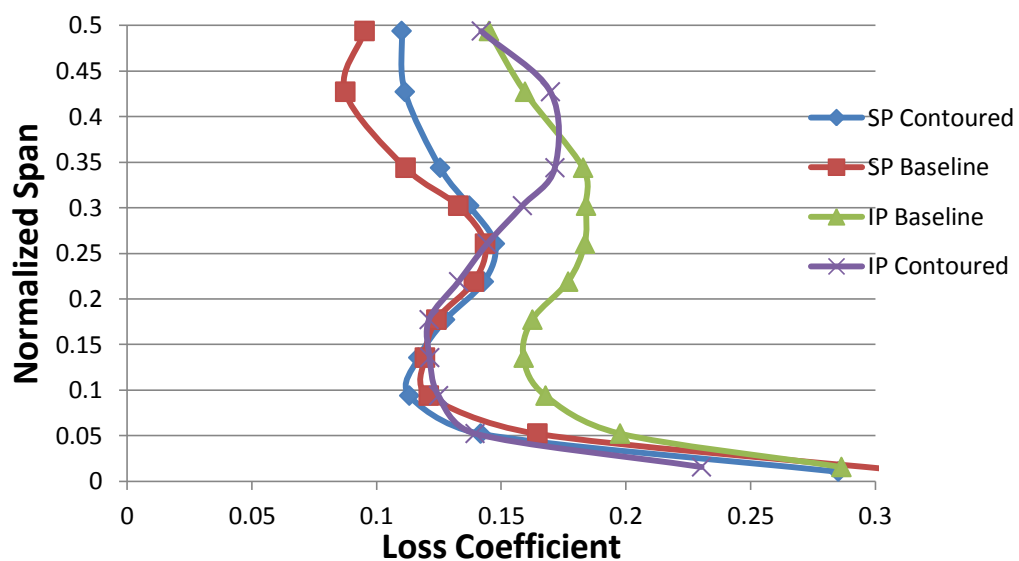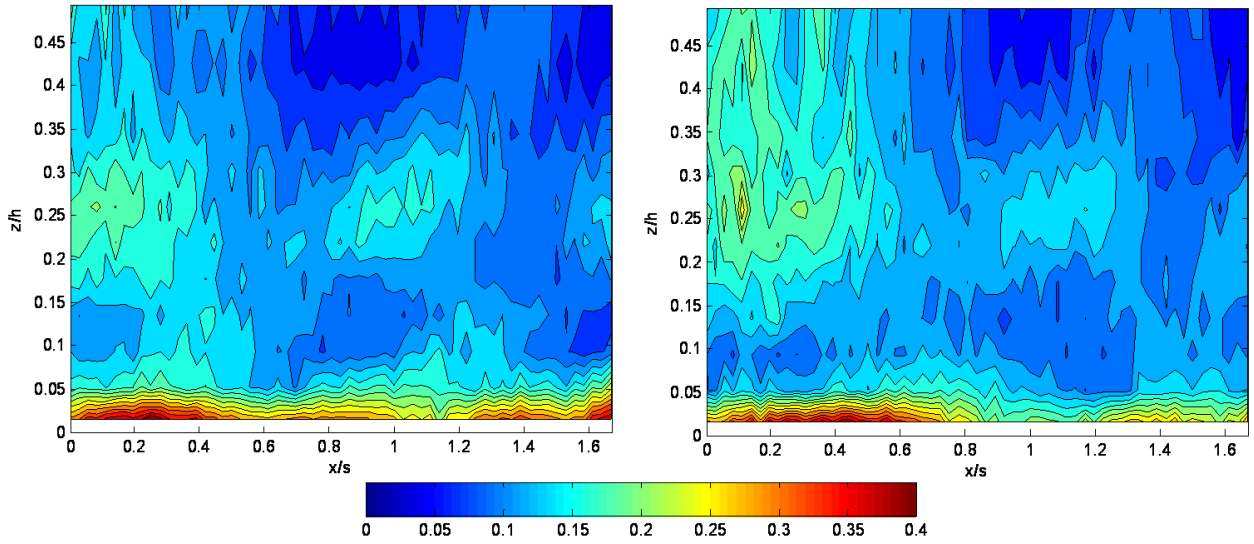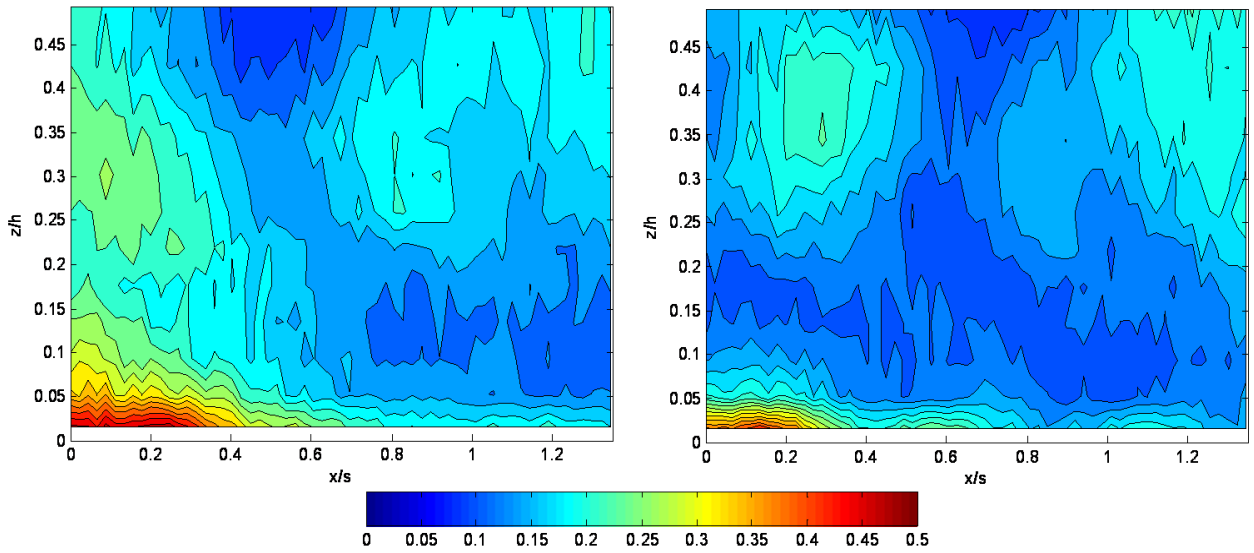

Figure 57: Spanwise variation of losses: 1.0 Cax downstream

(a) SP cascade

(b) IP cascade

Figure 58: 2D plot of losses with and without endwall contouring at 1.0 Cax location

Conclusions

In this study, experimental measurements were conducted to understand the effect of endwall contouring on two high turning cascades with varying airfoil spacing. Blade loading measurements and loss measurements were carried out. The increase in spacing led to an increase in the secondary flows generated. The loading on the airfoil with the increased pitch was higher, which led to higher pressure gradients across the passage. The strength and direction of the passage vortex is governed by this pressure gradient.

The cascade with the lower pitch (SP) showed lower strength of secondary flow structures. Profile losses played a more important role in total pressure loss as compared to the secondary losses. Endwall contouring is designed to reduce the adverse effects of secondary flows. The SP cascade, which already has low secondary losses, did not see any benefits with endwall contouring.

The IP case however, revealed large contribution of secondary losses to the overall total pressure loss. The pressure gradient across the passage was significantly stronger which led to a strong passage vortex moving in a predominantly pitchwise direction. The contours succeed in altering the flow path into a more favorable streamwise direction. This also delays the meeting of the passage vortex and suction side leg of the horseshoe vortex, which in turn delays the lift-off the vortex from the endwall. Significant reduction in overall area averaged loss coefficient was achieved with endwall contouring for the IP case, while very little change in loss profile was observed for the SP case.

Therefore, endwall contouring could be more beneficial in cases where the secondary losses are predominant. Low aspect ratio airfoils wherein the effects of secondary flows are seen across the entire span of the airfoil could benefit from endwall contouring. Highly front loaded airfoil and airfoils with high inlet/turning angles will have a strong pressure gradient

created across the passage due to difference in loading between the suction side and pressure sides of the airfoils. Strong passage vortex structures will be created in these cases and endwall contouring could be beneficial in reducing the secondary losses.

11.0 CONCLUSIONS

Part I: Aerodynamic performance of high turning airfoils

A comprehensive study on the aerodynamic performance of 5 different turbine blades with high turning angles, operating at transonic conditions was conducted at design and off-design conditions. Analysis of the loss behavior indicates that loss generation is mainly governed by three physical phenomena:

- Deceleration of flow on the suction side of the airfoil plays a major role in higher loss production.

- With higher aft diffusion, flow separation on the rear part of the suction surface of the airfoil occurs, which leads to higher losses.

- Shocks originating from the trailing edge of the adjacent airfoil and impinging on the rear of the airfoil suction surface affect losses adversely.

Part II: The effect of endwall contouring on turbine performance

At the end of the above study, the best airfoil in terms of aerodynamic performance was selected and the effect of endwall contouring in reducing secondary losses was conducted. For the cascade studied, the contribution of the secondary losses was small as compared to the profile losses. The contouring did not succeed in significantly altering the passage vortex flow path and no improvement was observed in either heat transfer through the endwall or in terms of aerodynamic loss reduction.

To further investigate the influence of endwall contouring in altering secondary flow patterns, a study was performed on a cascade with increased spacing between the airfoils. By

increasing the spacing, the airfoil would be more loaded, thereby increasing the difference between the pressure side and suction side pressure distributions on the airfoils. This creates a larger cross passage pressure gradient, leading to stronger secondary flow generation and a larger contribution of secondary losses to the total pressure losses. Additionally, by increasing the area of the passage, the contours can be more aggressively designed without creating steep gradients in the trough and peak regions. Two contoured endwalls, one with the objective of total pressure loss reduction and the other with the objective of reduced heat transfer from the hot gas to the endwall were tested.

The aero-optimized contoured endwall reduced the strength of the passage vortex that moves cross passage in the pitchwise direction. The contouring causes the meeting of the passage vortex and the suction side leg of the horseshoe vortex to be delayed, and thereby pulls down the vortex in the spanwise direction. A 3% reduction in area averaged losses was achieved at 0.1 Cax downstream of the trailing edge and a 17% reduction in mixed out losses was achieved at 1.0 Cax downstream location. The heat transfer optimized contoured endwall also altered the pressure gradient across the endwall passage, which helps in moving the passage vortex in the stream wise direction. The heat transfer optimized case was not as effective in reducing the total pressure loss as the aero-optimized case. The overall area averaged loss coefficient, in this case, was comparable to the baseline case.

REFERENCES

[1]   Goobie, S. M., Moustapha, S. H., and Sjolander, S. A., 1989, ''An Experimental Investigation of the Effect of Incidence on the Two-Dimensional Flow,'' Proc, IX International Symposium on Air Breathing Engines ~ISABE!, Sept., pp. 197–204.

[2]   Rodger, P., Sjolander, S. A., and Moustapha, S. H., 1992, ''Establishing Two-Dimensional Flow in a Large-Scale Planar Turbine Cascade,'' AIAA Paper, No. 92-3066.

[3]   Whitehouse, D. R., Moustapha, S. H., and Sjolander, S. A., 1993, ''The Effects of Axial Velocity Ratio, Turbulence Intensity, Incidence, and Leading Edge Geometry on the Midspan Performance of a Turbine Cascade,'' Can. Aeronautics Space J., 39, No. 3, Sept., pp. 150–156.

[4]   Prakash, C., Cherry, D. G., Shin, H. W., Machnaim, J., Dailey, L., Beacock, R., Halstead, D., Wadia, A. R., Guillot, S., and Ng, W. F., "Effect of Loading Level and Distribution on LPT Losses," *ASME Paper* GT2008-50052, 2008.

[5]   Corriveau, D., and Sjolander, S. A., 2004, "Influence of Loading Distribution on the Performance of Transonic HP Turbine Blades," ASME J. Turbomach., 126, pp. 288–296.

[6]   Funazaki. K., Takahiro, S. and Haruyuki, T., "Effects of Blade Loading Distribution on Aerodynamic Performance of Ultra-High Lift LP Turbine Airfoils Under the Influences of Wake Passing and Freestream Turbulence", ASME paper GT-2010-22134.

[7]   Popovic, I., Zhu, J., Dai, W., Sjolander, S. A., Praisner, T. and Grover, E., "Aerodynamics of a Family of Three Highly Loaded Low-Pressure Turbine Airfoils: Measured Effects of Reynolds Number and Turbulence Intensity in Steady Flow", ASME paper GT-2006-91271.

[8]   Zoric, T., Popovic, I., Sjolander, S. A., Praisner, T. and Grover, E., "Comparative Investigation of Three Highly Loaded LP Turbine Airfoils: Part I – Measured Profile and Secondary Losses at Design Incidence", ASME paper GT- 2007-27537.

[9]   Zoric, T., Popovic, I., Sjolander, S. A., Praisner, T. and Grover, E., "Comparative Investigation of Three Highly Loaded LP Turbine Airfoils: Part I – Measured Profile and Secondary Losses at Off-Design Incidence", ASME paper GT- 2007-27538.

[10]   Benner, M. W., Sjolander, S. A., and Moustapha, S. H., 2004, "The Influence of Leading Edge Geometry on Secondary Losses in a Turbine Cascades at the Design Incidence," ASME J. Turbomach., 126, pp. 277–287.

[11] MacIsaac, G.D., Sjolander, S.A. and Praisner, T.J., 2010, "Measurements of Losses and Reynolds Stresses in the Secondary Flow Downstream of a Low Speed Linear Turbine Cascade," ASME paper GT2010-22727.

[12] Jouini, D. B. M., Sjolander, S. A., and Moustapha, S. H., 2001, "Aerodynamic Performance of a Transonic Turbine Cascade at Off-Design Conditions," ASME J. Turbomach., 123, pp. 510–518.

[13] Jouini, D. B. M., Sjolander, S. A., and Moustapha, S. H., 2002, "Midspan Flow-Field Measurements for Two Tran-Sonic Linear Turbine Cascades at Off-Design Conditions," ASME J. Turbomach., 124, pp. 176–186.

[14] Taremi, F., Sjolander, S.A. and Praisner, T.J., 2010, "Measurements of Endwall Flows in Transonic Linear Turbine Cascades: Part I Low Flow Turning," ASME paper GT2010-22759.

[15] Taremi, F., Sjolander, S.A. and Praisner, T.J., 2010, "Measurements of Endwall Flows in Transonic Linear Turbine Cascades: Part II High Flow Turning," ASME paper GT2010-22760.

[16] Praisner, T. J. and Clark, J. P., "Predicting Transition in Turbomachinery, Part I – A Review and New Model Development", ASME paper GT-2004-54108.

[17] Praisner, T. J., Grover, E. A., Rice, M. J. and Clark, J. P., "Predicting Transition in Turbomachinery, Part II – Model Validation and Benchmarking", ASME paper GT-2004-54109.

[18] Menter, F. R., Langtry, R. B., Likki, S. R., Suzen, Y. B., Huang, P. G., "A Correlation-Based Transition Model Using Local Variables: Part I – Model Formulation", ASME GT-2004-53452.

[19] Langtry, R. B., Menter, F. R., Likki, S. R., Suzen, Y. B., Huang, P. G., "A Correlation-Based Transition Model Using Local Variables: Part II – Test Cases and Industrial Applications", ASME GT-2004-53454.

[20] Nagel, M. G., and Baier, R.-D., 2005, "Experimentally Verified Numerical Optimization of a Three-Dimensional Parameterized Turbine Vane With Nonaxisymmetric End Walls," ASME J. Turbomach., 127, pp. 380–387

[21] Morris, A. W. H., Hoare, R. G., 1975, "Secondary loss measurements in a cascade of turbine blades with meridional wall profiling," ASME Paper 75-WA/GT-13.

[22] Kopper, F. C., Milano, R., 1981, "Experimental investigation of endwall profiling in a turbine vane cascade," AIAA Journal, Vol. 19(8), pp 1033-1040

[23] Duden, A., Raab, I., Fottner, L., 1998, "Controlling the secondary flow in a turbine cascade by 3D airfoil design and endwall contouring," International gas turbine & aero engine conference & Exhibition, Stockholm, Sweden, 98-GT-72.

[24] Saha, A. K., Acharya, S., 2006, "Computations of turbulent flow and heat transfer through a three-dimensional non-axisymmetric blade passage," Proceedings of GT2006, ASME Turbo Expo 2006: power for land, sea and air, May 8-11, Barcelona, Spain, GT2006-90390.

[25] Gustafson, R., Mahmood, G., Acharya, S., 2007, "Aerodynamic measurements in a linear turbine blade passage with three-dimensional endwall contouring," Proceedings of GT2007, ASME Turbo Expo 2007: power for land, sea and air, May 14-17, Montreal, Canada, GT2007-28073.

[26] Praisner, T. J., Allen-Bradley, E., Grover, E. A., Knezevici, D. C., Sjolander, S. A., 2007, "Application of non-axisymmetric endwall contouring to conventional and high-lift turbine airfoils," Proceedings of GT2007, ASME Turbo Expo 2007: power for land, sea and air, May 14-17, Montreal, Canada, GT2007-27579.

[27] Snedden, G., Dunn D., Ingram, G., Gregory-Smith D., 2009, "The application of non-axisymmetric endwall contouring in a single stage, rotating turbine," Proceedings of GT2009, ASME Turbo Expo 2009: Power for land, sea and air, June 8-12, Orlando, Florida, GT2009-59169.

[28] Harvey, N. W., Rose, M. G., Taylor, M. D., Shahpar, S., Hartland, J., Gregory-Smith, D. G., 2000, "Nonaxisymmetric turbine end wall design: Part I- three-dimensional linear design system," ASME Jl. of turbomachinery, Vol. 122, April 2000, pp278-285.

[29] Hartland, J. C., Gregory-Smith, D. G., Harvey, N. W., Rose, M. G., 2000, " Nonaxisymmetric turbine end wall design: Part II – Experimental validation," ASME Jl. of turbomachinery, Vol. 122, April 2000, pp286-293.

[30] Lynch, S.P., Sundaram, N., Thole, K.A., "Heat transfer for a turbine blade with Non-Axisymmetric Endwall Contouring," Proceedings of GT2009, ASME Turbo Expo 2009: Power for land, sea and air, June 8-12, Orlando, Florida, GT2009-60185.

[31] Gregory-Smith, D. G., and Cleak, J. G. E., 1992, "Secondary Flow Measurements in a Turbine Cascade with High Inlet Turbulence," ASME J. Turbomach., **114**, pp. 173–183.

[32] Taremi, F., Sjolander, S.A. and Praisner, T.J., 2011, "Application of Endwall Contouring to Transonic Turbine Cascades: Experimental Measurements at Design Conditions," ASME paper GT2011-46511.

[33] Panchal, K., Abraham, S., Ekkad, S., Ng, W.F., Malandra, T. and Brown, B.J., 2011, "Investigation of Effect of end wall contouring methods on a transonic turbine blade passage", ASME paper GT2011-45192.